CARACTÉRISATION DES COMMUNAUTÉS PHYTOPLANCTONIQUES ET DES PROPRIÉTÉS OPTIQUES DE L'ESTUAIRE MARITIME ET DU GOLFE DU SAINT-LAURENT

Mémoire présenté

dans le cadre du programme de maîtrise en océanographie

en vue de l'obtention du grade de maître ès sciences

PAR

© ALYCIA BOISMENU

Octobre 2025

Composition du jury :

El Mahdi Bendif, président du jury, Institut des sciences de la mer, Université du Québec à Rimouski

Simon Bélanger, directeur de recherche, Université du Québec à Rimouski

Christian Nozais, codirecteur de recherche, Université du Québec à Rimouski

Michel Gosselin, codirecteur de recherche, Institut des sciences de la mer, Université du Québec à Rimouski

Emmanuel Devred, examinateur externe, Bedford Institute of Oceanography, Darmouth, Canada

Dépôt initial le 01 mai 2025 Dépôt final le 23 octobre 2025

REMERCIEMENTS

Je tiens tout d'abord à remercier Simon Bélanger, mon superviseur de recherche, pour m'avoir soutenu tout au long de mon parcours. Merci de m'avoir offert l'opportunité de participer à une campagne océanographique dans notre magnifique Saint-Laurent lorsque j'étais encore au baccalauréat. Cela a définitivement éveillé mon intérêt pour l'océanographie. Ensuite, merci de m'avoir permis de faire partie de ce projet qui a été très formateur pour moi. Un énorme merci également à Michel Gosselin et Christian Nozais, mes deux co-directeurs de recherche, pour votre support constant et vos commentaires constructifs tout au long de cette maîtrise ! Merci à vous trois de m'avoir permis d'apprendre à vos côtés.

Je tiens également à remercier El Mahdi Bendif et Emmanuel Devred pour avoir accepté de faire partie du jury d'évaluation en tant que président du jury et membre externe, respectivement. Je remercie également Hongyan Xi de m'avoir fourni les coefficients et valeurs nécessaires pour me permettre d'appliquer l'algorithme EOF-SST à ma région d'étude.

Je remercie également les organismes qui ont financé ce projet, les campagnes de terrain ainsi que les déplacements pour aller présenter mes résultats dans des conférences : le Réseau Québec maritime, l'Agence spatiale canadienne et le regroupement stratégique Québec-Océan.

Merci à tous.tes mes collègues du laboratoire AQUATEL : Brigitte, Raphael, Soham, Daniela, Carlos, Josiane, Mayssa, Gabriella, Matthieu et Véronique. Merci pour vos précieux conseils tout au long de mon parcours! Merci également à Lauriane pour son aide durant la mission AlgaeWISE. Un grand merci à toutes les personnes qui m'ont aidé pour les analyses en laboratoire : Mélanie Simard et Caroline Fink-Mercier pour les analyses des pigments par

chromatographie liquide à haute performance, Claude Belzile pour les analyses de cytométrie en flux, Pascal Rioux pour les analyses de nutriments et Pascal Guillot pour le traitement des données CTD.

Finalement, merci à ma famille et mes ami.es qui m'ont permis de rire et de me changer les idées lorsque j'en avais besoin. Merci à mes colocs d'avoir écouté mes multiples pratiques de présentations orales comme si c'était la première fois. Merci Félix pour ton soutien, ton écoute et ta compréhension inégalée, au moment où tu traversais toi aussi ta propre aventure académique.

AVANT-PROPOS

Ce mémoire de maîtrise est organisé en trois sections principales. Il comprend tout d'abord une introduction générale exposant le contexte de l'étude ainsi que quelques notions nécessaires à sa compréhension, suivie d'un chapitre présentant les résultats sous forme d'un article scientifique. Il se termine par une conclusion générale qui fait la synthèse des travaux, met en lumière les limites de l'étude ainsi que les perspectives du projet. Au cours de mon parcours de maîtrise, les résultats ont été présenté sous forme d'affiche lors de deux congrès, soit :

Boismenu, A., Nozais, C., Gosselin, M. et Bélanger, S. (2024) Télédétection des assemblages phytoplanctoniques dans l'estuaire maritime et le golfe du Saint-Laurent. Réunion scientifique annuelle de Québec-Océan, Rivière-du-Loup, Canada, 6 – 7 février 2024 (Affiche).

Boismenu, A., Nozais, C., Gosselin, M., Mukherjee, S. et Bélanger, S. (2024) Assessment of phytoplankton communities from ocean color in the St. Lawrence Lower Estuary and Gulf. 45th Canadian Symposium on Remote Sensing, Halifax, Canada, 10 – 13 juin 2024 (Affiche).

RÉSUMÉ

Le phytoplancton joue un rôle fondamental dans la fixation du carbone et en tant que producteur primaire à la base des réseaux trophiques dans les écosystèmes marins. Dans un contexte de changements climatiques et de pressions anthropiques, comprendre sa dynamique spatio-temporelle est crucial. Ce mémoire de maîtrise répond au besoin de mieux caractériser les communautés phytoplanctoniques et les propriétés optiques de l'estuaire maritime et du golfe du Saint-Laurent (EGSL), un système côtier complexe et productif. Il vise également à évaluer la performance d'algorithmes de télédétection des types fonctionnels de phytoplancton (PFTs), conçus principalement pour les océans ouverts, mais souvent inadaptés aux eaux côtières complexes comme celles de l'EGSL. Pour atteindre ces objectifs, deux campagnes océanographiques ont été réalisées durant les étés 2021 et 2022. Des échantillons d'eau ont été prélevés pour des analyses pigmentaires par chromatographie liquide à haute performance (HPLC) et pour des analyses de cytométrie en flux permettant d'identifier la distribution des classes de taille. Des mesures des propriétés optiques intrinsèques (absorption particulaire et absorption de la matière organique dissoute colorée) et apparentes (réflectance de la surface de l'eau) ont également été réalisées. Une classification hiérarchique sur composantes principales a permis d'identifier cinq communautés phytoplanctoniques distinctes, montrant une forte variabilité spatiale entre l'estuaire et le golfe. Selon une analyse de pigments diagnostiques, les diatomées dominaient la plupart des groupes, surtout dans l'estuaire et à l'ouest de l'île d'Anticosti. Les haptophytes étaient plus abondants dans le golfe et autour de l'île d'Anticosti, les prokaryotes dans les eaux libres du golfe, et les algues vertes à l'est de l'île d'Anticosti. L'analyse des propriétés optiques a révélé que l'absorption de la lumière aux courtes longueurs d'onde était majoritairement due à la matière organique dissoute colorée, caractéristique des eaux de type Cas 2. L'étude des spectres de réflectance a permis d'identifier quatre types optiques d'eau, bien que leur correspondance avec les communautés phytoplanctoniques soit restée limitée. L'évaluation de l'algorithme opérationnel du *Copernicus Marine Service* pour les PFTs (Xi et al., 2021) a montré une faible performance dans l'EGSL, soulignant l'importance d'adapter les algorithmes aux spécificités optiques régionales. Cette étude met ainsi en évidence la diversité des communautés phytoplanctoniques, l'influence majeure de la matière organique dissoute colorée sur les propriétés optiques ainsi que la nécessité de développer des outils de télédétection mieux calibrés pour les environnements côtiers complexes et pour pallier les limites des méthodes utilisées.

Mots clés : phytoplancton, pigments, propriétés optiques, Saint-Laurent, télédétection

ABSTRACT

Phytoplankton play a fundamental role in carbon fixation and as primary producers at the base of the food webs in marine ecosystems. In a context of climate change and anthropogenic pressures, understanding their spatio-temporal dynamics is crucial. This master's thesis responds to the need to better characterize phytoplankton communities and optical properties of the Lower Estuary and Gulf of St. Lawrence (EGSL), a complex and productive coastal system. It also aims to evaluate the performance of phytoplankton functional types (PFTs) remote sensing algorithms, designed primarily for open oceans, but often unsuited to complex coastal waters such as those of the EGSL. To achieve these objectives, two oceanographic campaigns were carried out during the summers of 2021 and 2022. Water samples were collected for pigment analysis by high-performance liquid chromatography and for flow cytometry analysis to assess size class distribution. Measurements of inherent (particle absorption and colored dissolved organic matter absorption) and apparent optical properties (water surface reflectance) were also carried out. A hierarchical clustering on principal components identified five distinct phytoplankton communities, showing strong spatial variability between the estuary and the gulf. According to a diagnostic pigment analysis, diatoms dominated most groups, especially in the estuary and to the west of Anticosti Island. Haptophytes were more abundant in the gulf and around Anticosti Island, prokaryotes in the open waters of the gulf, and green algae in the eastern part of Anticosti Island. Analysis of optical properties revealed that light absorption at short wavelengths was predominantly due to colored dissolved organic matter, characteristic of Case 2 waters. The study of reflectance spectra identified four optical water types, although their correspondence with phytoplankton communities remained limited. The evaluation of the Copernicus Marine Service algorithm for PFTs (Xi et al., 2021) showed poor performance in the EGSL, underlining the importance of adapting algorithms to regional optical specificities. This study thus highlights the diversity of phytoplankton communities, the strong influence of colored dissolved organic matter on optical properties and the need to develop better-calibrated remote sensing tools for complex coastal environments and to overcome the limitations of existing methods.

Keywords: phytoplankton, pigments, optical properties, St. Lawrence, remote sensing

TABLE DES MATIÈRES

LISTE DES TABLEAUX

LISTE DES FIGURES

LISTE DES ABRÉVIATIONS, DES SIGLES ET DES ACRONYMES

$a_{cdom}(\lambda)$	Colored dissolved organic matter absorption coefficient
$a_{nap}(\lambda))$	Non-algal particle absorption coefficient
$a_{p}(\lambda)$	Total particle absorption coefficient
$a_{ph}(\lambda)$	Phytoplankton absorption coefficient
$a^*_{ph}(\lambda)$	Chl *a*-specific absorption coefficient
Allo	Alloxanthin
But-fuco	19'-butanoyloxyfucoxanthin
CDOM	Colored dissolved organic matter (Matière organique dissoute colorée)
Chl *a*	Chlorophyll *a* (Chlorophylle *a*)
Chl a_{Fluo}	Chlorophyll *a* obtained from fluorometry
Chl *b*	Chlorophyll *b*
Chl c_1	Chlorophyll c_1
Chl c_2	Chlorophyll c_2
Chl c_3	Chlorophyll c_3
Chlide *a*	Chlorophyllide *a*
CMEMS	Copernicus Marine Environment Monitoring Service
C-neo	9'-cis-neoxanthin

C-OPS	Compact optical profiling system
Croco	Crocoxanthin
Diadino	Diadinoxanthin
Diato	Diatoxanthin
DMSP	Dimethylsufoniopropionate
DPA	Diagnostic pigment analysis (Analyse par pigment diagnostique)
EGSL	Lower Estuary and Gulf of St. Lawrence (Estuaire maritime et golfe du Saint-Laurent)
Fuco	Fucoxanthin
GSL	Gulf of St. Lawrence
HCPC	Hierarchical clustering on principal component
Hex-fuco	19'hexanoyloxyfucoxanthin
HPLC	High performance liquid chromatography (Chromatographie liquide à haute performance)
LSLE	Lower St. Lawrence Estuary
Lut	Lutein
MgDVP	Magnesium 2,4-divinylpheoporphyrin a_5 monomethyl ester
Nano-PC	Nanophycocyanin
Nano-PE	Nanophycoerythrin
OWT	Optical water types (Type optique d'eau)

PAR	Photosynthetically active radiation (Rayonnement solaire photosynthétiquement actif)
PFT	Phytoplankton functional type (Type fonctionnel de phytoplancton)
Peri	Peridinin
Phe *a*	Pheophytin *a*
Pheide *a*	Pheophorbide *a*
Pico-PC	Picophycocyanin
Pico-PE	Picophycoerythrin
PSC	Phytoplankton size classes (Classes de taille du phytoplancton)
PSD	Particle size distribution (Distribution des tailles de particules)
PTC	Phytoplankton taxonomic composition (Composition taxonomique du phytoplancton)
Pras	Prasinoxanthin
QWIP	Quality water index polynomial
$\boldsymbol{R_{rs}}$	Remote sensing reflectance
SAM	Spectral angle mapper
SCM	Subsurface chlorophyll fluorescence maximum depth
TChl $\boldsymbol{a}_{\mathbf{DPA}}$	Total chlorophyll *a* obtained from diagnostic pigment analysis
TChl *a*	Total chlorophyll *a* obtained from high performance liquid chromatography
TChl *b*	Total chlorophyll *b* obtained from high performance liquid chromatography

Viola	Violaxanthin
Zea	Zeaxanthin
βƐ-car	β,Ɛ-carotene
ββ-car	β,β-carotene

INTRODUCTION GÉNÉRALE

MISE EN CONTEXTE ET PROBLÉMATIQUE

Les changements climatiques qui se produisent depuis maintenant plusieurs décennies exercent un impact notable sur les océans (Garcia-Soto et al., 2021). L'estuaire maritime et le golfe du Saint-Laurent (EGSL) ne font pas exception à la règle. En effet, l'EGSL est confronté à des changements tels que la diminution de la concentration en oxygène dissous de ses eaux de fond (Gilbert et al., 2005; Jutras et al., 2020), l'augmentation de la température des eaux de surface (Galbraith et al., 2023, 2024), la réduction de l'étendue et de la durée du couvert de glace (Galbraith et al., 2023) ainsi que des changements dans la stratification de la colonne d'eau (Lavoie et al., 2020). Outre les changements climatiques, le Saint-Laurent est également confronté à d'autres perturbations telles que : (1) l'augmentation du transport maritime qui engendre une pollution acoustique et accroît le risque d'introduction d'espèces envahissantes ou toxiques dans les écosystèmes lors du déballastage (Simard et al., 2010; Dhifallah et al., 2022), et (2) l'intensification des activités anthropiques le long de ses rives, qu'il s'agisse d'activités industrielles ou agricoles, modifiant les apports de matière organique, de polluants et de nutriments (Hudon et al., 2017; Paradis-Hautcoeur et al., 2023).

Le système estuarien du Saint-Laurent est divisé en trois sections de l'amont vers l'aval, soit l'estuaire moyen (de la pointe Est de l'Île d'Orléans à Tadoussac), l'estuaire maritime (de Tadoussac à Pointe-des-Monts) et finalement le golfe qui se jette dans l'océan Atlantique. L'estuaire du Saint-Laurent est l'un des plus vastes au monde (El-Sabh & Silverberg, 1990) et présente un schéma de circulation complexe, notamment en raison de ses dimensions importantes, des marées et de sa topographie complexe (Figure 1). Le golfe du Saint-Laurent est quant à lui considéré comme étant une mer semi-enclavée, avec le détroit de Cabot et le détroit de Belle Isle comme ouverture vers l'océan Atlantique. Divers

phénomènes océanographiques, tels que des remontées d'eau froide, des gyres et des zones de mélange, y sont retrouvés. Cet environnement côtier dynamique est influencé notamment par les vents, les marées, les apports fluviaux et la présence de glace en hiver, induisant d'importantes variations spatiales et temporelles dans ses caractéristiques biogéochimiques.

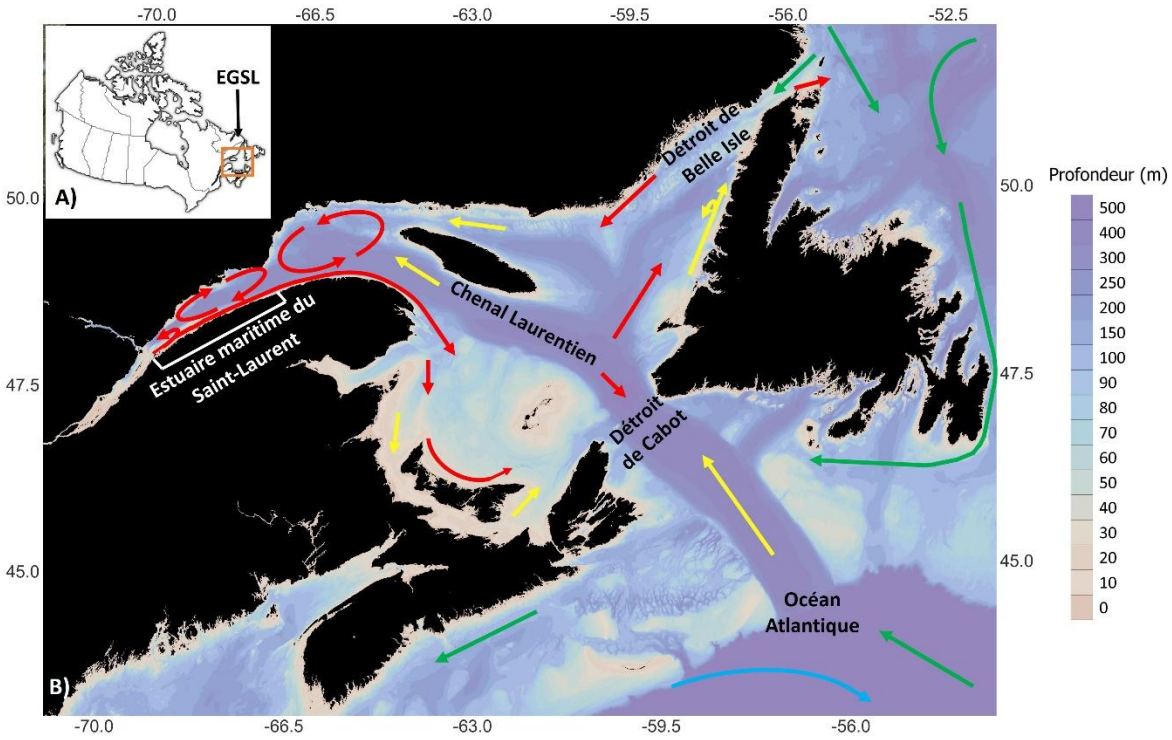

Figure 1. (A) Localisation de l'EGSL par rapport au Canada. (B) Carte représentant les principaux schémas de circulation des eaux de surface (en rouge) et des masses d'eaux profondes (en jaune) dans l'EGSL, qui sont une combinaison du courant du Labrador (en vert) et du Gulf Stream (en bleu). Les données bathymétriques proviennent de GEBCO (2024). Carte modifiée de Sharpe et al. (2023)

Les milieux côtiers océaniques comme l'EGSL sont des environnements actifs où une forte production primaire est observée. Les producteurs primaires, principalement le phytoplancton, sont des contributeurs majeurs à la fixation du carbone inorganique dissous par photosynthèse dans les milieux marins, participant ainsi à la pompe biologique en séquestrant le CO_2 atmosphérique dans les sédiments marins (Volk & Hoffer, 1985; Basu & Mackey, 2018). L'efficacité de la séquestration du carbone dépend de plusieurs facteurs comme la concentration de biomasse produite, la composition taxonomique des producteurs

primaires, la composition biochimique et la structure de taille des organismes phytoplanctoniques, ainsi que du recyclage de cette matière organique par les réseaux trophiques pélagiques. Par exemple, une grosse cellule à masse volumique élevée, comme une diatomée dont la paroi cellulaire est composée de silice, coule rapidement au fond de l'eau, ce qui réduit ses chances d'être reminéralisée par les bactéries à la surface ou broutée par le zooplancton, et facilite ainsi l'exportation du carbone vers les fonds marins sous forme de cellule entière (Bopp et al., 2005).

La répartition spatio-temporelle des communautés phytoplanctoniques, c.-à-d. une association de plusieurs espèces ou de groupes d'espèce de phytoplancton (Lalli & Parsons, 2002), dépend de facteurs abiotiques et biotiques, comme la disponibilité en lumière, la turbulence, les apports en nutriments et leur composition relative (stœchiométrie), la salinité, la température ainsi que la pression du broutage (Levasseur et al., 1984, 1992; Le Fouest et al., 2005; Cloern et al., 2014). En affectant ces facteurs, les changements climatiques pourraient entraîner des conséquences importantes sur la production, la biomasse et la composition taxonomique des différentes communautés de phytoplancton (Winder & Sommer, 2012; Barton et al., 2016).

Les organismes phytoplanctoniques présentent une grande diversité d'espèces (Bérard-Therriault et al., 1999) avec des tailles variables et des rôles écologiques distincts (Nair et al., 2008; IOCCG, 2014; Hillebrand et al., 2022). Au-delà de la diversité taxonomique, d'autres caractéristiques peuvent être utilisées pour les distinguer. Les types fonctionnels de phytoplancton (PFTs) peuvent être classés sur la base de critères tels que la taille (Hillebrand et al., 2022), les caractéristiques optiques (Bracher et al., 2017) ou bien sur le fait qu'ils remplissent des fonctions biogéochimiques similaires au sein de l'écosystème (Le Quéré et al., 2005; Nair et al., 2008; IOCCG, 2014). Parmi les principaux types fonctionnels, on retrouve :

- les silicificateurs (c.-à-d., le phytoplancton avec des parois cellulaires en silice : principalement les diatomées, mais aussi les chrysophytes, les silicoflagellés et les xanthophytes);

- les fixateurs d'azote (c.-à-d., le phytoplancton qui fixe l'azote moléculaire (N_2) : les cyanobactéries);

- les calcifiants (c.-à-d., le phytoplancton qui produit des coquilles de carbonate de calcium ou coccolithes : les coccolithophores, un groupe appartenant aux haptophytes);

- et les producteurs de diméthylsulfoniopropionate (DMSP), un précurseur du sulfure de diméthyle, un composé organique volatil (IOCCG, 2014) qui est particulièrement élevé chez les dinoflagellés et les haptophytes (Sunda et al., 2002).

Le type de classification adopté pour décrire les PFTs peut dépendre du niveau de précision souhaité, du type de recherche effectué et de l'objectif de celle-ci; il n'y a donc pas de manière universelle pour classifier ceux-ci (Reynolds et al., 2002).

Le phytoplancton, en tant que base de la chaîne trophique, constitue une source essentielle de matière organique pour les organismes marins, influençant ainsi la dynamique des populations aux niveaux trophiques supérieurs (Bryndum-Buchholz et al., 2020). L'industrie de la pêche intègre déjà certaines données phytoplanctoniques dans ses plans de gestion, notamment pour la surveillance des efflorescences de phytoplancton nuisibles ou bien seulement pour maintenir de bonnes pratiques de pêche (Cetinić et al., 2024). Le suivi de la répartition des principaux groupes de phytoplancton permet donc d'améliorer notre compréhension de leur rôle dans les écosystèmes (Bracher et al., 2017). Il constitue également un indicateur clé de la santé et de l'évolution des milieux marins.

LES MÉTHODES D'OBSERVATION DU PHYTOPLANCTON

Le suivi de la dynamique des communautés phytoplanctoniques pour étudier les réponses du système océanique aux changements climatiques est une avenue de recherche en plein essor. Plusieurs méthodes *in situ* existent pour l'observation et la caractérisation du phytoplancton, dont le volume des cellules peut varier de plus de neuf ordres de grandeur (de

0,1 à 1 × 10^8 μm^3; Marañón, 2015). Parmi ces méthodes, les plus communes incluent l'identification et le dénombrement des grosses cellules (>2 µm) par microscopie, l'analyse de la signature pigmentaire (approche chimiotaxonomique) ainsi que le dénombrement des cellules procaryotes et eucaryotes (0,2-20 µm) par cytométrie en flux. De plus, la télédétection optique (multispectrale ou hyperspectrale) est également une méthode utilisée depuis une vingtaine d'année. La concentration de la chlorophylle *a* (Chl *a*), couramment utilisée comme un proxy de la biomasse phytoplanctonique, est une mesure de base dont les résultats ont été rapporté à de nombreuses reprises dans l'EGSL, tant par des méthodes *in situ* (p. ex., Sinclair, 1978; Therriault & Levasseur, 1986; Roy et al., 1996; Bérard-Therriault et al., 1999; Blais et al., 2023a; Blais et al., 2023b) que par télédétection (p. ex., Fuentes-Yaco et al., 1997; Laliberté et al., 2018; Laliberté & Larouche, 2023).

Chacune de ces méthodes présente des avantages et des inconvénients (voir le Tableau 1), et leur utilisation dépend de l'objectif et du niveau de précision taxonomique recherché. Par exemple, pour la détection d'algues potentiellement nuisibles ou toxiques dans un milieu, où une grande précision taxonomique est nécessaire, l'identification des cellules phytoplanctoniques par microscopie optique est essentielle. En revanche, pour un suivi des changements des communautés phytoplanctoniques à l'échelle de l'EGSL au cours des dernières décennies, la télédétection par satellite est plus adaptée. Également, les méthodes ne permettent pas d'obtenir les mêmes informations. Par exemple, la cytométrie en flux et la microscopie optique permettent d'obtenir des résultats d'abondance (par exemple en nombre de cellules L^{-1}) tandis que les analyses pigmentaires et certains algorithmes de télédétection permettent d'obtenir des résultats de biomasses (par exemple en mg m^{-3}). Dans la majorité des cas, il est important de combiner plusieurs approches afin d'obtenir des résultats plus robustes (Kramer et al., 2024). Pour bien comprendre la portée de ce mémoire, les prochaines sous-sections mettront l'accent sur deux méthodes, soit la télédétection et l'analyse pigmentaire, qui seront spécifiquement utilisées dans le chapitre 1 du présent mémoire.

Tableau 1. Liste non exhaustive des caractéristiques (taille détectée, résolution taxonomique, avantages et limites) de quatre méthodes utilisées pour la caractérisation du phytoplancton. Tableau inspiré de Cetinić et al. (2024) et Kramer et al. (2024)

	Taille détectée (diamètre de la cellule)	**Résolution taxonomique**	**Avantage**	**Limite**
Microscopie optique	10-200 µm	Espèces	Une grande précision taxonomique	Difficulté à identifier les cellules de petite taille; travail laborieux ultraspécialisé et couteux
Analyse des signatures pigmentaires	> 0,3 µm (ou 0,7 µm pour les filtres GF/F non-brulés)	Groupes	Facilement associable aux propriétés optiques; Grande base de données mondiale	Variations pigmentaires inter- et intra-groupes; Résolution taxonomique limitée
Cytométrie en flux	0,5-50 µm (dépend de l'instrument utilisé)	Pico- et nano-procaryotes (*Prochlorococcus* et *Synechococcus*) et eucaryotes	Dénombrement cellulaire	Résolution de taille limité
Télédétection	Dépend de l'algorithme utilisé	Dépend de l'algorithme utilisé	Bonne résolution spatiale et temporelle	Applicabilité plus difficile aux eaux côtières; méthodes indirectes (proxy); incertitudes non-négligeables

Observation du phytoplancton par télédétection satellitaire

C'est à bord du satellite Nimbus-7 que le premier capteur dédié à la surveillance des propriétés bio-optiques des océans, le capteur Coastal Zone Color Scanner (CZCS), a été lancé en 1978. Ce capteur expérimental avait pour objectif principal d'observer la couleur de l'eau, notamment dans les zones côtières (IOCCG, 2014). Or, l'expérience a montré que le capter CZCS était limité par sa résolution spectrale pour le suivi des zones côtières, et ainsi mieux adapté au suivi de l'océan ouvert (McClain, 2009). Par la suite, de nombreux autres satellites et capteurs dédiés à la détection de la couleur de l'eau ont été mis en orbite. Ils ont en commun la capacité de mesurer quotidiennement et avec grande précision les variations spectrales subtiles de la couleur de l'eau à plusieurs longueurs d'onde du visible et du proche infrarouge, mais ce avec une résolution spatiale relativement grossière (souvent de l'ordre du km). Parmi ceux-ci se trouvent, entre autres, le capteur SeaWIFS (Sea-viewing Wide Field-of-View Sensor; 1997-2010), le capteur MODIS (Moderate Resolution Imaging Spectroradiometer; 2002-présent) ainsi que le capteur MERIS (Medium Resolution Imaging Spectroradiometer; 2002-2012) (IOCCG, 2014). Plus récemment, l'Agence spatiale européenne a mis au point le capteur OLCI (Ocean and Land Colour Instrument) à bord du satellite Sentinel-3, qui avec une résolution spatiale de 300 mètres et une excellente résolution spectrale dans le visible et le PIR (21 bandes), est conçu pour le suivi biologique et optique des eaux côtières et océaniques. Plus récemment, en 2024, la NASA a lancé le satellite PACE (Plankton, Aerosol, Cloud, ocean Ecosystem), le premier instrument capable de fournir des données hyperspectrales sur la couleur de l'eau, c.-à-d. un spectre continu de réflectance allant de l'ultra-violet au proche infra-rouge.

La télédétection du phytoplancton fait ainsi partie depuis longtemps des axes de recherche océanographique prioritaires (Sathyendranath et al., 2001). Les caractéristiques du phytoplancton, telles que la taille des cellules et la composition pigmentaire, influencent l'absorption et la diffusion de la lumière, deux propriétés optiques qui déterminent la couleur de l'eau observable par télédétection. Au cours des deux dernières décennies, plusieurs algorithmes de télédétection ont été développés pour cartographier les PFTs à partir

d'observations spatiales de la couleur des océans. Parmi ces nombreux algorithmes, on retrouve, entre autres, ceux de Sathyendranath et al. (2004), Alvain et al. (2005, 2008), Kostadinov et al. (2009, 2010), Brewin et al. (2010), Devred et al. (2011), Hirata et al. (2011), Li et al. (2013), Roy et al. (2013), Bracher et al. (2015), ainsi que de Xi et al. (2020, 2021). La majorité de ces travaux a été réalisée dans les eaux océaniques ouvertes, où la couleur de l'eau est essentiellement déterminée par les propriétés du phytoplancton (eaux dites de Cas 1; Morel & Prieur, 1977).

Plusieurs approches existent pour le développement d'algorithmes de télédétection. Mouw et al. (2017) présentent une revue de la littérature sur quatre des principales approches utilisées, excluant les méthodes basées sur l'écologie, qui nécessitent des caractéristiques physiques et spatio-temporelles additionnelles (p. ex., Raitsos et al., 2008). La première approche, basée sur l'abondance, suppose qu'il existe un lien entre la concentration de Chl *a* et la structure de taille ou la composition du phytoplancton (p. ex., Uitz et al., 2006). Cette approche est simple à mettre en œuvre et utilise le signal dominant dans les données de réflectance, mais elle est sensible à la variabilité régionale, notamment celle des eaux du Cas 2 (Mouw et al., 2017). À noter que le terme abondance est utilisé ici afin de rester cohérent avec l'article de référence. Toutefois, il s'agit en réalité plutôt d'une mesure de biomasse, puisqu'elle est exprimée en concentration en Chl a et non en nombre de cellules. Deuxièmement, les algorithmes basés sur la luminance spectrale émergeant de l'eau classifient les PFTs en fonction de la forme ou de l'amplitude de la réflectance observée par satellite, parfois après normalisation (p. ex., Alvain et al., 2008). Leur avantage est qu'ils dépendent peu, voire pas du tout, de produits dérivés de la réflectance brute, réduisant ainsi les erreurs. Toutefois, ils ne permettent pas de distinguer de façon optimale deux PFTs ayant une réflectance similaire (Mouw et al., 2017). Troisièmement, les algorithmes basés sur l'absorption exploitent les caractéristiques spectrales de l'absorption par le phytoplancton (p. ex., Ciotti & Bricaud, 2006). La première étape consiste à estimer le spectre d'absorption du phytoplancton à l'aide une approche semi-analytique qui décompose le spectre de réflectance de l'eau en spectre d'absorption et de rétrodiffusion (propriétés optiques intrinsèques; IOPs). Ils ont l'avantage de pouvoir utiliser les IOPs plutôt que la chlorophylle

comme entrée, ce qui réduit l'incertitude initiale. Toutefois, ils sont sensibles à la variabilité physiologique et ont de la difficulté à distinguer des groupes aux signatures d'absorption similaires (Mouw et al., 2017), mais également à l'incertitudes des estimations des IOPs. Finalement, les algorithmes basés sur la diffusion s'appuient sur le coefficient de rétrodiffusion, dont la pente spectrale est liée à la taille des particules (p. ex., Kostadinov et al., 2009). Bien que moins fréquents dans la littérature, ils sont généralement moins sensibles à la variabilité physiologique, cependant la rétrodiffusion n'est pas exclusivement influencée par le phytoplancton, mais bien par toutes les particules dans l'eau (Mouw et al., 2017).

Tel que rapporté par Mouw et al., (2017), les différentes définitions de PFTs obtenues par les algorithmes les plus utilisés sont basées sur les classes de taille (PSC; *Phytoplankton size classes*), la composition taxonomique (PTC; *Phytoplankton taxonomic composition*) ou la distribution de taille de particules (PSD; *Particules size distribution*) (Figure 2). La classification PSC la plus courante permet de répartir le phytoplancton en trois groupes : picoplancton (0,2 à 2 µm), nanoplancton (2 à 20 µm), et microplancton (> 20 µm). Les PTC concernent les groupes taxonomiques présents, mais leurs résultats dépendent fortement de la qualité des données *in situ* utilisées pour la calibration. Les PSD décrivent la variabilité de taille de l'ensemble des particules, incluant le phytoplancton, les sédiments en suspension, etc. (Mouw et al., 2017).

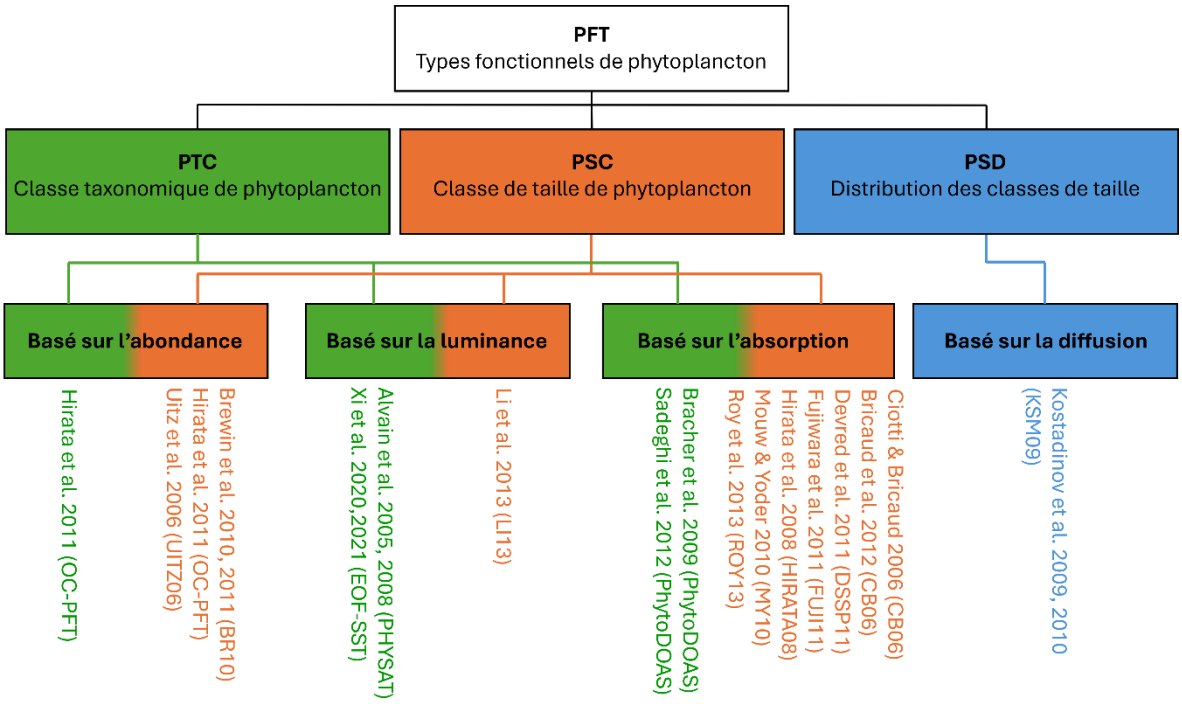

Figure 2. Schéma des différents algorithmes de PFTs regroupés selon leur classification de sortie (PTC, PSC ou PSD) et leur type de développement (basé sur l'abondance, la luminance, l'absorption ou la diffusion). L'abréviation inscrite à la suite des citations correspond au nom de l'algorithme. À noter que le terme abondance est utilisé ici afin de rester cohérent avec l'article de référence. Toutefois, il s'agit en réalité plutôt d'une mesure de biomasse, puisqu'elle est exprimée en concentration en Chl a et non en nombre de cellules. Figure modifiée de Mouw et al. (2017)

Depuis juillet 2020, le service *Copernicus Marine Environment Monitoring Service* (CMEMS) produit en temps quasi réel des cartes globales de la concentration en Chl *a* pour six groupes majeurs de PFTs : les diatomées, les haptophytes, les dinoflagellés, les algues vertes, les procaryotes et les *Prochlorococcus*. Ces estimations reposent sur l'algorithme développé par Xi et al. (2020, 2021) qui utilise les données de réflectance de l'eau obtenues à partir d'observations satellitaires ainsi que les mesures de température de surface. Cet algorithme repose sur une approche statistique basée notamment sur l'analyse des fonctions orthogonales empiriques. Les produits distribués par le CMEMS sont régulièrement mis à jour et couvrent la période allant de 1997 à aujourd'hui, tout en fournissant une estimation

globale de la répartition et de l'abondance des principaux PFTs dans l'océan mondial, avec une incertitude associée à chaque pixel (Figure 3 et 4).

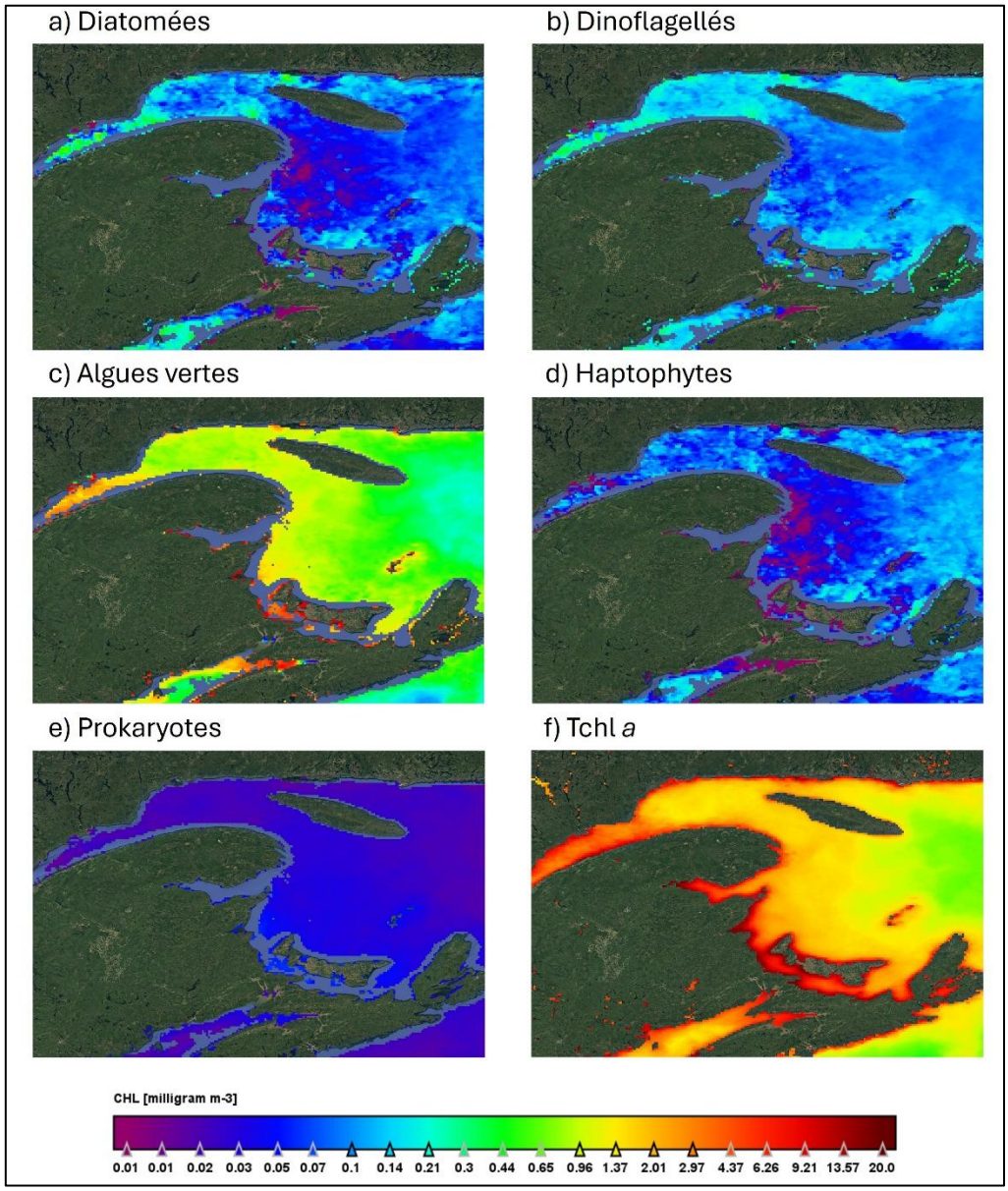

Figure 3 : Moyenne mensuelle des PFTs pour le mois d'août 2021 dans l'EGSL. Produits distribués par le CMEMS (utilisant l'algorithme de Xi et al. 2021). https://data.marine.copernicus.eu/product/OCEANCOLOUR_GLO_BGC_L4_MY_009_104/download.

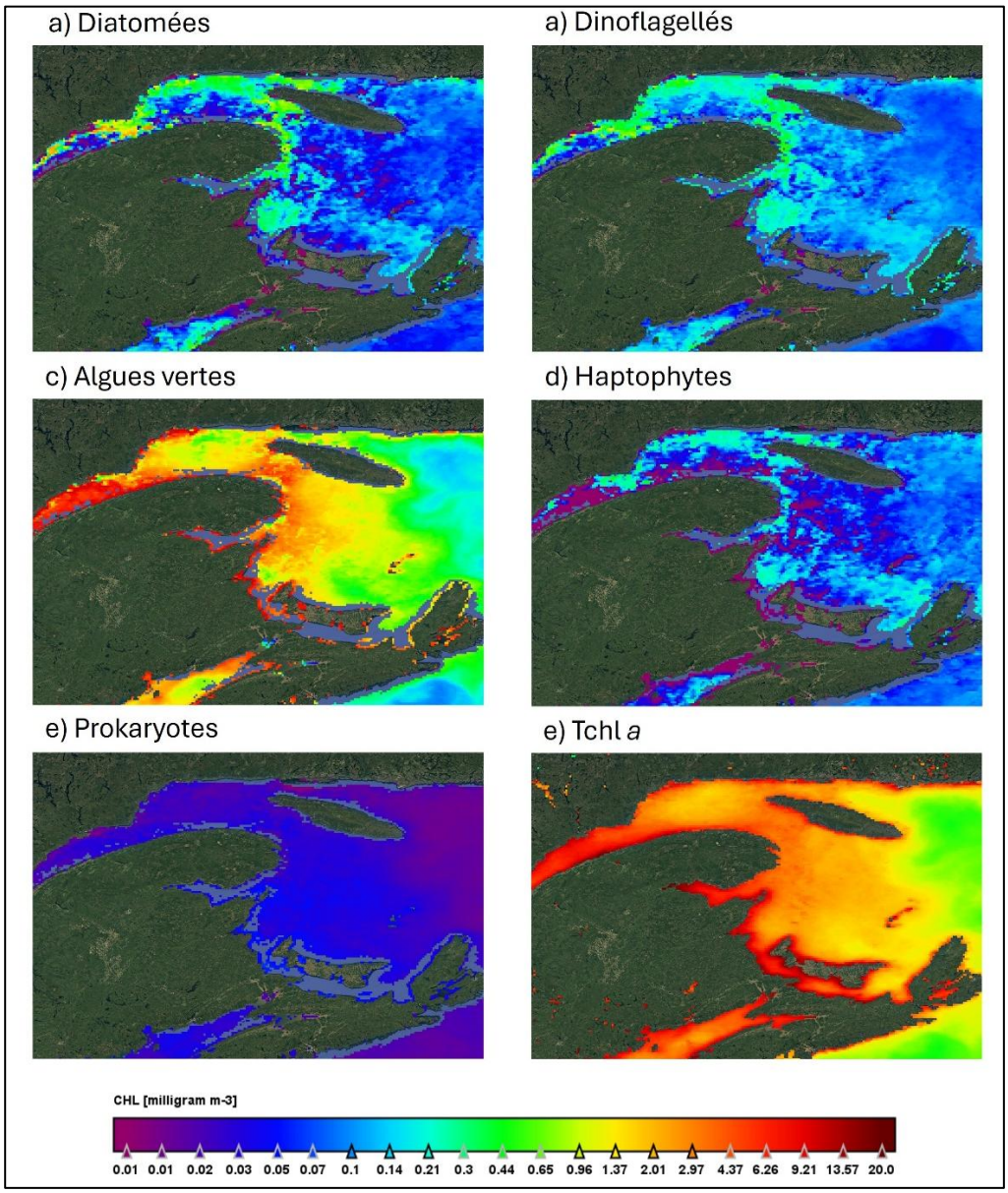

Figure 4 : Moyenne mensuelle des PFTs pour le mois de juillet 2022 dans l'EGSL. Produits distribués par le CMEMS (utilisant l'algorithme de Xi et al. 2021). https://data.marine.copernicus.eu/product/OCEANCOLOUR_GLO_BGC_L4_MY_009_104/download.

Cependant, les algorithmes, comme celui de Xi et al. (2020, 2021), reposent souvent sur des relations empiriques établies à partir d'observations à l'échelle globale. Ils peuvent donc être mal adaptés aux environnements côtiers, comme celui de l'EGSL, et conduire à

des résultats biaisés. Par exemple, sur les figures 3 et 4, on remarque une forte concentration d'algues vertes en surface, ce qui n'est pas nécessairement un résultat attendu pour cette zone d'étude durant les mois de juillet et août. En effet, les propriétés optiques des eaux océaniques dites de Cas 1 sont dominées principalement par l'absorption des molécules d'eau et du phytoplancton (Morel & Prieur, 1977). Dans ce cas, la télédétection permet d'établir un lien entre la signature spectrale et les PFTs présents (Johnsen et al., 2011). En revanche, les eaux de l'EGSL sont majoritairement classées comme des eaux de Cas 2 (Babin et al., 1993; Nieke et al., 1997; Bélanger et al., 2017), ce qui signifie qu'elles sont influencées non seulement par le phytoplancton, mais également par d'autres types de matières en suspension, telles que les sédiments en suspension et la matière organique dissoute colorée (CDOM) d'origine terrigène (Morel & Prieur, 1977). Dans ce type d'eau, tel qu'observé dans les eaux côtières de la côte nord de l'EGSL (Araújo et al., 2022), c'est la couleur de l'eau elle-même qui semble déterminer les communautés phytoplanctoniques et non l'inverse. En effet, la qualité spectrale de la lumière joue un rôle clé pour déterminer l'habitat et les niches écologiques du phytoplancton (Frenette et al. 2012; Hintz et al., 2021).

Sans cartographier précisément les différents PFTs, la Chl *a* a néanmoins été cartographiée à l'échelle de l'EGSL depuis plusieurs années. Fuentes-Yaco et al. (1997) ont été les premiers à cartographier la Chl *a* dans l'EGSL en utilisant des images du capteur CZCS. Par la suite, d'autres algorithmes ont été développés ou adaptés aux conditions de l'EGSL (p. ex., Jacques, 2001). Plus récemment, Laliberté et al. (2018) ont publié une carte climatologique de la concentration de Chl a dans l'EGSL produite à l'aide d'un algorithme régional, utilisant les fonctions orthogonales empiriques pour relier les valeurs de réflectances aux concentrations *in situ* de Chl a, appliqué aux données du capteur SeaWiFS. Quelques années plus tard, cet algorithme a été utilisé avec des données de plusieurs capteurs combinés (Laliberté & Larouche, 2023). Cette dernière étude a permis de mettre en évidence des concentrations de Chl *a* relativement élevées dans le courant de Gaspé, le long de la Côte-Nord du golfe, ainsi que dans les zones de fort brassage dû aux marées. D'importantes différences de phénologie du phytoplancton ont également observées entre entre les différentes sous-régions (estuaire maritime; nord, centre et sud du golfe), avec une tendance

générale à des floraisons printanières plus précoces et plus intenses. Enfin, Laliberté et Larouche (2023) rapportent une augmentation moyenne positive de la Chla de 1,1 % par an sur l'ensemble de l'écosystème du sud du golfe du Saint-Laurent, avec des tendances fortement positives dans les hauts-fonds madeliniens et à l'ouest de l'île d'Anticosti. De plus, depuis plusieurs années, le ministère des Pêches et des Océans utilise les outils de télédétection pour cartographier la Chl *a* dans ses rapports annuels sur l'état des composantes biologiques et chimiques de l'EGSL (p. ex., Blais et al., 2023a). Cependant, à notre connaissance, aucune étude n'a tenté de cartographier les PFTs à l'échelle de l'EGSL. Ce constat s'explique principalement par la rareté des observations *in situ* spécifiquement dédiées au développement ou à la validation d'algorithmes de télédétection pour les PFTs, mais également par le défi que représentent les eaux optiquement complexes de l'EGSL.

En résumé, la télédétection est un outil largement utilisé en raison de sa capacité à fournir une résolution spatiale et temporelle particulièrement pertinente pour cartographier les changements majeurs des PFTs au sein de nos écosystèmes. En effet, cette technique permet d'atteindre des résolutions spatiales inaccessibles par les techniques d'échantillonnage *in situ* traditionnelles. Toutefois, l'intégration de méthodes complémentaires reste indispensable pour valider les algorithmes de télédétection ou pour améliorer la précision taxonomique.

Observation du phytoplancton par approches pigmentaires

Les pigments sont synthétisés par les cellules phytoplanctoniques afin d'absorber le rayonnement solaire photosynthétiquement actif (PAR, 400-700 nm). Ceux-ci peuvent être utilisés comme biomarqueurs taxonomiques de certains types de phytoplancton (Roy et al., 1996; Vidussi et al., 1996). L'analyse en laboratoire des concentrations pigmentaires s'effectue à l'aide de la chromatographie liquide à haute performance (HPLC). L'application de cette technique permet une estimation précise de la Chl *a*, ainsi qu'une identification et une quantification d'environ 50 pigments chlorophylliens, caroténoïdes et pigments de dégradation du phytoplancton marin (Wright et al., 1991). Jeffrey (1961) fut l'un des

premiers à utiliser des méthodes de chromatographie pour la séparation des pigments du phytoplancton. L'un des avantages de cette méthode est sa large utilisation à l'échelle mondiale, ce qui permet un contrôle de qualité standardisé et l'accès à une vaste base de données disponible (Roy et al., 2011).

L'utilisation des pigments pour une analyse chimiotaxonomique, qui vise à classer les organismes en fonction de leur composition pigmentaire, est d'ailleurs une technique d'autant plus pertinente dans l'EGSL, car ce milieu est caractérisé par une forte abondance de cellules de petite taille (<5 μm; Roy et al., 1996). En effet, cette technique permet notamment d'analyser les cellules de très petite taille piégées sur des filtres d'une porosité de 0,7 μm. Roy et al. (1996) ont d'ailleurs été les premiers à utiliser cette technique dans l'EGSL. Outre son aspect taxonomique, l'analyse pigmentaire fournit également des informations sur l'état physiologique et les propriétés optiques des algues unicellulaires, comme leur acclimatation à la lumière (Demers et al., 1991; Bricaud et al., 2004).

Cependant, l'attribution des pigments à des groupes taxonomiques précis demeure complexe. En effet, la plupart des pigments ne sont pas spécifiquement associés à un seul groupe (Jeffrey et al., 2011; Roy et al., 2011; Kramer & Siegel, 2019). Ainsi, l'utilisation combinée de plusieurs pigments marqueurs, couplée à une bonne connaissance du milieu étudié, est essentielle. Par exemple, la fucoxanthine, habituellement associée aux diatomées, est aussi présente chez d'autres groupes tels que les haptophytes, les chrysophytes, les pélagophytes, les dinoflagellés, les dictyochophytes et les bolidophytes (Kramer et al., 2024). À l'inverse, les dinoflagellés peuvent être sous-estimés par leur pigment associé, car certaines espèces ne contiennent pas de péridinine ou en présentent des concentrations plus faibles (Brotas et al., 2022). Ces limitations doivent être prises en compte lors de l'interprétation des résultats. En revanche, les groupes phylogénétiquement proches partagent souvent des profils pigmentaires similaires (Falkowski et al., 2004). Par exemple, les algues rouges (diatomées, dinoflagellés et haptophytes) possèdent davantage de pigments en commun entre elles qu'avec d'autres groupes tels que les cyanobactéries ou les algues vertes (Kramer et al., 2018). Certains pigments sont néanmoins des marqueurs plus fiables, comme l'alloxanthine,

presqu'exclusivement associée aux cryptophytes, ou la chlorophylle *b* qui est un marqueur spécifique associé aux algues vertes (p. ex., les prasinophytes) (Roy et al., 2011). Malgré ces contraintes, notamment la faible précision dans l'identification des rangs taxonomiques spécifiques, cette approche permet de mettre en évidence les principales communautés phytoplanctoniques, offrant ainsi une complémentarité avec les informations obtenues par télédétection.

Plusieurs méthodes utilisent les signatures et concentrations pigmentaires afin de caractériser les PFTs. Parmi celles-ci figurent, entre autres, l'analyse de pigments diagnostiques (DPA; Claustre, 1994; Vidussi et al., 2001; Uitz et al., 2006; Devred et al., 2011; Hirata et al., 2011; Losa et al., 2017), l'analyse par regroupement hiérarchique et fonctions orthogonales empiriques (p. ex., Catlett & Siegel, 2018; Araújo et al., 2022) ou bien la méthode d'inversion matricielle CHEMTAX (CHEMical TAXonomy; p. ex., Mackey et al., 1996). Chacune de ces approches permet de fournir des informations complémentaires sur la composition des communautés phytoplanctoniques. La méthode CHEMTAX est une des méthodes les plus répandues en chimiotaxonomie (Hayward et al., 2023). Elle repose sur une factorisation matricielle qui estime la contribution relative des PFTs à la Chl *a* totale. L'analyse par regroupement hiérarchique regroupe les observations selon la similarité des profils pigmentaires, tandis que la DPA utilise des pigments spécifiques pour dériver la concentration en Chl *a* des PFTs (Kramer & Siegel, 2019).

Dans le cadre du chapitre 1 de ce mémoire, le terme PFTs sera utilisé puisque c'est celui qui est employé par les auteurs et autrices des méthodes utilisées. Cependant, l'analyse des signatures pigmentaires ou les méthodes de télédétection ne permettent pas nécessairement de classer le phytoplancton selon ses fonctions au sein de l'écosystème. Par exemple, chez les haptophytes — souvent considérés comme un groupe fonctionnel à part entière — on retrouve des organismes aussi variés que les coccolithophoridés, qui jouent un rôle de calcificateurs (IOCCG, 2014), ou les *Phaeocystis*, considérés comme des producteurs de DMSP (Schoemann et al., 2005), remplissant ainsi des fonctions écologiques différentes au sein de l'écosystème.

Enfin, l'analyse des concentrations pigmentaires est largement utilisée pour la validation des algorithmes de télédétection du phytoplancton. Les pigments influencent directement la forme spectrale de l'absorption de la lumière, et par conséquent, la réflectance, qui peut être mesurée par télédétection (Kramer & Siegel, 2019).

QUESTIONS DE RECHERCHE ET OBJECTIFS DE L'ÉTUDE

Cette étude s'inscrit dans le cadre du projet AlgaeWISE, financé par l'Agence spatiale canadienne, qui vise à démontrer le potentiel de l'imagerie hyperspectrale pour la détection et la quantification des algues marines, y compris le phytoplancton.

À la lumière de la revue de littérature, est-il possible de détecter les PFTs à partir d'observations satellitaires de la couleur de l'eau dans un système productifs comme celui de l'EGSL influencé par des apports terrigènes significatifs? Les assemblages phytoplanctoniques se retrouvent-ils dans des masses d'eau optiquement distinctes détectables par satellites ?

L'objectif général de ce projet de maîtrise est de caractériser spatialement les communautés phytoplanctoniques et leur environnement optique dans l'EGSL durant la période estivale. Cet objectif principal se décline en trois objectifs spécifiques :

- caractériser les communautés phytoplanctoniques présentes à l'aide des pigments et d'analyses de cytométrie en flux;
- analyser les relations entre les propriétés optiques apparentes et intrinsèques et le phytoplancton, et vice-versa;
- évaluer les performances de l'algorithme empirique opérationnel de Xi et al. (2020, 2021) appliqué à la région d'étude.

CHAPITRE 1
CHARACTERIZATION OF PHYTOPLANKTON COMMUNITIES AND OPTICAL PROPERTIES OF THE LOWER ESTUARY AND GULF OF ST. LAWRENCE

1.1 RÉSUMÉ

Étant donné le rôle essentiel du phytoplancton dans la fixation du carbone et de son importance dans les réseaux trophiques marins, il est nécessaire de surveiller sa variabilité spatio-temporelle dans un contexte de changements climatiques. Cette étude porte sur la caractérisation des communautés phytoplanctoniques et des propriétés optiques dans l'estuaire maritime et le golfe du Saint-Laurent (EGSL), un système marin côtier productif et complexe. Les principaux objectifs étaient de caractériser les communautés phytoplanctoniques de l'EGSL durant l'été à l'aide d'analyses pigmentaires (chromatographie liquide à haute performance; HPLC) et d'abondance cellulaire (cytométrie en flux), de caractériser leur environnement optique et d'évaluer la performance d'un algorithme opérationnel de télédétection des types fonctionnels de phytoplancton (PFTs) dans cette région. Deux campagnes océanographiques ont été menées durant les saisons estivales de 2021 et 2022, au cours desquelles des mesures radiométriques de la surface de l'eau ont été effectuées et des échantillons d'eau ont été récoltés. Les résultats ont révélé cinq communautés phytoplanctoniques, déterminées de manière statistique à l'aide de l'abondance des pigments et des cellules, présentant une forte variabilité spatiale au sein de l'EGSL. La fucoxanthine dominait dans la plupart des groupes, mais la contribution des autres pigments et l'abondance des classes de cellules variaient notablement entre l'estuaire et le golfe. L'analyse des propriétés optiques a démontré que l'absorption de la lumière dans les eaux de surface était principalement dominée par la matière organique dissoute colorée, caractéristique des eaux de type Cas 2. Bien que quatre types d'eaux optiques aient été

identifiés grâce à l'analyse de la réflectance, il s'est avéré difficile de lier directement ces types d'eaux optiques aux communautés phytoplanctoniques identifiées. En conséquence, l'application de l'algorithme de télédétection des PFTs de Xi et al. (2021) a montré une faible concordance avec les données *in situ* obtenues de l'analyse de pigments diagnostiques, suggérant que les coefficients de cet algorithme global ne sont pas adaptés aux eaux optiquement complexes de l'EGSL. Cette étude souligne la nécessité d'ajuster les algorithmes de télédétection à l'échelle régionale pour une estimation plus précise des PFTs dans les environnements côtiers comme l'EGSL.

1.2 ABSTRACT

Given the essential role of phytoplankton in carbon fixation and their importance in marine food webs, it is necessary to monitor their spatio-temporal variability in the context of climate change. This study focuses on the characterization of phytoplankton communities and optical properties in the Lower Estuary and Gulf of St. Lawrence (EGSL), a productive and complex coastal marine system. The main objectives were to characterize the phytoplankton communities of the EGSL during summer using pigment analyses (High performance liquid chromatography) and cell abundance (flow cytometry), to characterize their optical environment and to evaluate the performance of an operational algorithm for remote sensing of phytoplankton functional types (PFTs) in this region. Two oceanographic campaigns were carried out during the summer seasons of 2021 and 2022, during which radiometric measurements of the water surface were made and water samples were collected. The results revealed five phytoplankton communities, statistically determined using pigment and cell abundance, exhibiting high spatial variability within the EGSL. A dominance of fucoxanthin was observed in most groups, but with notable differences in the contribution of other pigments and in the abundance of cell classes between the estuary and the gulf. The analysis of optical properties showed that light absorption in surface waters was due to colored dissolved organic matter, characteristic of Case 2 waters. Although four optical water types were identified through hyperspectral reflectance analysis, it proved difficult to directly link these optical water types to the identified phytoplankton communities. As a result, the application of the PFTs remote sensing algorithm of Xi et al. (2021) showed poor agreement with *in situ* data obtained from diagnostic pigment analysis, suggesting that the coefficients of this global algorithm are not suitable for the optically complex waters of the EGSL. This study highlights the need to adjust remote sensing algorithms at a regional scale for more accurate estimation of PFTs in coastal environments such as the EGSL.

1.3 INTRODUCTION

Phytoplankton are major contributors to the fixation of dissolved inorganic carbon through photosynthesis in marine environments (Field et al., 1998; Häder & Gao, 2015), supporting most marine food webs through their basal position (Not et al., 2012). Due to their essential ecological role and the ability of satellite imagery to detect phytoplankton blooms, these primary producers serve as key indicators for monitoring the health of marine ecosystems. The distribution and composition of phytoplankton communities depend on both abiotic and biotic factors, e.g., salinity, temperature, light availability, vertical mixing, nutrient inputs and grazing (Levasseur et al., 1984, 1992; Le Fouest et al., 2005; Cloern et al., 2014). By altering these factors, climate change could significantly affect the spatio-temporal variation of different phytoplankton communities (Winder & Sommer, 2012; Barton et al., 2016; Mei et al., 2024). Therefore, characterizing these variations is essential for a better understanding of marine ecosystems.

Phytoplankton communities exhibit a great diversity of species (Bérard-Therriault et al., 1999), varying in traits and fulfilling different functions (Nair et al., 2008; IOCCG, 2014; Hillebrand et al., 2022). Beyond species diversity, they can be characterized according to their functions within marine ecosystems. This is how phytoplankton functional types (PFTs) are defined, which can be classified based on criteria such as size, shape, optical characteristics (Bracher et al., 2017) or directly on the fact that they perform similar biogeochemical functions within the ecosystem (Nair et al., 2008; IOCCG, 2014).

Compared to the open ocean, coastal zones are dynamic environments with higher nutrient concentrations due to tidal mixing, upwelling and terrigenous inputs, supporting significant primary production (Cloern et al., 2014). Pigment signatures, a proxy for different phytoplankton communities, were first measured in the Lower Estuary and Gulf of St. Lawrence (EGSL) by Roy et al. (1996). Since then, several studies have focused on these highly productive marine systems. A recent analysis of satellite data in the EGSL revealed an upward trend in chlorophyll *a* (Chl *a*) concentration, a proxy for phytoplankton biomass,

since 1998 (Laliberté & Larouche, 2023). Blais et al. (2023a) showed that smaller planktonic taxa (e.g., flagellates and ciliates) abundance has tended to increase in proportion in the Gulf of St. Lawrence (GSL) since 2014. However, there is limited knowledge about the structure and taxonomic composition of the communities and how they are specifically changing in response to the observed warming.

The EGSL is a large estuarine system (~226,000 km^2) in eastern Canada, and it includes the Laurentian Channel, an underwater valley 300-500 m deep extending from the Saguenay to the Atlantic Ocean. The GSL is a semi-enclosed sea with different biophysical subregions. The circulation of the EGSL is typically estuarine with three distinct layers. There is the surface layer, formed mainly by the freshwater inflow, flowing towards the ocean, the cold intermediate layer that occurs in winter (Galbraith, 2006) and the bottom layer of Atlantic origin that flows through the gulf and upstream of the estuary (Lauzier & Trites, 1958). The waters of the St. Lawrence are predominantly classified as Case 2 waters (Babin et al., 1993; Nieke et al., 1997), meaning their optical signature are influenced not only by phytoplankton but also by other optically active substances, such as suspended sediments and terrestrially-derived colored dissolved organic matter (CDOM) (Morel & Prieur, 1977). These optically complex waters make the remote sensing of phytoplankton biomass and PFTs more challenging (Craig et al., 2012; IOCCG, 2014; Mouw et al., 2017).

Several remote sensing algorithms for mapping PFTs based on observations of water reflectance spectra have been proposed over the last decades (Nair et al., 2008; Bracher et al., 2017; Mouw et al., 2017). Among these, the empirical algorithm of Xi et al. (2020, 2021) is now used operationally by the Copernicus Marine Environment Monitoring Service (CMEMS) since 2020 to estimate the Chl *a* concentration of six PFTs at the water surface on a global scale: diatoms, dinoflagellates, haptophytes, green algae, prokaryotes (i.e., cyanobacteria other than *Prochlorococcus*; e.g., *Synechococcus*) and *Prochlorococcus*. However, due to the empirical nature of the relationships derived from global observations, they are not necessarily suited for coastal waters such as those of the EGSL, yielding

inaccurate results. An assessment of the accuracy (or inaccuracy) for this operational algorithm is needed to inform the potential end-users of these satellite products.

Therefore, the first objective of this study is to characterize the phytoplankton communities and their optical properties of the EGSL. The second objective is to assess the performance of the PFTs algorithm of Xi et al. (2021) in the EGSL.

1.4 MATERIALS AND METHODS

1.4.1 Sampling

Water sampling and radiometric measurements were conducted during two cruises aboard the research vessel *Coriolis II*. The first campaign took place during the Odyssée oceanographic cruise from August 7 to 20, 2021, during which 37 stations were visited (see Table S1) along a transect of approximately 660 km extending from the entrance of the Lower St. Lawrence Estuary (LSLE), near the mouth of the Saguenay Fjord, to the center of the GSL (Figure 5). The second sampling took place during the AlgaeWISE oceanographic cruise from June 30 to July 7, 2022, when 38 stations were visited (Table S2) in the coastal waters of Anticosti Island in the GSL (Figure 5).

At each station, water samples were collected using a rosette sampler equipped 12 Niskin bottles (12 liters each) and a conductivity, temperature, depth (CTD) probe (Sea-Bird SBE911 plus) for salinity and temperature vertical profiles. The CTD-rosette also included an *in vivo* Chl *a* fluorometer (Wet Labs ECO-AFL/FL sensor and seapoint chlorophyll fluorometer). Water samples were collected at the surface (~1.5 m) and at the subsurface chlorophyll fluorescence maximum depth (SCM) during the Odyssée campaign, and at one to six depths in the euphotic zone (i.e., from the surface to a maximum of 50 m) during AlgaeWISE.

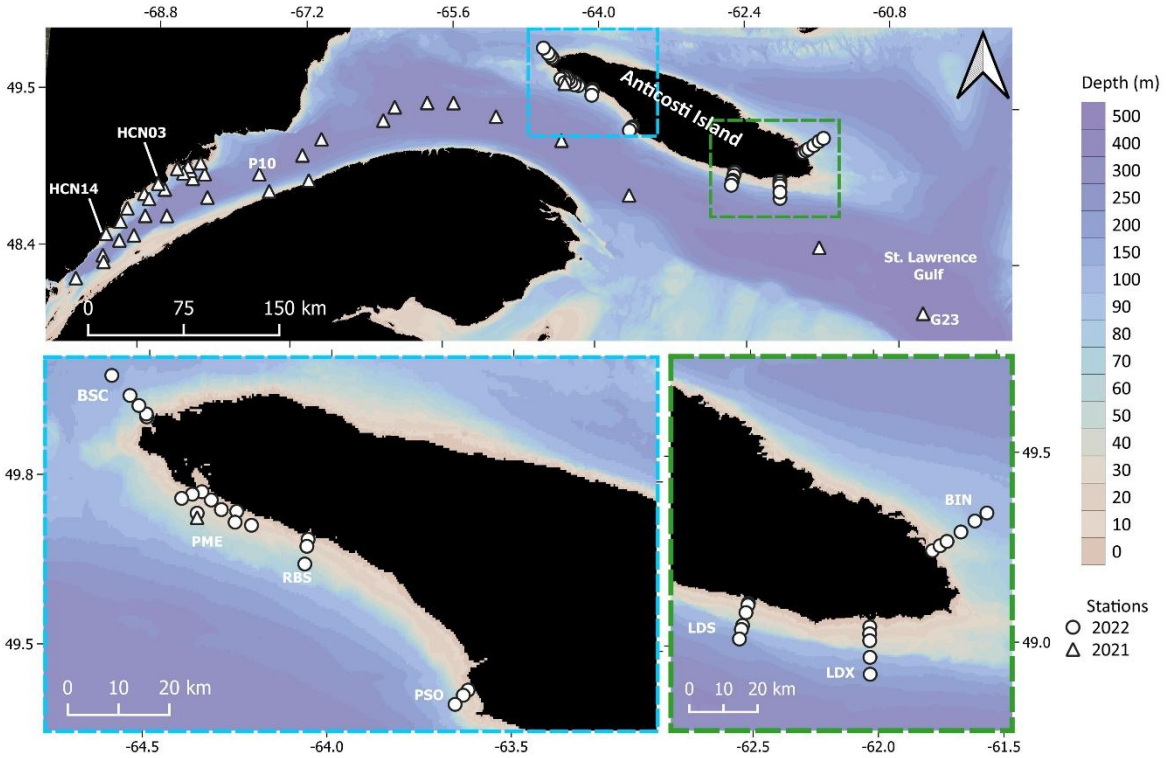

Figure 5. Maps of the EGSL showing sampling locations and bottom depths. Triangles represent stations visited during 2021 and circles represent stations visited during 2022. Bathymetry data are from GEBCO (2024). The names of four stations in the EGSL and seven transect lines surrounding Anticosti Island are shown on the maps.

1.4.2 Physical and biological variables

1.4.2.1 Sensor calibration from discrete samples

Salinity was measured on discrete water samples using a Portasal Salinometer 8410A (accuracy < ± 0.003 PSU). Chlorophyll *a* (Chl a_{Fluo}) concentration was determined onboard using the fluorometric method of Parsons et al. (1984). Briefly, water samples (between 0.2 and 1 L) were filtered through 25 mm glass microfiber filters (Whatman GF/F; 0.7 µm nominal pore size) and extracted in 90% acetone for 18 to 24 h in the dark at 4 °C. Fluorescence was then measured before and after acidification using a Turner Designs 10-AU fluorometer. Salinity and Chl a_{Fluo} concentration were used to calibrate the conductivity and *in vivo* fluorescence sensors, respectively.

1.4.2.2 Pigment concentrations

Water samples (about 2 L) were filtered through 47 mm Whatman GF/F filters to analyze pigment concentration using high-performance liquid chromatography (HPLC). After filtration, filters were immediately flash-frozen in liquid nitrogen and stored at -80 °C until analysis. In the laboratory, algal pigments were extracted in 95% methanol, sonicated and centrifuged. Extracts were filtered through a 0.22 µm polytetrafluoroethylene syringe filter and poured into an auto-sampler vial, which was gently sparged with argon to limit oxidation. Pigment concentration analysis was then carried out by reverse-phase HPLC using an Agilent Technologies 1200 series device according to the methods described in Zapata et al. (2000) and Bidigare et al. (2005). A known concentration of an internal standard, apo-carotene, was added to each sample before analysis to identify possible biases linked to manipulations and extraction. The concentration of 24 chlorophyll pigments and carotenoids were identified: chlorophyll c_1 (Chl c_1), chlorophyll c_2 (Chl c_2), chlorophyll c_3 (Chl c_3), chlorophyllide *a* (Chlide *a*), Magnesium 2,4-divinylpheoporphyrin a_5 monomethyl ester (MgDVP), peridinin (Peri), pheophorbide *a* (Pheide *a*), 19'-butanoyloxyfucoxanthin (But-fuco), fucoxanthin (Fuco), 9'-cis-neoxanthin (C-neo), prasinoxanthin (Pras), violaxanthin (Viola), 19'hexanoyloxyfucoxanthin (Hex-fuco), diadinoxanthin (Diadino), alloxanthin (Allo), diatoxanthin (Diato), zeaxanthin (Zea), lutein (Lut), crocoxanthin (Croco), chlorophyll *b*, pheophytin *a* (Phe *a*), β,Ɛ-carotene (βƐ-car) and β,β-carotene (ββ-car). Pheide *a* and Phe *a* are alteration products of Chl *a*, referred to as degradation pigments. In this study, the total chlorophyll *b* (TChl *b*) concentration obtained by HPLC includes chlorophyll *b* and its allomers and epimers. The total Chl *a* (TChl *a*) concentration obtained by HPLC is the sum of Chl *a*, its allomers and epimers, and Chlide *a*. Pigment concentrations below the detection limit of the device have been set to zero.

1.4.2.3 Flow cytometry

To determine the abundance of pico- (0.2 to 2 µm) and nanophytoplankton (2 to 20 µm) cells by flow cytometry, water samples were fixed with Grade I glutaraldehyde (Sigma)

to a final concentration of 0.1%, flash frozen in liquid nitrogen and then stored at -80 °C until laboratory analysis. The abundances of nano- and picophycoerythrin-containing cyanobacteria (nano-PE and pico-PE), nano- and picophycocyanin-containing cyanobacteria (nano-PC and pico-PC), and pico- and nanoeukaryotes were determined in duplicates using a CytoFLEX flow cytometer, as described in more detail by Araújo et al. (2022). Although the abundances of nano-PC and pico-PC remained low (below 100 cells/mL) for most stations, these size classes were still included in the analysis, as some stations exhibited considerable abundances, reaching ~4000 cells/mL for pico-PC and ~200 for nano-PC.

1.4.3 Particulate and colored dissolved organic matter absorption

To determine the spectral absorption coefficient of suspended particulate matter, water samples (between 0.2 and 0.7 L, depending on the area) were filtered onto 25 mm Whatman GF/F filters to retain the suspended particles. Filters were immediately stored in the dark at -80 °C until analysis. Total particle absorbance values were then measured using a Perkin Elmer lambda-850 dual-beam spectrophotometer equipped with a 150 mm integral sphere in which the filter was placed (Röttgers & Gehnke, 2012; IOCCG, 2018). Non-algal particle absorbance values were obtained after extracting the pigments from the filter with methanol (Kishino et al., 1985). Blank filters were subjected to the same steps in the laboratory. They were subsequently used as a reference and to assess if there was any contamination during the laboratory manipulations. The absorbance values of the samples were then subtracted from the absorbance of the blank (OD_f). The absorbance values were converted to total particle absorption coefficients, $a_p(\lambda)$, using this equation:

$$a_p(\lambda) = \ln(10) \cdot OD_f(\lambda) \cdot \frac{F_{area}}{V\beta} \quad (1)$$

where $OD_f(\lambda)$ is the measured absorbance (or optical density) of the sample filter corrected for the blank baseline, F_{area} (m^2) is the filtered clearance area of the particles and V (m^3) is the filtered volume, and β is the pathlength amplification factor calculated following Stramski et al. (2015). Next, phytoplankton absorption coefficient, $a_{ph}(\lambda)$, was determined by

subtracting the non-algal particle absorption coefficient ($a_{nap}(\lambda)$) from $a_p(\lambda)$. The Chl *a* specific absorption coefficient, $a^*_{ph}(\lambda)$, was then obtained by normalizing $a_{ph}(\lambda)$ to TChl *a*.

For CDOM analysis, water samples were filtered through polyethersulfone membrane filters (0.22 µm pore size) and then stored at 4 °C in the dark until analysis shortly after each cruise (within 3 weeks). Only surface water samples were analyzed for this parameter. In the laboratory, water samples were placed in 10 cm long quartz cuvettes inside the spectrophotometer. A cuvette with nanopure water was also put in the reference beam of the spectrophotometer, beside the filtered seawater sample. The absorbance values were converted into CDOM absorption coefficients, $a_{cdom}(\lambda)$, using this equation:

$$a_{cdom}(\lambda) = \frac{\ln(10) \cdot OD(\lambda)}{L} \quad (2)$$

where $OD(\lambda)$ is the absorbance (optical density) and L (m) is the length of the cuvette (i.e., 0.1 m). The *R* package used to obtain the particles and CDOM absorption values is available at https://github.com/belasi01/RspectroAbs (last access: 11 March 2024).

1.4.4 Water remote sensing reflectance

At each station visited during the sunlight hours of the 2021 cruise, a handheld spectroradiometer (type HR-12i from Spectra Vista Corporation; SVC) was used to produce above-water remote sensing reflectance (R_{rs}) spectra of the water surface. The spectral radiance of three targets was measured in a systematic sequence, namely that of a white spectralon plate (L_g; $W \cdot m^{-2} \cdot sr^{-1} \cdot nm^{-1}$), of the sky ($L_{sky}$; $W \cdot m^{-2} \cdot sr^{-1} \cdot nm^{-1}$), and of the water surface (L_t; $W \cdot m^{-2} \cdot sr^{-1} \cdot nm^{-1}$). The viewing geometry followed the recommendations of Mobley (1999), i.e., a viewing zenith angle (θ_v) around 40 degrees and an azimuthal difference between the solar and viewing direction ($\Delta\phi$) ranging between 90 and 135 degrees. Theses parameters were carefully documented. In 2022, radiometric measurements were carried out simultaneously using a HyperSAS system deployed at the bow of the Coriolis II, which included a downwelling irradiance measurement (E_d; $W \cdot m^{-2} \cdot nm^{-1}$), L_{sky} and L_t,

respectively. The *in situ* spectral remote sensing reflectance (R_{rs}; sr^{-1}) was calculated using the following equation:

$$R_{rs}(\lambda) = \frac{L_w(\lambda)}{E_d(\lambda)} = \frac{L_t(\lambda) - \rho_{sky} L_{sky}(\lambda)}{E_d(\lambda)} - \Delta \quad (3)$$

where L_w ($W \cdot m^{-2} \cdot sr^{-1} \cdot nm^{-1}$) is the water leaving radiance; E_d is the downwelling irradiance; ρ_{sky} is the air-water interface reflectance factor; and Δ is a correction factor. For the SVC measurements, E_d was calculated $as\ \pi \cdot L_g/\rho_g$, where ρ_g is the reflectance of the calibrated spectralon plate (i.e., 99.8%). The radiance data from the SVC were processed using an R package available on GitHub (https://github.com/belasi01/asdsvc/; last access: 5 June 2023), which applies the ρ_{sky} from Mobley (1999) and various methods to assess Δ were implemented (e.g., null near infrared reflectance residual; Ruddick et al., 2006; Kutser et al., 2013; Jiang et al., 2020). The Δ correction method was chosen for each spectrum as a function of environmental conditions (i.e., clear versus turbid water, dark CDOM-rich water; cloudy versus clear sky) and the *Quality water index polynomial* (QWIP; Dierssen et al., 2022) value. Similarly, HyperSAS data were processed using the R package *HyperocR* (https://github.com/belasi01/HyperocR; last access: 5 June 2023), which include a Δ correction based on independently measured R_{rs} made using in-water radiometric measurements obtained from a Compact optical profiling system (C-OPS; Biospherical). This correction method estimates Δ at two wavelengths in the ultraviolet and near infrared using measured in-water R_{rs} and interpolates the values to yield a spectrally dependent Δ.

To identify the similarities and differences between the different reflectance spectral shapes, the spectral angle mapper (SAM; rad) (Kruse et al., 1993) was used, following equation 4:

$$\mathrm{SAM} = cos^{-1}\left(\frac{\sum_{k=1}^{B} d_k i_k}{(\sum_{k=1}^{B} d_k^2)^{\frac{1}{2}} \cdot (\sum_{k=1}^{B} i_k^2)^{\frac{1}{2}}}\right) \quad (4)$$

where d and i are the spectra to compare, and B is the number of spectral bands.

1.4.5 Data analyses

The normality of the data was tested with the Shapiro-Wilk test with a significant threshold of 0.05. For non-parametric data, the Kruskal-Wallis test (one-way ANOVA by ranks) was used. Afterward, the Dunn test was used with the Bonferroni correction method. All statistical analyses were performed using the RStudio interface of the R programming software (version 4.3.0).

1.4.5.1 Hierarchical clustering on principal components

A hierarchical clustering of principal components (HCPC) was applied to cell-class abundance and pigment concentration data following the method of Araújo et al. (2022). First, pigment concentration data were normalized to TChl *a* concentration to remove the effect of biomass. Cell-class abundance and normalized pigment concentration data were then mean-centered and divided by their standard deviation to account for differences in units.

These normalized and standardized data were then subjected into a principal component analysis to reduce the dimensions from 28 variables (i.e., 22 normalized pigments from HPLC, plus the six cell-classes from cytometry) to a few components while retaining as much information as possible about the data. The first seven principal components, which cumulatively explained 71.04% of the variability, were selected for inclusion in the hierarchical clustering. The HCPC was performed using Ward's method.

Following the HCPC, five different groups of samples were obtained. These HCPC groups are made up of samples collected at the surface and other depths. Each group differs from the others in terms of pigment concentration and cell-class abundance. The cophenetic coefficient of the clustering tree is 0.84, which is similar to other studies (Araújo et al., 2022; Sun et al., 2022).

1.4.5.2 Diagnostic pigment analysis

Diagnostic pigment analysis (DPA) was applied to the pigment concentrations obtained by HPLC. The DPA method was first established by Vidussi et al. (2001) and subsequently adapted numerous times (e.g., Uitz et al., 2006; Hirata et al., 2011; Soppa et al., 2014; Brewin et al., 2015; Losa et al., 2017). This analysis links diagnostic pigments (DP) to specific phytoplankton types and was used to obtain Chl *a* concentration of PFTs for comparison with the algorithm results. The pigments used in this analysis are Fuco, Peri, Hex-fuco, But-fuco, Allo, TChl *b,* and Zea. The total Chl *a* concentration, estimated from the weighted sum of the diagnostic pigments (TChl a_{DPA}), is calculated with this equation:

$$TChla_{DPA} = \sum_{1}^{n} w_n \cdot DP_n \tag{5}$$

where w is the coefficient of each DP. The coefficients used to obtain the Chl *a* concentration of the five PFTs can be found in Table S1 of the Supplementary Materials of Losa et al. (2017). This specific DPA was chosen for consistency with the method adopted in Xi et al. (2021).

1.4.5.3 PFTs algorithm application

The remote sensing *EOF-SST* hybrid algorithm of Xi et al. (2020, 2021) was used to determine the Chl *a* concentration of six PFTs from our *in situ* R_{rs} dataset. The PFTs included diatoms, dinoflagellates, haptophytes, green algae, photosynthetic prokaryotes other than *Prochlorococcus,* and *Prochlorococcus*, as well as the total Chl *a* concentration. However, in this study, *Prochlorococcus* were excluded since they are not found in the study area. To apply the algorithm to the R_{rs} data, the hyperspectral reflectance spectra were first transformed into ten spectral bands (from 400 to 681 nm) using the Ocean and Land Colour Instrument (OLCI) relative spectral response (RSR) and then standardized by subtracting the mean spectral value and dividing by the spectral standard deviation. The regression coefficients used for the algorithm's application are from Xi et al. (2021), updated in August

2023 (H. Xi, personal communication; 07 December 2023). The sea surface temperature used in the algorithm equations was obtained from the CTD data.

1.4.5.4 Optical water types

The reflectance data were also classified into one of 21 inland and coastal optical water types (OWT) according to the classification and typology proposed by Spyrakos et al. (2018). Briefly, the data were first normalized to the area under the curve. Then, a SAM analysis (as described in section 1.4.4) was performed between the normalized R_{rs} data and the reflectance spectra of each OWT. The normalized Rrs spectra were associated with the OWT for which they had the lowest SAM value. Four different OWTs were observed in our study area.

1.5 RESULTS

1.5.1 Physico-chemical water conditions during sampling campaigns

The Odyssée sampling campaign included nearshore and offshore stations with bottom depths varying between 22 m at station HCN14 in the LSLE and 448 m at station G23 in the GSL (Figure 5). The warmest sea surface temperatures (SST) were recorded in the GSL, reaching up to 17.5°C (G26), while the coldest SST in the LSLE was as low as 4.4°C (HCN11). Surface salinity was lower upstream of the LSLE (~ 27), especially for the stations close to the coast, and gradually increased towards the GSL (~ 30) (Figure 6).

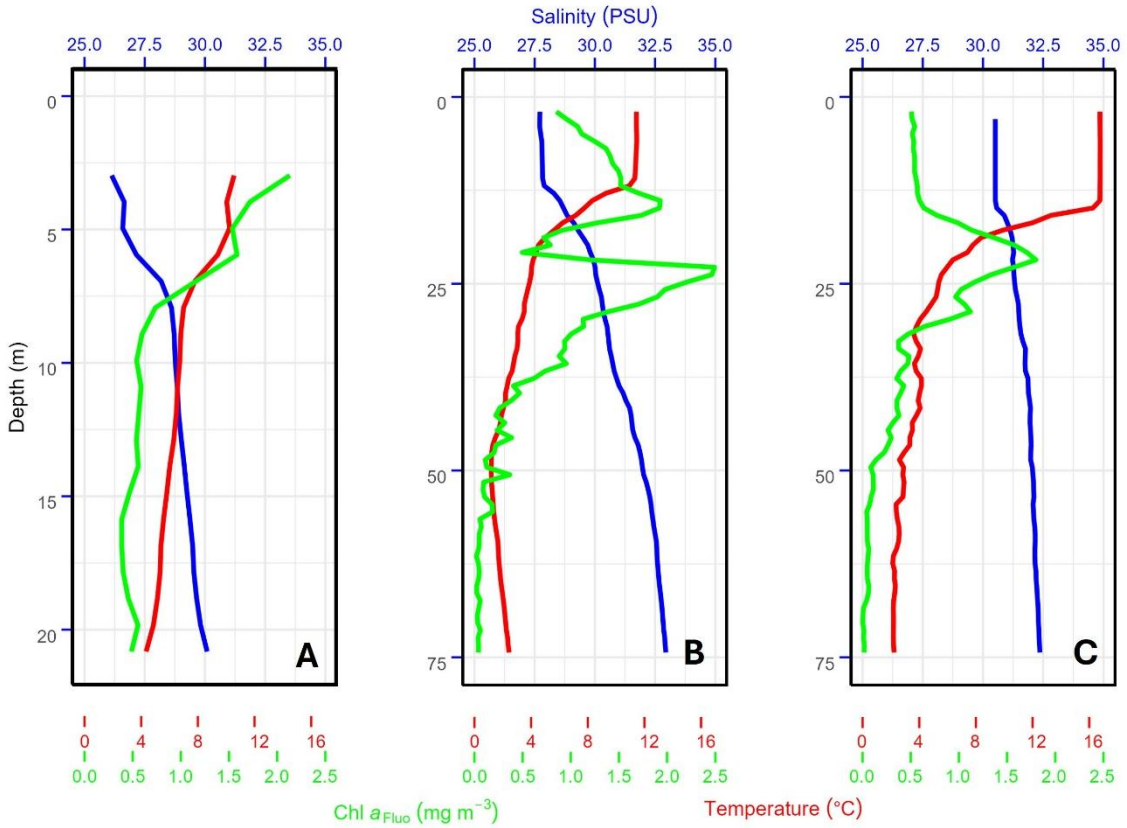

Figure 6. Salinity, water temperature and calibrated Chl *a* concentration profiles at stations (A) HCN03, (B) P10, and (C) G23 during the Odyssée sampling campaign in August, 2021 (see Fig. 1 for their locations). Stations are in order from upstream to downstream

Overall surface Chl a_{Fluo} concentrations from Odyssée ranged from 0.44 to 6.81 mg m^{-3} (with a median concentration of 1.27 mg m^{-3}). Stations in the LSLE generally had higher Chl a_{Fluo} concentrations than those in the GSL and around Anticosti Island, except for a few shallower stations on the north coast, which also had lower Chl a_{Fluo} concentrations. The stratification in the GSL was well established in August 2021 with a mixed layer depth (MLD) of ~15 m and a sub-surface chlorophyll-a maximum reaching 1.8 mg m^{-3} just below at 22 meters (Fig. 4c).

The AlgaeWISE sampling stations around Anticosti Island were organized into six transects perpendicular to the coast and one parallel to the coast (transect PME; Figure 5). The shallowest stations along these perpendicular transects ranged from 13 to 24 m, while

the deepest offshore stations reached up to 220 m. The coldest surface temperature (6.4°C) was recorded on the western side east of the island (Station RBS-01), while the warmest temperature (14.6°C) occurred on the eastern side (Station BIN-05). Surface Chl a_{Fluo} concentrations ranged from 0.26 to 3.20 mg m^{-3} (with a median concentration of 0.76 mg m^{-3}), with higher mean Chl a_{Fluo} concentrations on the western side (1.30 mg m^{-3}) than on the eastern side (0.55 mg m^{-3}). Figures 7 and 8 present CTD profiles taken at two transects at opposite ends of the island (see transect BIN and BSC in Figure 5).

The eastern transect presented surface salinity ranging from 29.1 (BIN-04) to 30.5 (BIN-06) and SST between 12.3°C (BIN-01) and 14.6°C (BIN-05). Interestingly, the shallow nearshore station had slightly higher salinity and lower SST than some of the offshore stations (Fig. 5). Surface salinity at stations in the western part of the island was slightly lower than in the eastern part, with mean values of 29.09 and 29.64, respectively. The MLD extended between ~15 to ~10 meters but often displaying multi-layer stratification with the first layer as thin as ~5 meters.

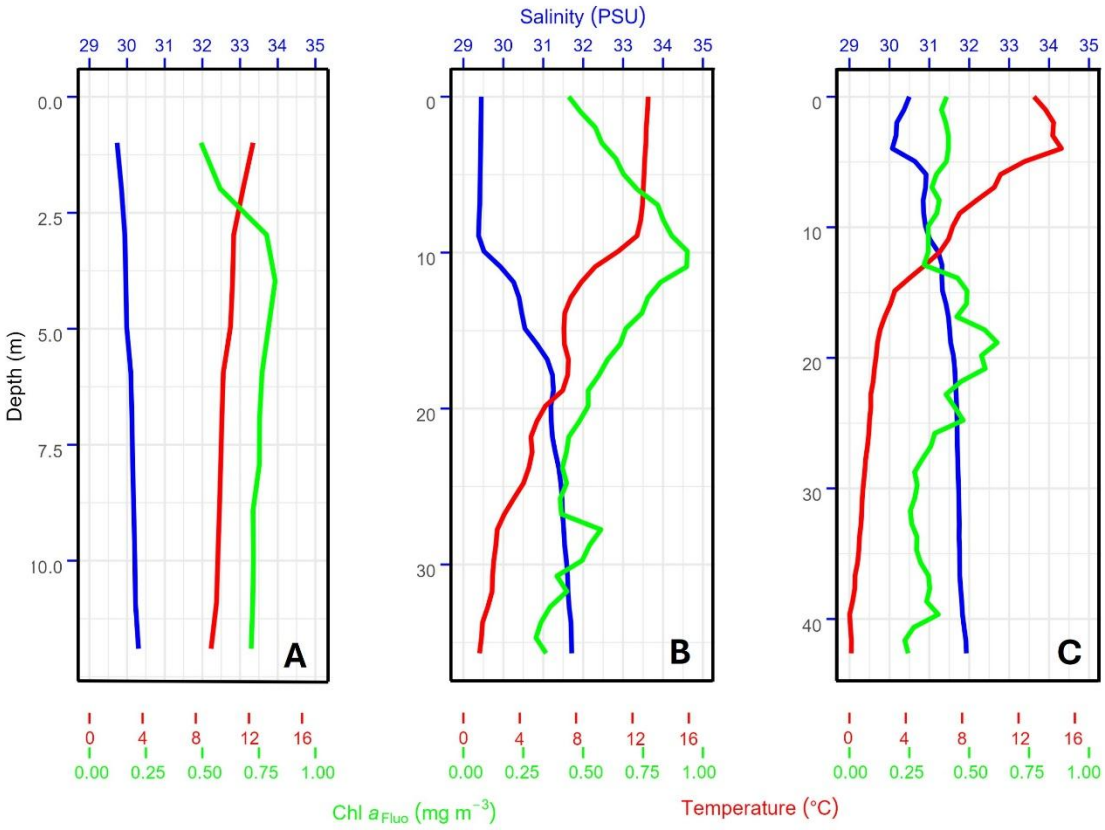

Figure 7. Salinity, water temperature and calibrated Chl *a* concentration profiles at stations (A) BIN-01, (B) BIN-03, and (C) BIN-06 along the transect on the eastern side of Anticosti Island on July 02, 2022 (see Fig.1 for the location of the transect). BIN-01 is the station closest to the coast while BIN-06 is the furthest offshore

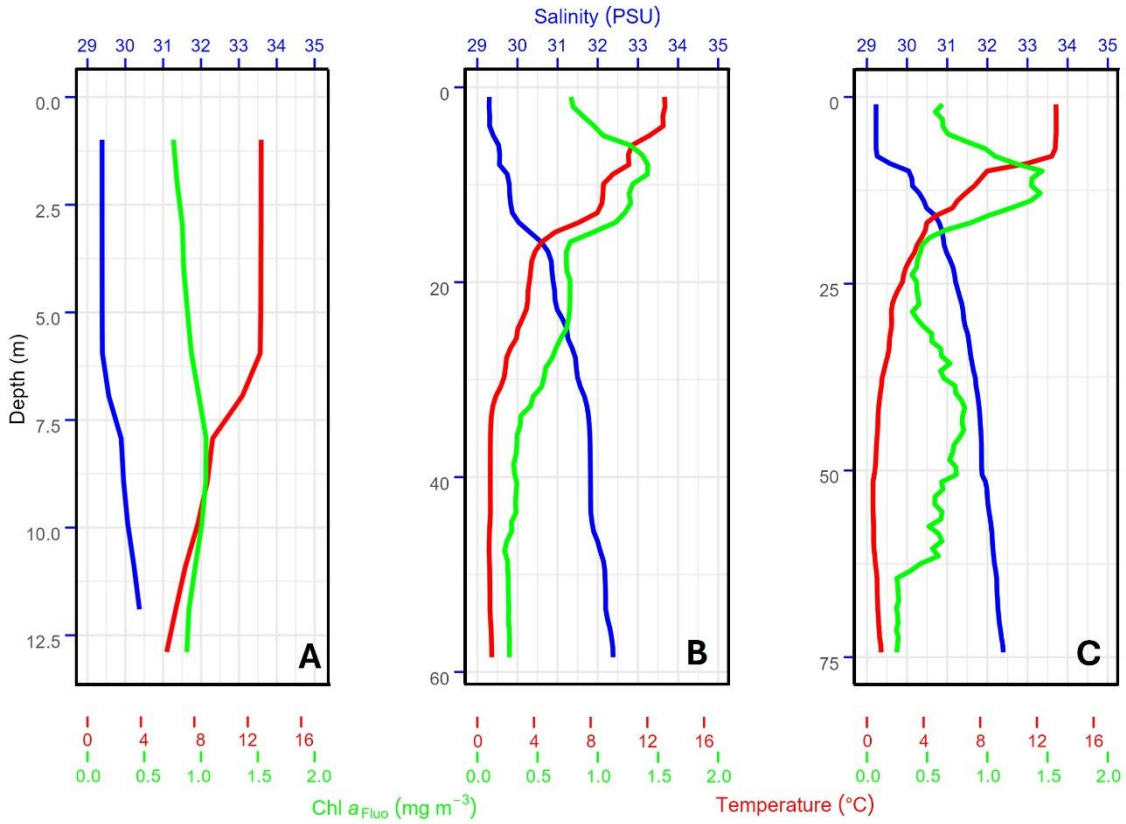

Figure 8. Salinity, water temperature and calibrated Chl *a* concentration profiles at stations (A) BSC-01 (B) BSC-03, and (C) BSC-05 along the transect on the western side of Anticosti Island on July 07, 2022 (see Fig.1 for the location of the transect). BCS-01 is the station closest to the coast while BSC-05 is the furthest offshore

SCM typically occurred between 4 and 12 m at shallower nearshore stations and between 11 and 30 m at the offshore stations. Figures 7 and 8 show the deepening of the SCM with increasing bottom depth along the transects.

1.5.2 Taxonomic composition of phytoplankton communities

1.5.2.1 Spatial distribution of groups identified by hierarchical clustering on principal components

The hierarchical clustering on principal components (HCPC) allowed the identification of five groups of samples differentiated by pigment concentration and cell class. Surface and

depth samples were included for this analysis. Figure 9 shows the spatial distribution of the five HCPC groups for the surface water samples.

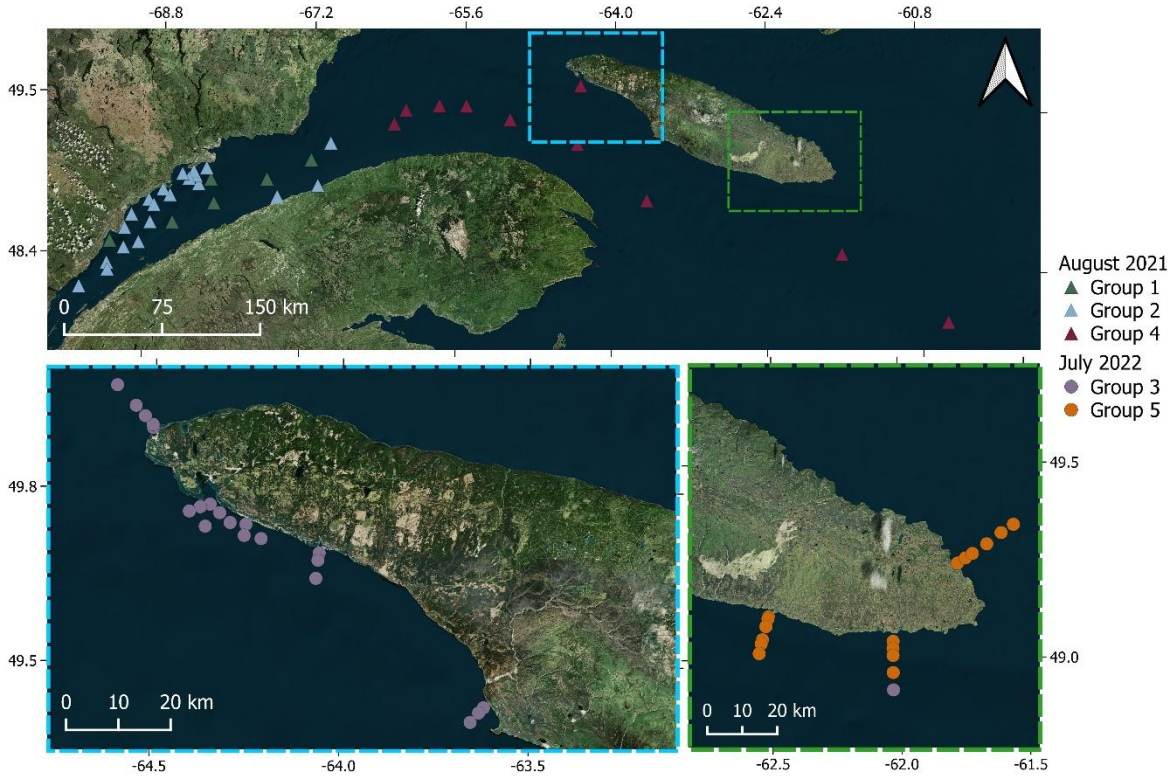

Figure 9. Spatial distribution of the five HCPC groups in the surface waters of the EGSL during Odyssée (August 2021) and AlgaeWISE (July 2022)

During Odyssée, the surface water samples from the LSLE were represented by groups 1 and 2 (Figure 9). Surface samples characterized as group 1 (n=6) were located in the Laurentian Channel. In contrast, group 2 stations (n=21) were located near the head of the channel and along the northern and southern coasts of the estuary. In the Anticosti Gyre and the GSL, the ten surface water samples were assigned to group 4. In the LSLE, surface dominance by a group generally extended to the SCM, with only a few exceptions (Figure S1). In the GSL, however, four groups of stations made up the SCM, namely groups 1 through 4.

During AlgaeWISE, which occurred about one month earlier in the summer season relative to the Odyssée cruise, surface water samples around Anticosti Island were classified into groups 3 and 5 (Figure 9). Surface samples classified in group 3 (n=21) were almost exclusively located northwest of the island, except for one station at the end of the LDX transect southeast of the island. Surface samples classified in group 5 (n=16) were exclusively located on the island's eastern side. The SCM around Anticosti Island was dominated by group 1, but the surface group was also observed at depth for a few stations (Figure S2).

Overall, the five HCPC groups were spatially distinct on the surface, and more mixed at depths. Considering all the samples, including those from the surface and other depths, groups 1, 2, 3, 4, and 5 characterize 55, 39, 34, 15, and 41 samples, respectively.

Regarding TChl *a*, group 2 had the highest mean concentration (Figure S3). However, considering only the surface samples, group 1 had the highest mean TChl *a* concentration. Group 5 was significantly different from the others in its low TChl *a* concentration. Flow cytometry analyses showed a shift in communities from the estuary to the gulf, with picoeukaryotes gradually giving way to pico-PE (Figure S4).

1.5.2.2 Taxonomic composition of groups identified by hierarchical clustering on principal components

The major photosynthetic pigments in each of the groups previously identified by HCPC are presented in Table 2. Figure S5 presents boxplots showing the distribution of photosynthetic pigments and carotenoids for each HCPC group.

Table 2. Distribution of normalized pigment and cell-class concentrations in each HCPC group. The asterisk (*) means that the concentration value is significantly different from the other four HCPC groups

HCPC groups	Number of samples	Top 3 pigments with the highest concentration in each group	Assignment of pigments in the group where they reach their highest concentration	Assignment of cell-class in the group where they reach their highest concentration
Group 1	55	Fuco Chl c_1 Chl c_3	Fuco* Chl c_1 Chl c_2	None
Group 2	39	Fuco Peri Chl c_2	βε-car Peri	Picoeukaryotes Pico-PC
Group 3	34	Fuco Chl c_2 Diadino	Diato Diadino	Nanoeukaryotes
Group 4	15	Fuco Hex-fuco Chl c_2	Zea Hex-fuco But-fuco Chl c_3	Pico-PE Nano-PE Nano-PC
Group 5	41	TChl *b* Fuco Hex-fuco	C-neo* Viola* Croco Pras* MgDVP* Lut ββ-car* Allo TChl *b**	None

DPA was applied on pigments concentration to estimate the relative contribution of five PFTs (i.e., diatoms, dinoflagellates, green algae, haptophytes and photosynthetic prokaryotes) to TChl a_{DPA} concentration for each HCPC group. The results are presented in Figure 10.

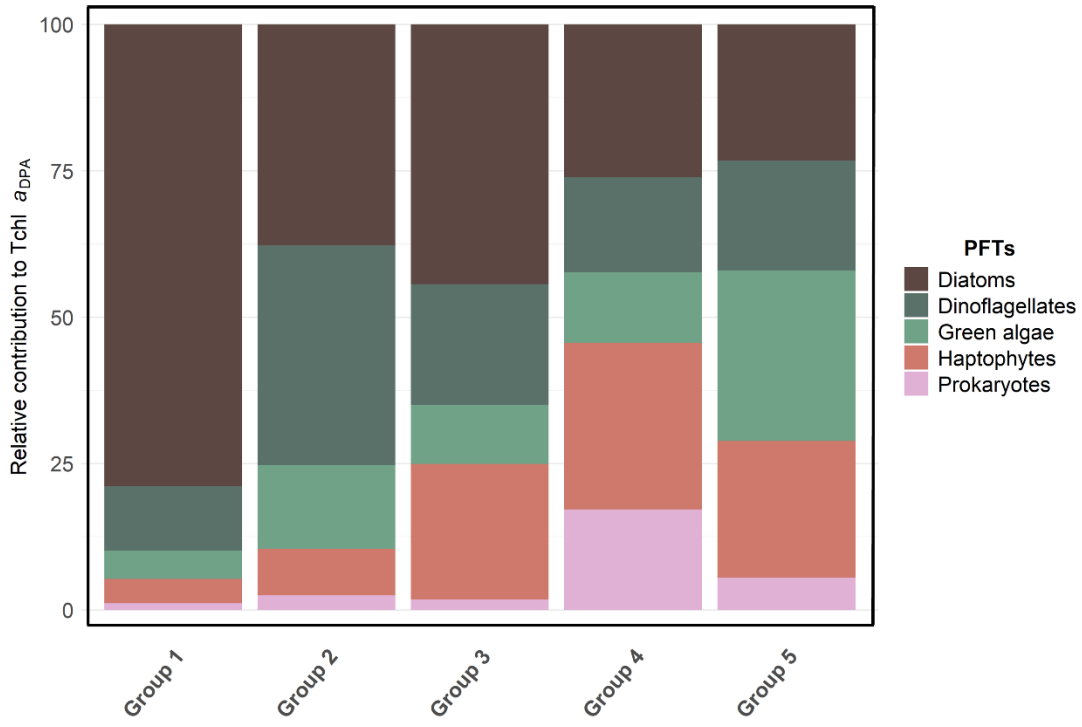

Figure 10. Mean relative contribution of five PFTs to TChl a_{DPA} determined by DPA for the five HCPC groups

Consistent with the dominance of Fuco in group 1 (Table 2), diatoms (DPA-based) accounted for most of the biomass in this HCPC group (78.9 ± 12.4%). Diatom biomass was also relatively high in groups 2 and 3. The normalized concentrations of Fuco are relatively high in each group with values ranging from 0.21 to 0.68, making it the most abundant accessory pigment overall, except in group 5, where TChl *b* dominates (see Table 2). Group 2 was almost equally composed of diatoms (37.8 ± 15.9%) and dinoflagellates (37.5 ± 16.2%). Note that this was the group with the highest mean percentage of dinoflagellates among all the HCPC groups. Group 3 was made up of diatoms (44.4 ± 13.9%), followed by haptophytes (23.2 ± 9.5%) and dinoflagellates (20.6 ± 5.7%). It was the group with the second highest biomass of diatoms and dinoflagellates. It was the group that stood out the least from the other HCPC groups. Group 4 was mainly composed of haptophytes (28.5 ± 9.3%) and diatoms (26.1 ± 8.6%), and had the highest relative contribution of photosynthetic prokaryotes (17.7 ± 8.1%). Finally, group 5 was very different from group 1 regarding

pigment concentrations. Indeed, it was the only group whose most abundant pigment was not Fuco, but rather TChl *b* and it stood out for its lower concentrations of Fuco and Chl c_2. Group 5 was dominated by green algae (29.1 ± 9.7%), followed by haptophytes (23.4 ± 9.4%) and diatoms (23.2 ± 8.4%). It was the group with the highest percentage of green algae. Overall, the major PFTs in the study area were diatoms in groups 1, 2 and 3 and flagellates (i.e., haptophytes and green algae) in groups 4 and 5.

1.5.3 Optical properties

In this section, we first examine the spectral light absorption of the water constituents measured for each of the HCPC groups described above. This inherent optical property is one of the main drivers of the remote sensing reflectance spectrum presented in section 1.5.3.3.

1.5.3.1 Light absorption budget

Total water absorption combines absorption by pure water, phytoplankton, non-algal particles and CDOM. Non-water absorption can therefore be defined by subtracting the contribution of pure water absorption from total water absorption. CDOM absorption was only measured in surface waters and at a few stations during Odyssée. As a result, the number of samples used to generate the light absorption budget was 3 for groups 1 and 2, respectively, 21 for group 3, 6 for group 4, and 16 for group 5. Figure 11 shows the relative contribution of $a_{ph}(\lambda)$, $a_{nap}(\lambda)$, and $a_{cdom}(\lambda)$ in the blue, green and red regions for the surface waters.

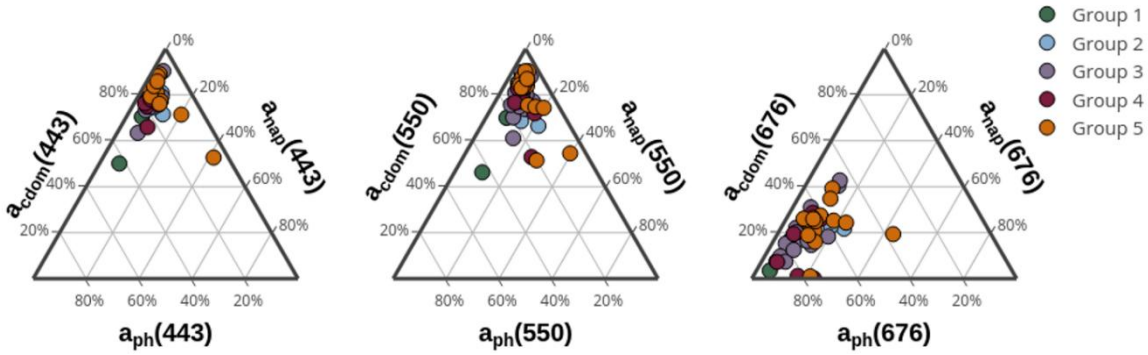

Figure 11. Relative contribution of phytoplankton (a_{ph}), non-algal particles (a_{nap}), and colored dissolved organic matter (a_{cdom}) absorption to the total non-water absorption coefficient for three wavelengths (443 nm, 550 nm and 676 nm) for the surface observations of the five HCPC groups

CDOM was the dominant light-absorbing compound at 443 and 550 nm in surface waters throughout the sampling area (Figure 11). For half of the stations, $a_{cdom}(443)$ contributed to more than 80% of the total non-water absorption. Groups 5 and 3 had the highest relative contribution of a_{cdom} at 443 and 550 nm among all HCPC groups. For most stations, a_{ph} at 443 and 550 nm accounted for less than 20% of the total non-water absorption, although the relative contribution of a_{ph} at 443 nm was slightly higher than at 550 nm. In contrast to a_{ph}, the relative contribution of a_{nap} was slightly higher at 550 nm.

As expected, a_{ph} dominated the light absorption budget at 676 nm for most stations, accounting for more than half of the contribution for 92% of the stations. At 676 nm, station LDX-1, located on the east coast of Anticosti Island, was the only station dominated by a_{nap} instead of a_{ph}. Group 1 had the highest relative contribution of a_{ph} among the five HCPC groups.

The highest and lowest mean $a_{cdom}(350)$ coefficients were measured in the LSLE (i.e., group 1) and in the GSL (i.e., group 4), respectively (data not shown). Stations on the west side (i.e., group 3) of Anticosti Island generally had higher $a_{cdom}(350)$ coefficients than those on the east side (i.e., group 5). Total particle absorption coefficients at 440 nm were mainly dominated by $a_{ph}(440)$ with a mean contribution of 70.8%. Only 12 water samples were dominated by $a_{nap}(440)$, half of them at depths below the SCM.

1.5.3.2 Chlorophyll *a*-specific absorption

Differences in the pigment composition of various phytoplankton communities and their packaging within the cells determine their light absorption signatures (Bricaud et al., 2004; Sun et al., 2022). The mean $a^*_{ph}(\lambda)$ spectra from 375 nm to 750 nm for the five HCPC groups are shown in Figure 12.

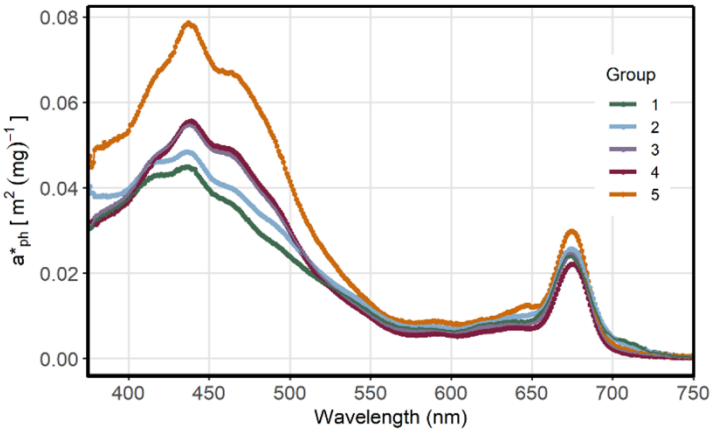

Figure 12. Mean total chlorophyll *a*-specific absorption coefficient of phytoplankton (a*ph) for the five HCPC groups

Overall, the HCPC groups had two main peaks, one located around 440 nm, where the influence of pigments is maximal (Bricaud et al., 2004), and a second around 676 nm. In terms of their magnitude, there were some differences between the $a^*_{ph}(\lambda)$ of the five HCPC groups. At 440 nm, group 5 has the most significant $a^*_{ph}(\lambda)$ coefficient, followed by groups 4, 3, 2, and 1. At 675 nm, the pattern is not the same. Group 5 still has the most important $a^*_{ph}(\lambda)$ coefficient, but is followed by groups 2, 3, 1, and 4. The $a^*_{ph}(\lambda)$ spectra of groups 3 and 4 had almost identical magnitude and spectral shapes, especially at shorter wavelengths.

The blue-to-red ratio (440 and 675 nm) allowed the slope between the two absorption peaks of the spectrum to be measured (Sun et al., 2022). The flatter the slope is, the lower

the ratio will be. Group 5 had the highest ratio (2.62) followed by groups 4 and 3 (2.50 and 2.25). Group 2 and 1 had the lowest ratios, 1.87 and 1.85, respectively.

When we focus only on the surface observations (data not shown), the spectral shapes are flatter, but the general pattern between each group remain the same.

1.5.3.3 Water remote sensing reflectance

Due to the daytime constraint, the number of observations for R_{rs} is more limited than for the other types of data. During Odyssée, several stations were visited outside of sunshine hours, which decreased the number of observations for most HCPC groups. The number of observations per group ranged from 8 to 20, except for group 1, which had only one observation. Mean values of R_{rs} spectra and normalized R_{rs} spectra for the five HCPC groups are shown in Figure 13. Normalization was done using the area under the curve. The standard deviations of the five HCPC groups were relatively large due to the high intra-group variability (Figure 13A). Groups 5 and 1 have very similar spectral shapes and magnitudes. In contrast, groups 2 and 3 have similar spectral shapes but different magnitudes. Group 2 peak in the green (550-570 nm) is slightly more pronounced than the other HCPC groups. Group 4 shows the bluest waters with a peak at 490-500 nm and presents the highest mean R_{rs} and standard deviation.

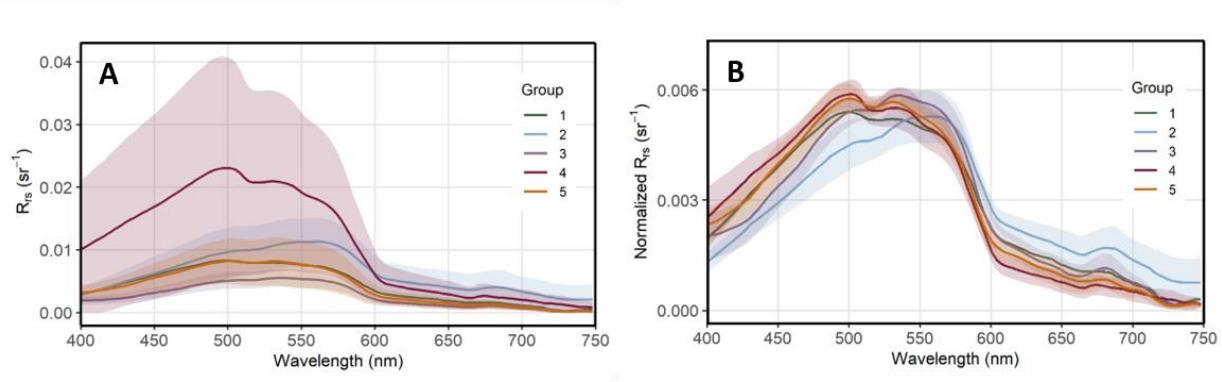

Figure 13. Spectra of the (A) water reflectance and (B) normalized water reflectance for the five HCPC groups. Mean and standard deviation are shown. The mean apparent visible wavelength (AVW; nm) for each group is 515, 532, 519, 508 and 511 for groups 1, 2, 3, 4, and 5, respectively.

The difference in spectral shapes is better seen in the normalized R_{rs} spectra (Figure 13B). The spectral angle mapper (SAM) was used to quantify the similarities and differences in spectral shapes between the normalized spectra (Figure S6). The 430 to 630 nm spectral range was considered for the statistical analysis of these optical data. The 430 to 630 nm spectral band was selected for the statistical analysis of these optical data. This selection was made to highlight the influence of accessory pigments while attempting to minimize the effects of CDOM absorption, which tends to occur at the extreme end of the spectrum in the UV, and the effects of Chl a absorption in the red. The difference between the spectral shapes of two groups increases with the SAM value.

Groups 2 and 4 had the most significant difference between their spectral shapes, followed closely by the difference between groups 2 and 5 (Figure S6). Overall, group 2 is the most different from the others (more greenish waters; AVW = 532). Conversely, according to the SAM results, the groups with the most similar spectral shapes were 5 and 1, followed by 5 and 4. Overall, this analysis indicates that it can be difficult to distinguish the different phytoplankton communities determined based on pigments concentrations and cell class abundances (obtained from HPLC and flow cytometry analysis) from most of the reflectance spectra.

1.5.3.4 Optical water types

Four different optical water types (OWT), as defined by Spyrakos et al. (2018), were identified from the reflectance spectra measured in the study area, demonstrating spatial variability in ocean color within the EGSL (Figure 14A). The OWT 4, 7, 8, and 9 include 5, 36, 3, and 8 observations, respectively (Figure 14B).

OWT 4 characterized blue-green water stations in the GSL and on the east coast of Anticosti Island. Of the four OWTs in the study area, OWT 4 stations had the lowest mean concentration of TChl *a* and suspended matter in particulate and dissolved forms. Stations from groups 4 (n=3) and 5 (n=2) were present in this OWT.

With its 36 observations, OWT 7 characterizes most of the stations. These stations are situated primarily in the GSL, particularly in transects around Anticosti Island, with a few in the LSLE. The characteristics of this OWT were similar to those of OWT 4, with low mean values of particulate and dissolved absorption, along with low mean concentrations of TChl *a*. Notably, some of these stations had high values of $a_{nap}(443)$. All HCPC groups were present in this OWT.

OWT 8 was associated with only three stations, all located in the LSLE. This OWT had the highest averages for $a_p(443)$, $a_{nap}(443)$, $a_{phy}(443)$, and TChl *a*. All three stations from this OWT were from group 2.

The eight stations classified as OWT 9 were closer to the coast, with some near the shores of the LSLE and others on the east coast of Anticosti Island. OWT 9 was characterized by the highest $a_{cdom}(443)$. It had the second highest mean values for $a_p(443)$, $a_{nap}(443)$, $a_{phy}(443)$ and TChl *a* after OWT 8 and was represented by phytoplankton communities from groups 2 (n=3) and 3 (n=5).

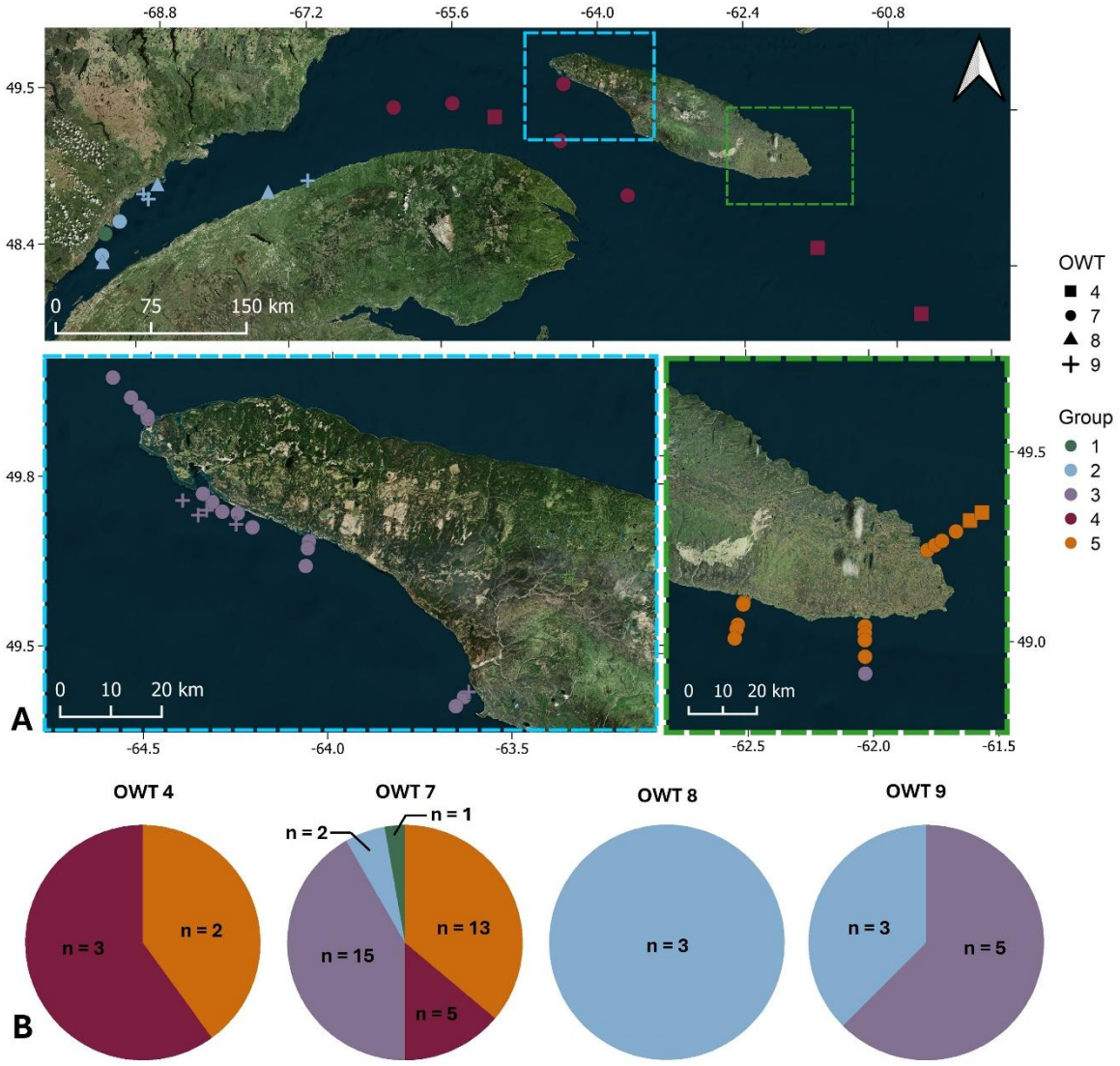

Figure 14. (A) Spatial distribution of the four optical water types identified in the EGSL surface waters. Stations shown are those for which a reflectance spectrum was measured. OWT are represented by the symbols and HCPC groups by the colors. (B) Pie charts illustrating the distribution of HCPC groups (1, 2, 3, 4, and 5) for each OWT (4, 7, 8, and 9). Each pie chart represents an OWT and is colored according to the HCPC groups. The colors used for each HCPC group are consistent with those used in Figure 14A. n is for the number of stations

1.5.4 Performance of the Xi's PFTs algorithm

The Chl *a* concentration of PFTs estimated using DPA was compared to that obtained by applying the *EOF-SST hybrid* algorithm (Xi et al., 2021) to standardized surface reflectance spectra. Figure 15 shows the scatterplots of the algorithm-retrieved PFTs Chl *a* concentration versus the DPA-derived PFTs Chl *a* concentration. Each station is plotted according to its group (color) and its OWT (symbols).

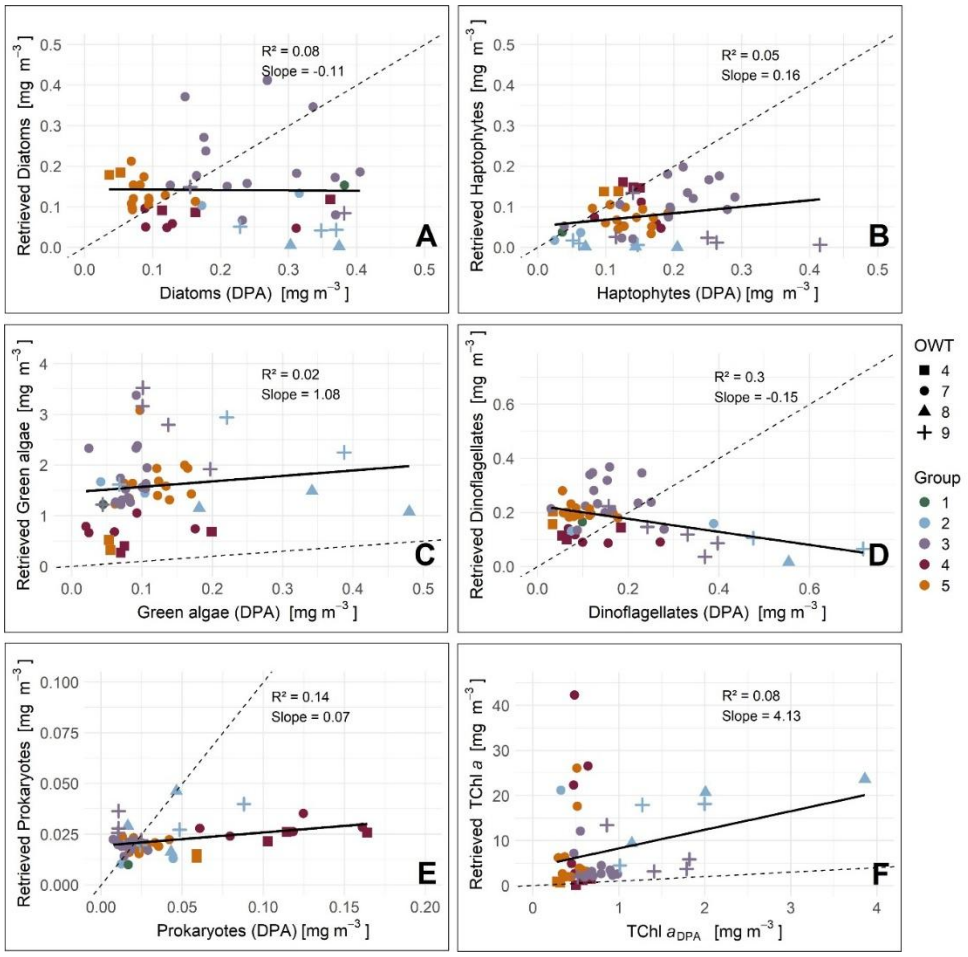

Figure 15. Linear regression between DPA-derived and EOF-SST hybrid algorithm-retrieved Chl *a* concentrations of (A) diatoms, (B) haptophytes, (C) green algae, (D) dinoflagellates, (E) photosynthetic prokaryotes and (F) total Chl *a*. Observations are colored according to the group obtained by the HCPC based on pigment concentrations and cell class abundances. Symbols represent the optical water types (OWT) into which they were classified. The dashed line represents the x=y line

Overall, the correlations between predicted and observed Chl *a* concentrations for all PFTs were weak, with all R^2 values ≤ 0.30, and even negative regression slopes for some PFTs (i.e., diatoms and dinoflagellates; Figure 15A, D). The TChl *a* is severely overestimated by the algorithm (a mean factor of ~12), with concentrations reaching as much as 42,29 mg m^{-3} (Figuire 13F). For diatoms, the algorithm underestimated the majority of observations, particularly for surface stations in groups 2 and 4 (Figure 15A). Similarly, haptophyte Chl *a* concentrations were mostly underestimated, but they fitted the 1:1 regression line slightly better than diatoms (Figure 15A, B). Note that most stations classified as OWT8 and OWT9 yield almost no haptophyte (<0.05).

In contrast, the predicted Chl *a* concentrations for green algae were greatly overestimated relative to the observed values, with a regression slope close to unity and an intercept of 0.21 (Figure 15C; note the scale of the y-axis). Dinoflagellates exhibited a negative slope, but the highest R^2 of all groups (Figure 15D). While most predictions overestimated the observations, most were closer to the 1:1 line compared to green algae. Finally, prokaryotes were underestimated by the algorithm, especially for stations belonging to group 4 (Figure 15E).

The performance of the algorithm for each OWT was assessed by calculating the mean distance between the points and the regression line where $y=x$ for each of them. In general, the predictions of the Chl *a* concentration of dinoflagellates, green algae, haptophytes, and TChl a_{DPA} were more accurate for stations classified as OWT 4, which are in offshore waters of the GSL (Figure 14). For predicting diatom Chl *a* concentrations, the algorithm performed best in waters classified as OWT 7. For prokaryotes, the best predictions were obtained in waters classified as OWT 8, closely followed by OWT 9.

1.6 DISCUSSION

1.6.1 Spatial variability of phytoplankton communities

Combining HPLC and light microscopy or flow cytometry data to identify major differences in the distribution of phytoplankton communities has been used successfully in previous studies in the St. Lawrence ecosystem (e.g., Roy et al., 1996; Araújo et al., 2022). The use of pigment biomarkers to determine PFTs has inherent limitations. Some pigments are not exclusive to a single phytoplankton type, and their presence can vary depending on environmental conditions (Schlüter et al., 2000). For example, fucoxanthin, which is typically associated with diatoms, is also found in prymnesiophytes, chrysophytes, pelagophytes, dinoflagellates, dictyochophytes, and bolidophytes (Kramer et al., 2024), while peridinin, a biomarker for dinoflagellates, is not present in all dinoflagellate species. It should be noted that dinoflagellates containing peridinin do not contain fucoxanthin, whereas those with fucoxanthin do not contain peridinin (Roy et al., 2011; Brotas et al., 2022). These limitations should be considered when interpreting the results. Also, the empirical relationships underlying DPA can vary regionally and are strongly influenced by environmental conditions, which may compromise the reliability of the estimates, particularly in coastal environments. Here, the specific method of Losa et al. (2017) was employed to maintain consistency with the approach used by Xi et al. (2021). In the future, to improve accuracy, we recommended applying DPA using region-specific coefficients, in order to reflect the composition and size structure of the phytoplankton community more accurately in the EGSL. Despite its limitations, this approach can effectively highlights key phytoplankton communities, making it comparable to information obtained through remote sensing methods.

Phytoplankton communities structure in the EGSL exhibits marked seasonal variability. Outside the bloom period, the surface waters of the EGSL are generally numerically dominated by small flagellated cells (Levasseur et al., 1984; Cantin et al., 1996; Roy et al., 1996; Blais et al., 2023). Our cytometry analyses confirmed this trend by detecting

an overall higher abundance of pico-sized cells than nano-sized cells. However, as flow cytometry analysis does not account for micro-sized cells (>20 μm), their potential numerical abundance remains unquantified. This limitation is particularly relevant given the observed dominance of fucoxanthin; a pigment typically linked to micro-sized cells. Micro-sized phytoplankton usually contribute more significantly to Chl *a* compared to other size classes in environments with high nutrient and Chl *a* concentration (Cloern, 2018), such as the St. Lawrence Estuary (Levasseur et al., 1984; Araújo et al., 2022).

This study revealed a general dominance of fucoxanthin, in most cases associated with diatoms, at surface stations in the study area for four out of five HCPC groups identified. Fucoxanthin, significantly abundant in group 1, was previously identified as a predominant pigment in the St. Lawrence Estuary (Roy et al., 2008). Blais et al. (2023b) reported a positive normalized annual anomaly for the diatom:dinoflagellate abundance ratio at a station near Rimouski for almost every year from 2014 to 2021. This finding aligns with the results for Group 1, which shows higher diatom biomass compared to dinoflagellates.

Stations located further into the GSL during August exhibited a stronger presence of prokaryotes and haptophytes. The high concentration of pico-PE for group 4 can be associated with marine cyanobacteria, making it possible to associate the pigment zeaxanthin with cyanobacteria. Of all PFTs, prokaryotes were present in the lowest biomass in the EGSL, consistent with their typically low abundance at high latitudes (Xi et al., 2023; Zhang et al., 2024).

A recent analysis of satellite-retrieved Chl *a* climatology in the EGSL showed marked Chl *a* values in the coastal waters of Anticosti between May and September (Laliberté & Larouche, 2023). In early July, stations east of Anticosti Island were dominated by green algae. However, phytoplankton communities at surface stations west of the island were not the same, being more dominated by diatoms and haptophytes. One hypothesis for this difference could be the occurrence of a coastal upwelling west of the island, leading to nutrients replenishing in the upper water column. This process could increase the algal biomass in this region, which is dominated by larger phytoplankton (Le Fouest et al., 2005).

The occurrence of coccolithophores (part of the haptophyte group) has been previously documented in the eastern GSL (Cantin et al., 1996; Genin et al., 2021) and also as sporadic blooms in the Laurentian Channel and east of Anticosti Island (Brown & Yoder, 1994).

However, the relatively low TChl *a* concentrations observed around Anticosti Island in July suggest that the sampling occurred during the post-bloom period. Typically, blooms in the GSL occur earlier in the year (April-May) compared to those in the estuary, which peak in June-July (Levasseur et al., 1984; Therriault & Levasseur, 1986; Zakardjian et al., 2000; Mei et al., 2010; Laliberté & Larouche, 2023). This temporal pattern may explain the observed spatial gradient in TChl *a* concentrations during both campaigns. The general gradient of decreasing Chl *a* from the estuary to the GSL during most of the year was also previously observed satellite (Fuentes-Yaco et al., 1997; Laliberté et Larouche, 2023). The GSL stations sampled in August 2021 showed a well-established stratification, with surface waters dominated by group 4 (characterised by a larger abundance of small cells), which were found in the warmest, clearest and bluest waters encountered (OWT 4).

1.6.2 Influence of pigments and cells class abundance on chlorophyll *a*-specific absorption coefficient

Our results show some differences in the specific absorption coefficient of the five phytoplankton groups obtained by HCPC. A key factor influencing phytoplankton-specific absorption coefficient is the packaging effect. The packaging effect refers to the reduction of the absorption efficiency of a cell depending on the organization and concentration of its photosynthetic pigments as well as the size of the cell (Kirk, 1975; Morel & Bricaud, 1981; Bricaud et al., 2004). For example, picophytoplankton are expected to have a higher specific absorption coefficient than nanophytoplankton in the blue wavelengths (Ciotti et al., 2002; Brewin et al., 2010). Since groups 1, 2, and 3 are predominantly composed of large cells such as diatoms and dinoflagellates, this is consistent with their lower blue-to-red absorption ratios. Previous studies (e.g., Babin et al., 1993; Roy et al., 2008) have identified this effect as the primary driver of variation in Chl *a*-specific absorption coefficient within the EGSL.

In addition to cell size, pigment composition also influences the spectral absorption characteristics of phytoplankton. A shoulder peak is visible for groups 3, 4 and 5 around 465 nm and a smaller one for groups 1 and 2. This peak may be due to the absorption of pigments such as alloxanthin, zeaxanthin and Chl c_2 (Sun et al., 2022). Group 5 shows an absorption peak around 650 nm, just after the prominent peak of 676 nm, most likely due to the high concentration of TChl *b* in this group, indicating the presence of green algae. Furthermore, groups 3, 4, and 5 show high concentrations of photoprotective pigments, namely Diadino, Diato, Viola, Zea and ββ-car. High concentrations of photoprotective pigments can result in high $a^*_{ph}(\lambda)$ values, particularly in the blue-green region of the spectrum (Morel & Bricaud, 1981; Eisner et al., 2003; Roy et al., 2008).

1.6.3 Algorithm performances and optical properties

The results indicate that the *EOF-SST hybrid* algorithm proposed by Xi et al. (2021), with the globally tuned coefficients used, does not perform adequately for systematic application in the EGSL. Although it was expected that an algorithm designed for oceanic waters would not be suitable for a productive environment influenced by terrigenous inputs such as the St. Lawrence, it was important to assess the extent of the errors and to identify the phytoplankton types that were the least accurately quantified. This evaluation was particularly important given that PFTs products are now distributed operationally by the Copernicus Marine Environment Monitoring Service and are potentially used by a wide range of end users. Several factors could explain the significant discrepancies observed between satellite and *in situ* data.

Remote sensing algorithms of PFTs retrieval have already been validated for some water types on a global scale, but their application remains limited in waters predominantly of the Case 2 type (IOCCG, 2014). The influence of CDOM absorption on the reflectance of the EGSL water could be one explanation for the reduced performance of the algorithm in the study site (Fuentes-Yaco et al., 1997). The results indicate that $a_{cdom}(\lambda)$ dominates the absorption budget at short wavelengths in the study region, which is consistent with other

studies conducted in the St. Lawrence (e.g., Xie et al., 2012; Araújo & Bélanger, 2022). This result is typical of coastal waters, in contrast to Case 1 waters where phytoplankton generally dominate absorption (Nieke et al., 1997). Differences in optical properties between the LSLE and the GSL have been previously documented in the literature (e.g., Babin et al., 1993; Nieke et al., 1997; Roy et al., 2008; Xie et al., 2012). For instance, the stations with the lowest contribution of $a_{cdom}(\lambda)$ to the total absorption are located in the GSL. Moreover, OWT 4, which consists of the stations with the lowest mean values of $a_{cdom}(443)$, is the one for which the algorithm performs best for the majority of PFTs, except for diatoms and prokaryotes. In contrast, we found that all five phytoplankton communities obtained from the HCPC can be represented in one single OWT (OWT 7), making challenging the distinction of PFTs from remote sensing. This pattern may be influenced by the limited summer sampling, conducted after the spring bloom, which constrained the variability in biomass captured by our dataset.

The results of the SAM index applied to the R_{rs} show that the five HCPC groups identified according to pigment concentrations and cell class abundances are difficult to discriminate based on reflectance alone. The regression slopes between the PFTs Chl *a* concentration obtained by DPA and by the algorithm are low, suggesting that the differences between the reflectance spectra of the stations may not be sufficiently marked to allow the algorithm to discriminate the various Chl *a* concentration, or that the coefficients are not adapted to the characteristics of our study area. The overall low Chl *a* concentration of certain PFTs, and therefore the limited detection signal, may partly explain some of the difficulties encountered by the algorithm (Vishnu et al., 2022).

Not only was the algorithm not explicitly adapted for our region, as it was designed globally, but it also excluded all stations located at depths shallower than 200 m during its development (Xi et al., 2020). Given that most of the stations studied are located in areas shallower than 200 m, this limitation may also explain the inapplicability of this algorithm in shallow coastal ecosystems.

According to the algorithm's predictions, green algae have the highest Chl *a* concentrations at most stations. However, this is not consistent with *in situ* observations.

Although chlorophyll *b*, which is associated with green algae, is high in group 5, it remains lower than many other pigment concentrations in the other four groups.

The unsatisfactory results highlight the need for specific regional adjustments for this type of algorithm, as demonstrated by Vishnu et al. (2022). In our study, the coefficients proposed by Vishnu et al. (2022) for the Canadian west coast were tested on the EGSL reflectance data but did not perform better than the global coefficients of Xi et al. (2021), further emphasizing the need to develop coefficients specifically adapted to this region. The coefficients have not been adapted to the EGSL yet, mainly due to the limited number of available data and their poor representativeness in terms of seasonality. Bracher et al. (2015) showed that a minimum number of 50 match points would be sufficient for statistically significant pigment estimation, but this is in an open ocean context. Under the optically complex conditions of the EGSL, the 52 reflectance spectra available may prove insufficient to obtain robust statistics and develop reliable coefficients for the algorithm. In addition, a better temporal resolution would also be required for more accurate regional adjustment.

1.6.4 Future perspectives

Given previous findings, the global algorithm of Xi et al. (2020, 2021) applied to our study region does not provide adequate results. This highlights the importance of fine-tuning algorithms for regional scales. Advances in sensor precision, mainly through hyperspectral missions such as NASA's Plankton, Aerosol, Cloud, and ocean Ecosystem (PACE), launched in February 2024, will greatly improve the detection and analysis of diverse phytoplankton communities from space. PACE provides hyperspectral ocean color data with a spatial resolution of ~1.2 km and global coverage every two days, enabling precise monitoring of phytoplankton composition and distribution (Werdell et al., 2019; Cetinić et al., 2024). Its Ocean Color Instrument (OCI) sensor provides imaging across a spectral range of 340-890 nm, with 2.5 nm steps and ~5 nm bandwidths, supporting improved atmospheric correction and detailed measurements of chlorophyll fluorescence and other key features (Frouin et al., 2019). These advances could help address the challenges of detecting PFTs in optically

complex coastal waters, where traditional remote sensing methods often struggle (Craig et al., 2012; Vishnu et al., 2022). However, detecting subtle differences in phytoplankton communities will remain a challenge in coastal waters, as different communities may occupy similar optical water types. Approaches will need to rely on other sources of information to discriminate PFTs in such optically complex environment, like sea surface salinity, SST, MLD, bathymetry, etc.

Future work should refine the pigment-based assessment of PFTs in the GSL by applying chemotaxonomic approaches, such as DPA or CHEMTAX, but using regionally adapted conversion coefficients derived from local taxonomic information obtained through techniques like light microscopy or metagenomic approaches.

In summary, ongoing developments in ocean color remote sensing and region-specific algorithms hold great promises for improving our ability to monitor and understand phytoplankton communities. The information gathered in this study on the optical properties of the water in the EGSL (i.e., absorption budget, reflectance) and the different phytoplankton communities will be valuable in the future to further develop algorithms that are precisely tailored to this region.

CONCLUSION GÉNÉRALE

Ce mémoire de maîtrise s'est penché sur la caractérisation spatiale des communautés phytoplanctoniques de l'EGSL durant la période estivale, à partir de données récoltées lors de deux campagnes océanographiques menées en 2021 et 2022. L'étude visait trois objectifs spécifiques : 1) caractériser les communautés phytoplanctoniques présentes; 2) analyser les relations entre certaines propriétés optiques intrinsèque (absorption) et apparentes (réfléctance) et le phytoplancton; et 3) évaluer les performances d'un algorithme empirique de télédétection (EOF-SST hybrid algorithm; Xi et al., 2020, 2021) des PFTs appliqué à la région d'étude.

Nos travaux ont permis de mettre en lumière la diversité des communautés phytoplanctoniques dans l'EGSL. Cinq groupes distincts ont été identifiés à l'aide de l'analyse de regroupement hiérarchique sur composantes principales basée sur les concentrations pigmentaires obtenues par HPLC et sur l'abondance des classes de taille obtenue par cytométrie en flux. Pour la majorité des groupes, en particulier ceux de l'estuaire maritime et ceux situés à l'ouest de l'île d'Anticosti, une dominance marquée de la fucoxanthine a été observée, un pigment couramment associé aux diatomées. Les dinoflagellés étaient également fortement présents dans l'estuaire maritime, notamment aux stations plus côtières. Néanmoins, la composition des communautés phytoplanctoniques présentait une variabilité spatiale notable. Les pigments ont révélé une contribution relative plus élevée d'haptophytes dans les trois groupes localisés dans le golfe du Saint-Laurent. Par ailleurs, une prédominance des algues vertes a été observée à l'est de l'île d'Anticosti, tandis qu'une plus forte contribution des procaryotes caractérisait le groupe associé aux eaux libres du golfe. L'analyse des propriétés optiques a révélé que l'absorption par la matière organique dissoute colorée (CDOM) dominait le budget d'absorption aux courtes longueurs d'ondes dans les eaux de surface de Cas 2 de l'EGSL. Les coefficients d'absorption spécifique du phytoplancton ont montré des variations entre les groupes, étant influencés par la taille des cellules et la composition pigmentaire. L'analyse des spectres de réflectance a démontré une variabilité de la couleur de l'eau dans l'EGSL, avec l'identification de quatre types d'eaux

optiquement différentes. Cependant, la distinction des différentes communautés phytoplanctoniques basée uniquement sur les spectres de réflectance s'est avérée difficile. Les communautés phytoplanctoniques n'étaient pas distribuées selon les différents types d'eau optiques retrouvés dans l'EGSL. Les résultats ont par ailleurs montré que l'algorithme de télédétection des PFTs *EOF-SST*, appliqué avec les coefficients globaux, ne fournit pas de résultats adéquats pour l'EGSL. Les estimations de la concentration en Chl *a* des différents PFTs présentaient de faibles corrélations avec les données *in situ* obtenues par l'analyse pigmentaire, avec des sous-estimations et des surestimations significatives. Ces résultats suggèrent que les relations empiriques globales sur lesquelles repose l'algorithme ne sont pas adaptées aux conditions optiquement complexes des eaux côtières de l'EGSL. Par conséquent, les produits satellitaires distribués par le service marin Copernicus ne devraient pas être utilisé pour étudier les PFTs dans l'EGSL.

Cette étude comporte certaines limites qu'il est important de souligner. L'analyse pigmentaire est efficace pour explorer la dynamique phytoplanctonique dans l'EGSL – une région dominée numériquement par de petites cellules – mais elle présente néanmoins une résolution taxonomique limitée, ce qui restreint l'identification précise des groupes phytoplanctoniques. Il serait intéressant de poursuivre l'étude et d'utiliser d'autres méthodes de chimiotaxonomie, comme la méthode CHEMTAX, avec des coefficients spécifiquement adaptés à la région d'étude et obtenus à partir de données taxonomiques issues de la microscopie optique. Cela permettrait d'améliorer la caractérisation des communautés phytoplanctoniques présentes dans le milieu. Une couverture temporelle plus étendue, incluant par exemple des échantillonnages répétés au cours de plusieurs saisons, aurait également permis une caractérisation des dynamiques saisonnières. De plus, le nombre restreint de spectres de réflectance disponibles, notamment en raison d'un échantillonnage parfois réalisé en dehors des heures d'ensoleillement, a limité la robustesse des analyses, comme en témoigne le groupe 1 qui ne comporte qu'une seule observation spectrale. D'autres variables, comme le CDOM, n'ont pas été mesurées à chacune des stations. Ces informations manquantes permettraient vraisemblablement d'obtenir une représentation plus complète de la variabilité optique au sein de la région à l'étude. L'utilisation de coefficients de calibration

générique dans l'algorithme de télédétection des PFTs constitue une autre limite. Le développement d'algorithmes adaptés spécifiquement à l'EGSL, en générant des coefficients de calibration propres à la région d'étude, constituerait une amélioration méthodologique pertinente pour les travaux futurs. Enfin, il est important de souligner que l'étude est temporellement et spatialement restreinte, et donc ne représente pas l'entièreté de l'EGSL, qui est un environnement dynamique.

Finalement, bien que cette étude comporte ses limites, les résultats mettent en lumière l'importance de poursuivre les efforts de suivi des PFTs dans l'EGSL, un environnement en constante évolution. Le développement d'algorithmes de télédétection des PFTs, spécifiquement adaptés aux eaux optiquement complexes de l'EGSL, apparait comme une avenue prometteuse pour assurer un suivi rigoureux à grande échelle. Contrairement aux méthodes d'échantillonnage *in situ*, la télédétection satellitaire permet une couverture spatiale étendue, essentielle pour documenter les dynamiques environnementales sur de vastes territoires. Les données récoltées dans le cadre de ce projet constitueront une base de données précieuse pour l'élaboration et la validation de tels algorithmes.

MATÉRIELS SUPPLÉMENTAIRES

Table S1. Date, geographic coordinates and water depth of the stations visited during the Odyssée campaign. The stations are listed in order of sampling time

Station	Date	Latitude	Longitude	Water depth (m)
P9	2021-08-07	48.6668	-68.582	330.1
P9b	2021-08-07	48.8165	-68.164	349.5
P10	2021-08-08	49.0038	-67.626	295.1
P11	2021-08-08	49.1543	-67.175	324.1
P11b	2021-08-08	49.4285	-66.321	324.9
P13b	2021-08-09	49.3260	-64.386	384.3
P14	2021-08-09	48.9457	-63.650	324.0
G23	2021-08-10	48.0842	-60.536	448.2
G26	2021-08-10	48.5696	-61.619	417.0
PM	2021-08-11	49.7291	-64.362	48.0
P13	2021-08-11	49.4852	-65.101	362.4
P11c	2021-08-11	49.5718	-65.567	320.2
P12b	2021-08-11	49.5661	-65.853	332.0
P12	2021-08-12	49.5263	-66.203	331.7
P10b	2021-08-12	49.2756	-66.979	313.5
M1	2021-08-12	48.9794	-67.092	115.3
M4	2021-08-13	48.8876	-67.509	58.0
MANIC4	2021-08-13	49.0552	-68.262	27.0
MANIC1	2021-08-14	48.9797	-68.210	232.5
MANIC8	2021-08-14	48.9410	-68.334	260.0
MANIC6	2021-08-14	48.9970	-68.369	130.0
MANIC5	2021-08-15	49.0251	-68.394	35.3
MANIC9	2021-08-15	48.9749	-68.439	157.3
MANIC11	2021-08-15	49.0032	-68.509	24.0
HCN1	2021-08-15	48.8517	-68.624	166.2
HCN3	2021-08-16	48.8887	-68.699	30.0
HCN4	2021-08-16	48.8110	-68.840	23.7
HCN6	2021-08-16	48.7777	-68.785	123.0
HCN10	2021-08-17	48.6998	-69.008	23.0
HCN11	2021-08-17	48.6032	-69.070	26.9
HCN14	2021-08-17	48.5081	-69.213	22.3
HCN16	2021-08-17	48.3558	-69.228	260.8

P7	2021-08-17	48.3095	-69.215	280.0
P6	2021-08-18	48.1791	-69.492	226.0
HCN13	2021-08-18	48.4690	-69.066	318.0
P8	2021-08-19	48.5132	-68.916	302.0
HCN7	2021-08-19	48.6564	-68.812	332.3

Table S2. Date, geographic coordinates and water depth of the stations visited during AlgaeWISE campaign. The stations are listed in order of sampling time

Station	Date	Latitude	Longitude	Water depth (m)
PME-4	2022-06-30	49.7469	-64.337	33.0
LDX-1	2022-07-01	49.0461	-62.029	15.0
LDX-2	2022-07-01	49.0277	-62.029	27.5
LDX-3	2022-07-01	49.0099	-62.030	40.0
LDX-4	2022-07-01	48.9661	-62.030	121.0
LDX-5	2022-07-01	48.9215	-62.030	200.0
BIN-1	2022-07-02	49.2445	-61.773	15.0
BIN-2	2022-07-02	49.2574	-61.742	33.0
BIN-3	2022-07-02	49.2685	-61.714	43.0
BIN-4	2022-07-02	49.2926	-61.657	75.0
BIN-5	2022-07-02	49.3208	-61.600	106.3
BIN-6	2022-07-02	49.3414	-61.551	114.3
LDS-1	2022-07-03	49.1116	-62.515	14.0
LDS-2	2022-07-03	49.1070	-62.517	19.0
LDS-3	2022-07-03	49.0870	-62.525	30.0
LDS-4	2022-07-03	49.0532	-62.539	68.0
LDS-5	2022-07-03	49.0427	-62.544	115.0
LDS-6	2022-07-03	49.0176	-62.552	200.0
PSO-1	2022-07-04	49.4301	-63.618	24.0
PSO-2	2022-07-04	49.4209	-63.631	34.8
PSO-3	2022-07-04	49.4046	-63.653	75.0
PME-1	2022-07-05	49.7171	-64.213	29.0
PME-2	2022-07-05	49.7414	-64.254	16.0
PME-3	2022-07-05	49.7221	-64.258	30.0
PME-4	2022-07-05	49.7439	-64.296	28.0
PME-5	2022-07-05	49.7606	-64.324	20.0
PME-6	2022-07-05	49.7750	-64.350	13.0

PME-7	2022-07-05	49.7703	-64.376	16.0
PME-8	2022-07-05	49.7626	-64.405	36.0
PME-9	2022-07-05	49.7369	-64.362	45.0
BSC-1	2022-07-06	49.9056	-64.505	19.1
BSC-2	2022-07-06	49.9107	-64.506	35.0
BSC-3	2022-07-06	49.9254	-64.527	67.0
BSC-4	2022-07-06	49.9429	-64.552	95.7
BSC-5	2022-07-06	49.9777	-64.603	164.4
RBS-1	2022-07-07	49.6937	-64.058	16.0
RBS-2	2022-07-07	49.6814	-64.061	30.4
RBS-3	2022-07-07	49.6498	-64.065	58.6

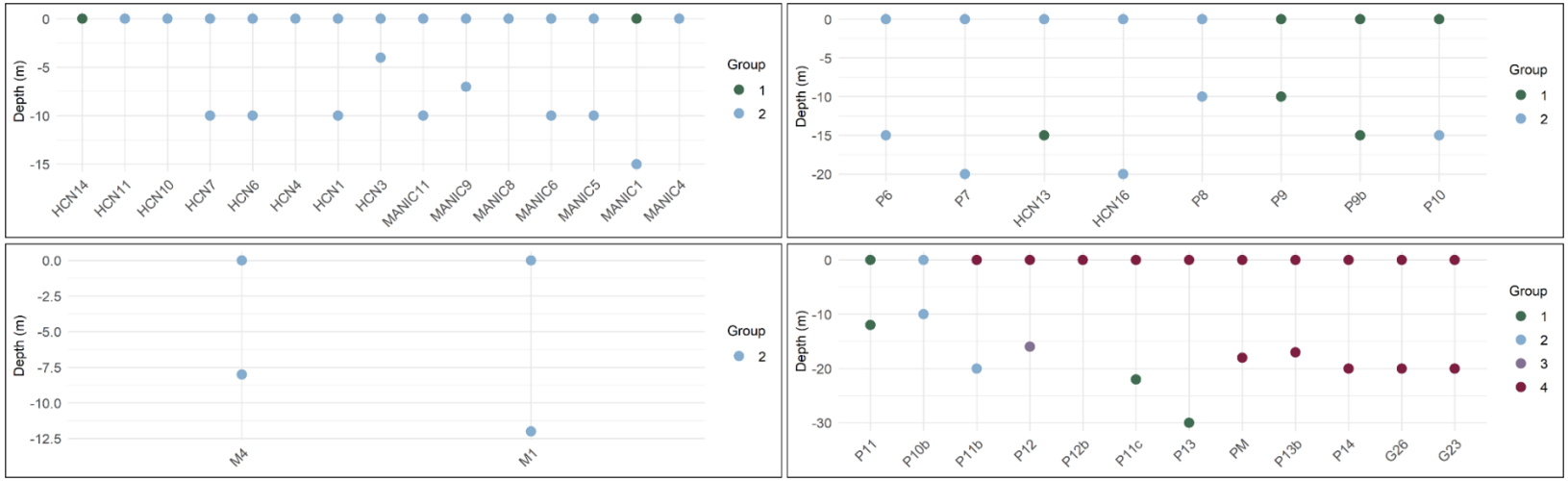

Figure S1. Vertical distribution of the five HCPC groups for each station visited during the Odyssée oceanographic cruise

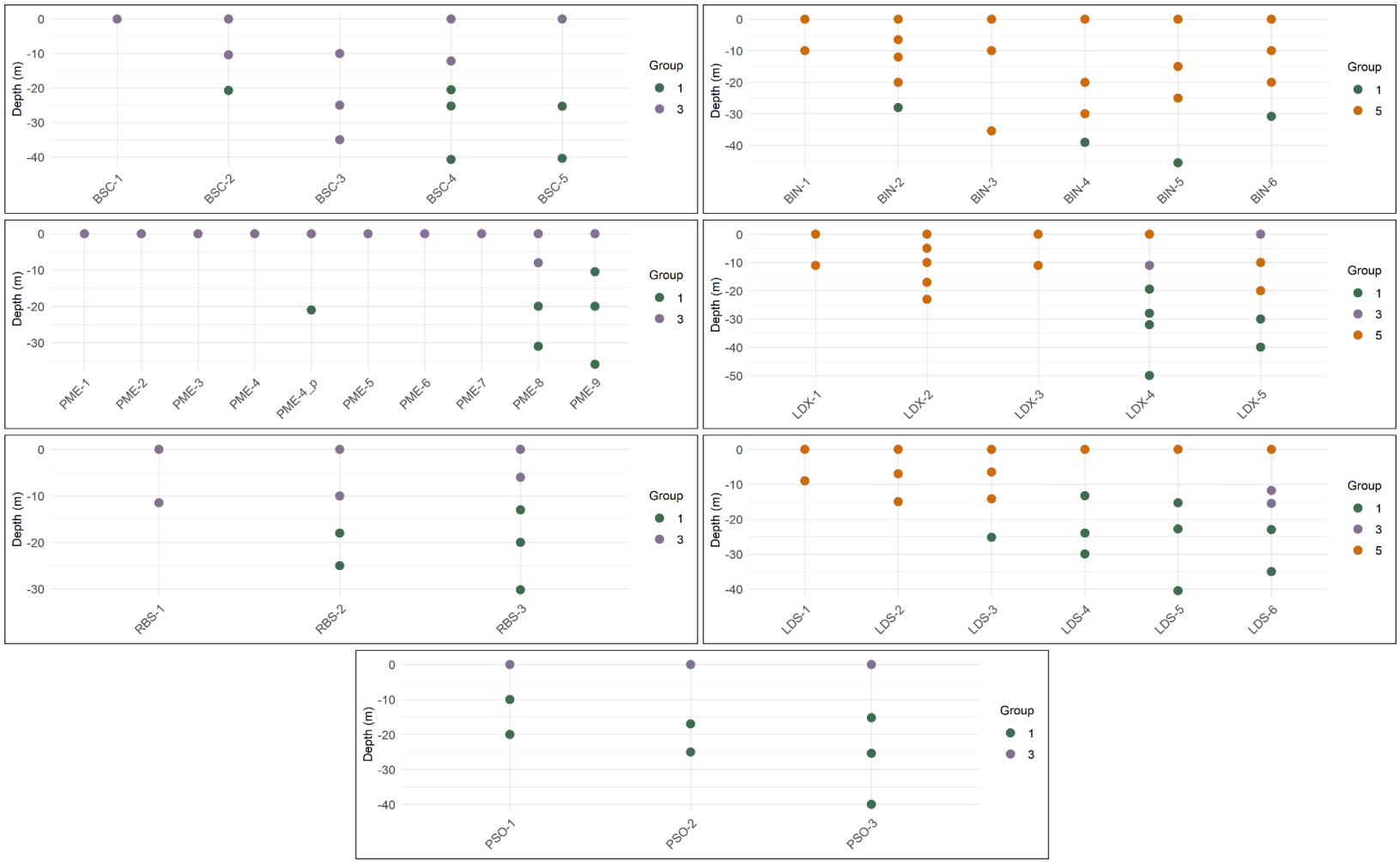

Figure S2. Vertical distribution of the five HCPC groups for each station visited during the AlgaeWISE oceanographic cruise

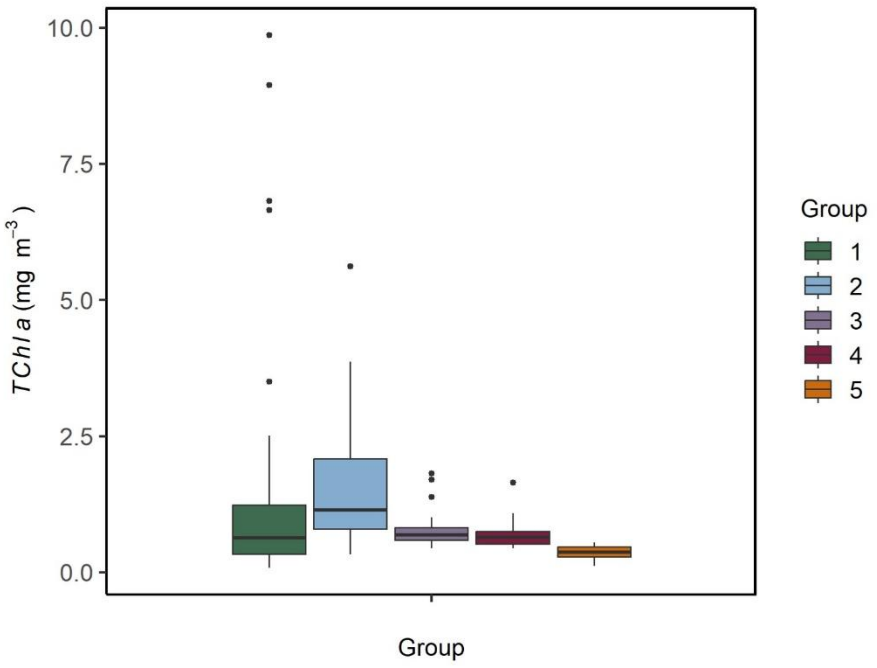

Figure S3. Box plots of the variability (minimum, lower quartile, median, upper quartile, maximum and outliers) of TChl *a* concentration for the five HCPC groups

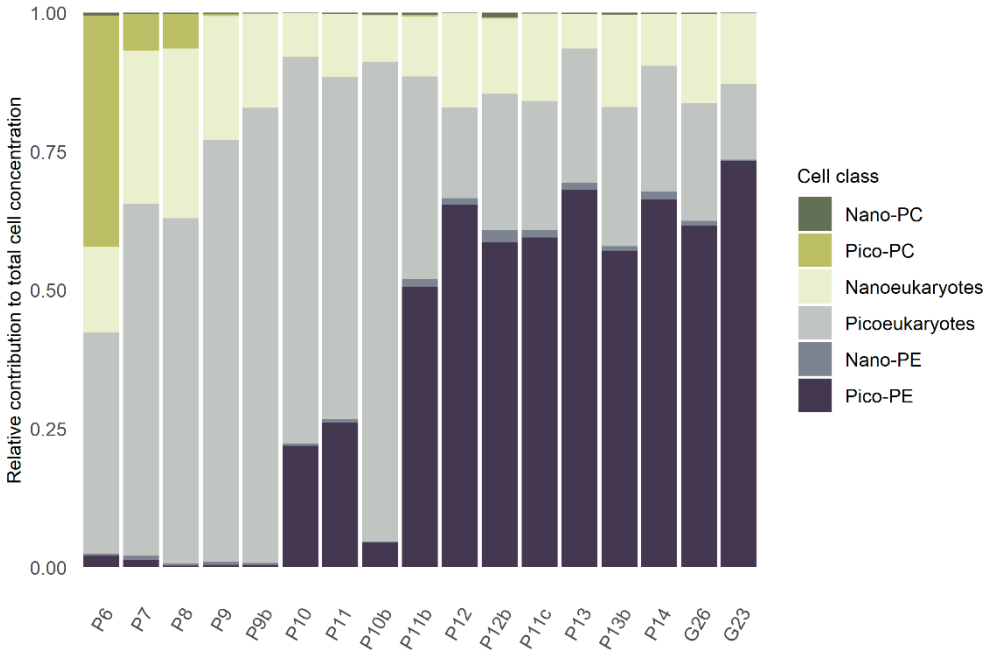

Figure S4. Relative contribution of each cell class to the total cell concentration (obtained from flow cytometry) at surface stations along the central transect from the LSLE to the GSL. Stations are arranged from upstream to downstream (left to right)

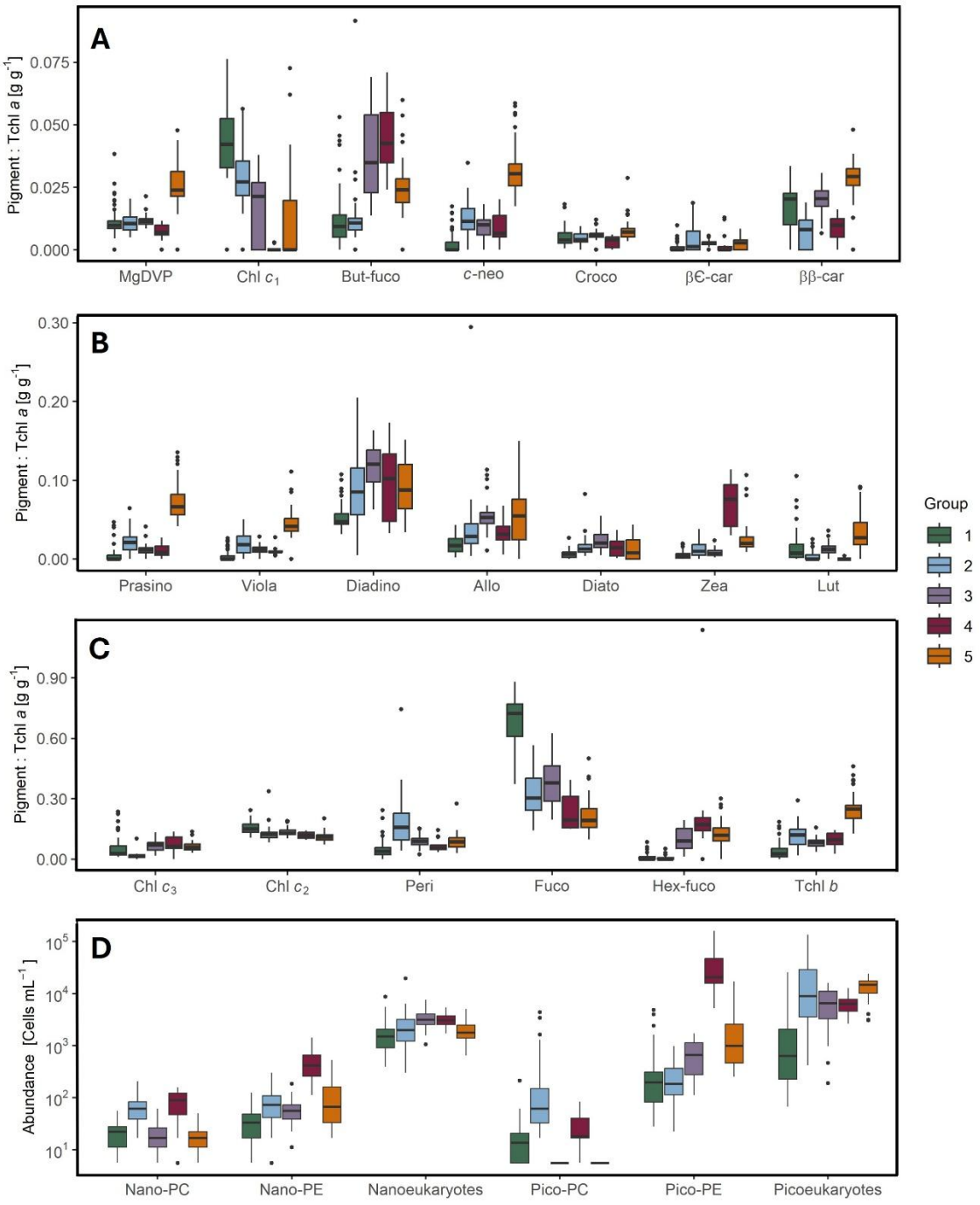

Figure S5. Box plots of the variability (minimum, lower quartile, median, upper quartile, maximum and outliers) of (A, B, C) the ratio of 20 accessory pigments to TChl *a* for the five HCPC groups and (D) the abundance of six phytoplankton cell classes for the five HCPC groups. The pigment ratios are listed according to their retention time for each graph. Note the differences in y-axis scales for each sub-plot

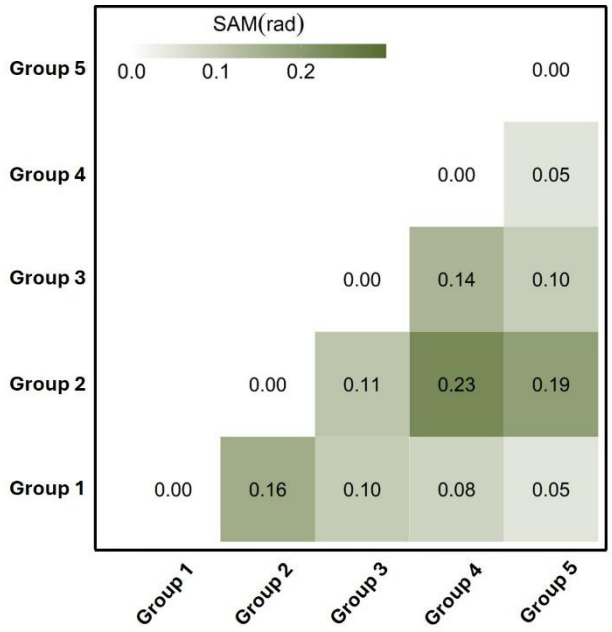

Figure S6. Spectral angle mapper (SAM) applied to the mean normalized reflectivity spectra for the five HCPC groups. Wavelength considered range from 430 to 630 nm

RÉFÉRENCES BIBLIOGRAPHIQUES

Alvain, S., Moulin, C., Dandonneau, Y., & Bréon, F. M. (2005). Remote sensing of phytoplankton groups in case 1 waters from global SeaWiFS imagery. *Deep-Sea Research Part I: Oceanographic Research Papers*, *52*(11), 1989–2004. https://doi.org/10.1016/j.dsr.2005.06.015

Alvain, S., Moulin, C., Dandonneau, Y., & Loisel, H. (2008). Seasonal distribution and succession of dominant phytoplankton groups in the global ocean: A satellite view. *Global Biogeochemical Cycles*, *22*(3). https://doi.org/10.1029/2007GB003154

Araújo, C. A. S., & Bélanger, S. (2022). Variability of bio-optical properties in nearshore waters of the estuary and Gulf of St. Lawrence: Absorption and backscattering coefficients. *Estuarine, Coastal and Shelf Science, 264*. https://doi.org/10.1016/j.ecss.2021.107688

Araújo, C. A. S., Belzile, C., Tremblay, J. É., & Bélanger, S. (2022). Environmental niches and seasonal succession of phytoplankton assemblages in a subarctic coastal bay: Applications to remote sensing estimates. *Frontiers in Marine Science*, *9*. https://doi.org/10.3389/fmars.2022.1001098

Babin, M., Therriault, J.-C., Legendre, L., & Condal, A. (1993). Variations in the specific absorption coefficient for natural phytoplankton assemblages: Impact on estimates of primary production. *Limnology and Oceanography*, *38*(1), 154–177. https://doi.org/10.4319/lo.1993.38.1.0154

Barton, A. D., Irwin, A. J., Finkel, Z. V., & Stock, C. A. (2016). Anthropogenic climate change drives shift and shuffle in North Atlantic phytoplankton communities. *Proceedings of the National Academy of Sciences of the United States of America*, *113*(11), 2964–2969. https://doi.org/10.1073/pnas.1519080113

Basu, S., & Mackey, K. R. M. (2018). Phytoplankton as key mediators of the biological carbon pump: Their responses to a changing climate. *Sustainability*, *10*(3), 869. https://doi.org/10.3390/su10030869

Bérard-Therriault, L., Poulin, M., & Bossé, L. (1999). Guide d'identification du phytoplancton marin de l'estuaire et du golfe du Saint-Laurent: incluant également certains protozoaires. *Canadian Manuscript report of Fisheries and Aquatic Sciences, 128*, 387p.

Bidigare, R. R., Van Heukelem, L., & Trees, C. C. (2005). Analysis of algal pigments by high-performance liquid chromatography. In R. A. Anderson (Ed.), *Algal Culturing Techniques* (p. 327–345) Elsevier Academic Press

Blais, M., Galbraith, P. S., Plourde, S., & Lehoux, C. (2023a). Chemical and biological oceanographic conditions in the Estuary and Gulf of St. Lawrence during 2022. *Canadian Technical Report of Hydrography and Ocean Sciences, 357,* 70 p.

Blais, M., Galbraith, P. S., Plourde, S., Lehoux, C., & Devine, L. (2023b). Chemical and biological oceanographic conditions in the estuary and Gulf of St. Lawrence during 2021. *DFO Canadian Science Advisory Secretariat*, *045*, 74 p.

Bopp, L., Aumont, O., Cadule, P., Alvain, S., & Gehlen, M. (2005). Response of diatoms distribution to global warming and potential implications: A global model study. *Geophysical Research Letters*, *32*(19). https://doi.org/10.1029/2005GL023653

Bracher, A., Bouman, H. A., Brewin, R. J. W., Bricaud, A., Brotas, V., Ciotti, A. M., Clementson, L., Devred, E., Di Cicco, A., Dutkiewicz, S., Hardman-Mountford, N. J., Hickman, A. E., Hieronymi, M., Hirata, T., Losa, S. N., Mouw, C. B., Organelli, E., Raitsos, D. E., Uitz, J.,Vogt, M., & Wolanin, A. (2017). Obtaining phytoplankton diversity from ocean color: A scientific roadmap for future development. *Frontiers in Marine Science*, *4*, 55. https://doi.org/10.3389/fmars.2017.00055

Bracher, A., Taylor, M. H., Taylor, B., Dinter, T., Röttgers, R., & Steinmetz, F. (2015). Using empirical orthogonal functions derived from remote-sensing reflectance for the prediction of phytoplankton pigment concentrations. *Ocean Science*, *11*(1), 139–158. https://doi.org/10.5194/os-11-139-2015

Bracher, A., Vountas, M., Dinter, T., Burrows, J. P., Röttgers, R., & Peeken, I. (2009). Quantitative observation of cyanobacteria and diatoms from space using PhytoDOAS on SCIAMACHY data. *Biogeosciences*, *6*(5), 751-764. https://doi.org/10.5194/bg-6-751-2009

Brewin, R. J., Devred, E., Sathyendranath, S., Lavender, S. J., & Hardman-Mountford, N. J. (2011). Model of phytoplankton absorption based on three size classes. *Applied Optics, 50*(22), 4535-4549. https://doi.org/10.1364/AO.50.004535

Brewin, R. J. W., Sathyendranath, S., Hirata, T., Lavender, S. J., Barciela, R. M., & Hardman-Mountford, N. J. (2010). A three-component model of phytoplankton size class for the Atlantic Ocean. *Ecological Modelling*, *221*(11), 1472–1483. https://doi.org/10.1016/j.ecolmodel.2010.02.014

Brewin, R. J. W., Sathyendranath, S., Jackson, T., Barlow, R., Brotas, V., Airs, R., & Lamont, T. (2015). Influence of light in the mixed-layer on the parameters of a three-component model of phytoplankton size class. *Remote Sensing of Environment*, *168*, 437–450. https://doi.org/10.1016/j.rse.2015.07.004

Bricaud, A., Ciotti, A. M., & Gentili, B. (2012). Spatial-temporal variations in phytoplankton size and colored detrital matter absorption at global and regional scales, as derived from twelve years of SeaWiFS data (1998–2009). *Global Biogeochemical Cycles*, *26*(1). https://doi.org/10.1029/2010GB003952

Bricaud, A., Claustre, H., Ras, J., & Oubelkheir, K. (2004). Natural variability of phytoplanktonic absorption in oceanic waters: Influence of the size structure of algal populations. *Journal of Geophysical Research: Oceans*, *109*(C11). https://doi.org/10.1029/2004JC002419

Brotas, V., Tarran, G. A., Veloso, V., Brewin, R. J. W., Woodward, E. M. S., Airs, R., Beltran, C., Ferreira, A., & Groom, S. B. (2022). Complementary approaches to assess phytoplankton groups and size classes on a long transect in the Atlantic Ocean. *Frontiers in Marine Science*, *8*. https://doi.org/10.3389/fmars.2021.682621

Brown, C. W., & Yoder, J. A. (1994). Distribution pattern of coccolithophorid blooms in the western North Atlantic Ocean. *Continental Shelf Research*, *14*(3), 175–197. https://doi.org/https://doi.org/10.1016/0278-4343(94)90012-4

Bryndum-Buchholz, A., Boyce, D. G., Tittensor, D. P., Christensen, V., Bianchi, D., & Lotze, H. K. (2020). Climate-change impacts and fisheries management challenges in the North Atlantic Ocean. *Marine Ecology Progress Series*, *648*, 1–17. https://doi.org/10.3354/meps13438

Catlett, D., & Siegel, D. A. (2018). Phytoplankton pigment communities can be modeled using unique relationships with spectral absorption signatures in a dynamic coastal environment. *Journal of Geophysical Research: Oceans*, *123*(1), 246–264. https://doi.org/10.1002/2017JC013195

Cantin, G., Levasseur, L., Gosselin, M., & Michaud, S. (1996). Role of zooplankton in the mesoscale distribution of surface dimethylsulfide concentrations in the Gulf of St. Lawrence, Canada. *Marine Ecology Progress Series*, *141*, 103–117. https://doi.org/10.3354/meps141103

Cetinić, I., Rousseaux, C. S., Carroll, I. T., Chase, A. P., Kramer, S. J., Werdell, P. J., Siegel, D. A., Dierssen, H. M., Catlett, D., Neeley, A., Soto Ramos, I. M., Wolny, J. L., Sadoff, N., Urquhart, E., Westberry, T. K., Stramski, D., Pahlevan, N., Seegers, B. N., Sirk, E., Lange, P. K., Vandermeulen, R. A., Graff, J. R., Allen, J. G., Gaube, P., McKinna, L. I. W., Mckibben, S. M., Binding, C. E., Calzado, V. S. & Sayers, M. (2024). Phytoplankton composition from sPACE: Requirements, opportunities, and challenges. *Remote Sensing of Environmen*t, *302*. https://doi.org/10.1016/j.rse.2023.113964

Ciotti, A. M., & Bricaud, A. (2006). Retrievals of a size parameter for phytoplankton and spectral light absorption by colored detrital matter from water-leaving radiances at SeaWiFS channels in a continental shelf region off Brazil. *Limnology and Oceanography: Methods*, *4*(7), 237–253. https://doi.org/10.4319/lom.2006.4.237

Ciotti, Á. M., Lewis, M. R., & Cullen, J. J. (2002). Assessment of the relationships between dominant cell size in natural phytoplankton communities and the spectral shape of the absorption coefficient. *Limnology and Oceanography*, *47*(2), 404–417. https://doi.org/10.4319/lo.2002.47.2.0404

Claustre, H. (1994). The trophic status of various oceanic provinces as revealed by phytoplankton pigment signatures. *Limnology and Oceanography*, *39*(5), 1206–1210. https://doi.org/10.4319/lo.1994.39.5.1206

Cloern, J. E. (2018). Why large cells dominate estuarine phytoplankton. *Limnology and Oceanography*, *63*(S1), S392–S409. https://doi.org/10.1002/lno.10749

Cloern, J. E., Foster, S. Q., & Kleckner, A. E. (2014). Phytoplankton primary production in the world's estuarine-coastal ecosystems. *Biogeosciences*, *11*(9), 2477–2501. https://doi.org/10.5194/bg-11-2477-2014

Craig, S. E., Jones, C. T., Li, W. K. W., Lazin, G., Horne, E., Caverhill, C., & Cullen, J. J. (2012). Deriving optical metrics of coastal phytoplankton biomass from ocean colour. *Remote Sensing of Environment, 119*, 72–83. https://doi.org/10.1016/j.rse.2011.12.007

Demers, S., Roy, S., Gagnon, R., & Vignault, C. (1991). Rapid light-induced changes in cell fluorescence and in xanthophyll-cycle pigments of *Alexandrium excavatum* (Dinophyceae) and *Thalassiosira pseudonana* (Bacillariophyceae): a photo-protection mechanism. *Marine Ecology Progress Series*, *76*(2), 185–193.

Devred, E., Sathyendranath, S., Stuart, V., & Platt, T. (2011). A three component classification of phytoplankton absorption spectra: Application to ocean-color data. *Remote Sensing of Environment*, *115*(9), 2255–2266. https://doi.org/10.1016/j.rse.2011.04.025

Dhifallah, F., Rochon, A., Simard, N., McKindsey, C. W., Gosselin, M., & Howland, K. L. (2022). Dinoflagellate communities in high-risk Canadian Arctic ports. *Estuarine, Coastal and Shelf Science*, *266*. https://doi.org/10.1016/j.ecss.2021.107731

Dierssen, H. M., Vandermeulen, R. A., Barnes, B. B., Castagna, A., Knaeps, E., & Vanhellemont, Q. (2022). QWIP: A quantitative metric for quality control of aquatic reflectance spectral shape using the apparent visible wavelength. *Frontiers in Remote Sensing*, *3*. https://doi.org/10.3389/frsen.2022.869611

Eisner, L. B., Twardowski, M. S., Cowles, T. J., & Perry, M. J. (2003). Resolving phytoplankton photoprotective: Photosynthetic carotenoid ratios on fine scales using *in situ* spectral absorption measurements. *Limnology and Oceanography*, *48*(2), 632–646. https://doi.org/10.4319/lo.2003.48.2.0632

El-Sabh, M. I., & Silverberg, Norman. (1990). *Oceanography of a large-scale estuarine system : the St. Lawrence*. Springer-Verlag.

Falkowski, P. G., Katz, M. E., Knoll, A. H., Quigg, A., Raven, J. A., Schofield, O., & Taylor, F. J. R. (2004). The evolution of modern eukaryotic phytoplankton. *Science*, *305*(5682), 354–360. http://science.sciencemag.org/

Field, C. B., Behrenfeld, M. J., Randerson, J. T., & Falkowski, P. (1998). Primary production of the biosphere: Intergrating terrestrial and oceanic components. *Science*, *281*(5374), 237–240. https://doi.org/10.1126/science.281.5374.237

Frenette, J. J., Massicotte, P., & Lapierre, J. F. (2012). Colorful niches of phytoplankton shaped by the spatial connectivity in a large river ecosystem: a riverscape perspective. *PLoS One*, 7(4). https://doi.org/10.1371/journal.pone.0035891

Frouin, R. J., Franz, B. A., Ibrahim, A., Knobelspiesse, K., Ahmad, Z., Cairns, B., Chowdhary, J., Dierssen, H. M., Tan, J., Dubovik, O., Huang, X., Davis, A. B., Kalashnikova, O., Thompson, D. R., Remer, L. A., Boss, E., Coddington, O., Deschamps, P. Y., Gao, B. C., Gross, L., Hasekamp, O., Omar, A., Pelletier, B., Ramon, D., Steinmetz, F. & Zhai, P. W. (2019). Atmospheric correction of satellite ocean-color imagery during the PACE era. *Frontiers in Earth Science*, *7*. https://doi.org/10.3389/feart.2019.00145

Fuentes-Yaco, C., Vézina, E. F., Larouche, P., Vigneau, C., Gosselin, M., & Levasseur, M. (1997). Phytoplankton pigment in the Gulf of St. Lawrence, Canada, as determined by the Coastal Zone Color Scanner - Part I: Spatio-temporal variability. *Continental Shelf Research*, *17*(12), 1421–1439. https://doi.org/10.1016/S0278-4343(97)00021-6

Fujiwara, A., Hirawake, T., Suzuki, K., & Saitoh, S. I. (2011). Remote sensing of size structure of phytoplankton communities using optical properties of the Chukchi and Bering Sea shelf region. *Biogeosciences, 8*(12), 3567-3580. https://doi.org/10.5194/bg-8-3567-2011

Galbraith, P. S. (2006). Winter water masses in the Gulf of St. Lawrence. *Journal of Geophysical Research: Oceans, 111*(C6). https://doi.org/10.1029/2005JC003159

Galbraith, P. S., Chassé, J., Shaw, J.-L., Dumas, J., Lefaivre, D., & Bourassa, M.-N. (2023). Physical Oceanographic Conditions in the Gulf of St. Lawrence during 2022. *Canadian technical report of hydrography and ocean sciences*, *354*, 88 p.

Galbraith, P. S., Sévigny, C., Bourgault, D., & Dumont, D. (2024). Sea ice interannual variability and sensitivity to fall oceanic conditions and winter air temperature in the Gulf of St. Lawrence, Canada. *Journal of Geophysical Research: Oceans*, *129*, e2023JC020784. https://doi. org/10.1029/2023JC020784

Garcia-Soto, C., Cheng, L., Caesar, L., Schmidtko, S., Jewett, E. B., Cheripka, A., Rigor, I., Caballero, A., Chiba, S., Báez, J. C., Zielinski, T., & Abraham, J. P. (2021). An overview of ocean climate change indicators: Sea surface temperature, ocean heat content, ccean pH, dissolved oxygen concentration, Arctic sea ice extent, thickness and volume, sea level and strength of the AMOC (Atlantic Meridional Overturning Circulation). *Frontiers in Marine Science*, *8*. https://doi.org/10.3389/fmars.2021.642372

GEBCO Compilation Group (2024) GEBCO 2024 Grid (doi:10.5285/1c44ce99-0a0d-5f4f-e063-7086abc0ea0f)

Genin, F., Lalande, C., Galbraith, P. S., Larouche, P., Ferreyra, G. A., & Gosselin, M. (2021). Annual cycle of biogenic carbon export in the Gulf of St. Lawrence. *Continental Shelf Research, 221*. https://doi.org/10.1016/j.csr.2021.104418

Gilbert, D., Sundby, B., Gobeil, C., Mucci, A., & Tremblay, G. H. (2005). A seventy-two-year record of diminishing deep-water oxygen in the St. Lawrence estuary: The northwest Atlantic connection. *Limnology and Oceanography*, *50*(5), 1654–1666. https://doi.org/10.4319/lo.2005.50.5.1654

Gregg, W. W., & Casey, N. W. (2004). Global and regional evaluation of the SeaWiFS chlorophyll data set. *Remote Sensing of Environment*, *93*(4), 463–479. https://doi.org/10.1016/j.rse.2003.12.012

Häder, D. P., & Gao, K. (2015). Interactions of anthropogenic stress factors on marine phytoplankton. *Frontiers in Environmental Science*, *3*. https://doi.org/10.3389/fenvs.2015.00014

Hayward, A., Pinkerton, M. H., & Gutierrez-Rodriguez, A. (2023). phytoclass: A pigment-based chemotaxonomic method to determine the biomass of phytoplankton classes. *Limnology and Oceanography: Methods*, *21*(4), 220–241. https://doi.org/10.1002/lom3.10541

Hillebrand, H., Acevedo-Trejos, E., Moorthi, S. D., Ryabov, A., Striebel, M., Thomas, P. K., & Schneider, M. L. (2022). Cell size as driver and sentinel of phytoplankton community structure and functioning. *Functional Ecology*, *36*(2), 276–293. https://doi.org/10.1111/1365-2435.13986

Hintz, N. H., Zeising, M., & Striebel, M. (2021). Changes in spectral quality of underwater light alter phytoplankton community composition. *Limnology and Oceanography*, 66(9), 3327-3337. https://doi.org/10.1002/lno.11882

Hirata, T., Aiken, J., Hardman-Mountford, N., Smyth, T. J., & Barlow, R. G. (2008). An absorption model to determine phytoplankton size classes from satellite ocean colour. *Remote Sensing of Environment*, *112*(6), 3153-3159. https://doi.org/10.1016/j.rse.2008.03.011

Hirata, T., Hardman-Mountford, N. J., Brewin, R. J. W., Aiken, J., Barlow, R., Suzuki, K., Isada, T., Howell, E., Hashioka, T., Noguchi-Aita, M., & Yamanaka, Y. (2011). Synoptic relationships between surface Chlorophyll-a and diagnostic pigments specific to phytoplankton functional types. *Biogeosciences*, *8*(2), 311–327. https://doi.org/10.5194/bg-8-311-2011

Hudon, C., Gagnon, P., Rondeau, M., Hébert, S., Gilbert, D., Hill, B., Patoine, M. & Starr, M. (2017) Hydrological and biological processes modulate carbon, nitrogen and phosphorus flux from the St. Lawrence River to its estuary (Québec, Canada). *Biogeochemistry, 135*, 251-276.

IOCCG (2014). *Phytoplankton functional types from space*. S. Sathyendranath (Ed.), Reports of the International Ocean-Colour Coordinating Group, No. 15, IOCCG, Dartmouth, Canada.

IOCCG (2018). IOCCG ocean optics and biogeochemistry protocols for satellite ocean colour sensor validation; Volume 1.0. Inherent optical oroperty measurements and protocols: Absorption coefficient. A. R. Neeley & A. Mannino (Eds.), Dartmouth, Canada. doi: 10.25607/OBP-119

Jacques, A. (2001). Télédétection passive de la chlorophylle dans l'estuaire maritime du Saint-Laurent: Optimisation spectrale des algorithmes et application au SeaWIFS [Thèse de doctorat, Université de Sherbrooke].

Jeffrey, S. W. (1961). Paper-Chromatographic separation of chlorophylls and carotenoids from marine algae. *Biochemical Journal*, *80*(2), 336–342.

Jeffrey, S. W., Wright, S., and M. Zapata. (2011). Microalgal classes and their signature pigments. In S. Roy, C. A. Llewellyn, E. S. Egeland, & G. Johnsen (Eds.), *Phytoplankton pigments: characterization, chemotaxonomy and applications in Oceanography* (p. 3–77). Cambridge University Press

Jiang, D., Matsushita, B., & Yang, W. (2020). A simple and effective method for removing residual reflected skylight in above-water remote sensing reflectance measurements. *ISPRS Journal of Photogrammetry and Remote Sensing*, *165*, 16–27. https://doi.org/10.1016/j.isprsjprs.2020.05.003

Johnsen, G., Moline, M. A., Pettersson, L. H., Pettersson, L. H., Pozdnyakov, D. V., Egeland, E. S., & Schofield, O. M. (2011). Optical monitoring of phytoplankton bloom pigment signature. In S. Roy, C. A. Llewellyn, E. S. Egeland, & G. Johnsen (Eds.), *Phytoplankton pigments: Characterization, Chemotaxonomy and Applications in Oceanography* (p. 538–581). Cambridge University Press.

Jutras, M., Dufour, C. O., Mucci, A., Cyr, F., & Gilbert, D. (2020). Temporal changes in the causes of the observed oxygen decline in the St. Lawrence Estuary. *Journal of Geophysical Research: Oceans, 125*(12). https://doi.org/10.1029/2020JC016577

Kirk, J. T. O. (1975). A theoretical analysis of the contribution of algal cells to the attenuation of light within natural waters. *New Phytologist*, *75*(1), 21–36. https://doi.org/10.1111/j.1469-8137.1975.tb01367.x

Kishino, M., Takahashi, M., Okami, N., & Ichimura, S. (1985). Estimation of the spectral absorption coefficients of phytoplankton in the sea. *Bulletin of Marine Science*, *37*(2), 634–642.

Kostadinov, T. S., Siegel, D. A., & Maritorena, S. (2009). Retrieval of the particle size distribution from satellite ocean color observations. *Journal of Geophysical Research: Oceans, 114*(9). https://doi.org/10.1029/2009JC005303

Kostadinov, T. S., Siegel, D. A., & Maritorena, S. (2010). Global variability of phytoplankton functional types from space: Assessment via the particle size distribution. *Biogeosciences*, *7*(10), 3239–3257. https://doi.org/10.5194/bg-7-3239-2010

Kramer, S. J., Bolaños, L. M., Catlett, D., Chase, A. P., Behrenfeld, M. J., Boss, E. S., Crockford, E. T., Giovannoni, S. J., Graff, J. R., Haëntjens, N., Karp-Boss, L., Peacock, E. E., Roesler, C. S., Sosik, H. M., & Siegel, D. A. (2024). Toward a synthesis of phytoplankton community composition methods for global-scale application. *Limnology and Oceanography: Methods*, *22*(4), 217–240. https://doi.org/10.1002/lom3.10602

Kramer, S. J., Roesler, C. S., & Sosik, H. M. (2018). Bio-optical discrimination of diatoms from other phytoplankton in the surface ocean: Evaluation and refinement of a model for the Northwest Atlantic. *Remote Sensing of Environment, 217,* 126–143. https://doi.org/10.1016/j.rse.2018.08.010

Kramer, S. J., & Siegel, D. A. (2019). How can phytoplankton pigments be best used to characterize surface ocean phytoplankton groups for ocean color remote sensing algorithms? *Journal of Geophysical Research: Oceans*, *124*(11), 7557–7574. https://doi.org/10.1029/2019JC015604

Kruse, F. A., Lefkoff, A. B., Boardman, J. W., Heidebrecht, K. B., Shapiro, A. T., Barloon, P. J., & Goetz, A. F. (1993). The spectral image processing system (SIPS)-interactive visualization and analysis of imaging spectrometer data. *Remote Sensing of Environment, 44*, 145–163. https://doi.org/10.1016/0034-4257(93)90013-N

Kutser, T., Vahtmäe, E., Paavel, B., & Kauer, T. (2013). Removing glint effects from field radiometry data measured in optically complex coastal and inland waters. *Remote Sensing of Environment*, *133*, 85–89. https://doi.org/10.1016/j.rse.2013.02.011

Laliberté, J., & Larouche, P. (2023). Chlorophyll-a concentration climatology, phenology, and trends in the optically complex waters of the St. Lawrence Estuary and Gulf. *Journal of Marine Systems, 238*. https://doi.org/10.1016/j.jmarsys.2022.103830

Laliberté, J., Larouche, P., Devred, E., & Craig, S. (2018). Chlorophyll-a concentration retrieval in the optically complex waters of the St. Lawrence Estuary and Gulf using principal component analysis. *Remote Sensing*, *10*(2). https://doi.org/10.3390/rs10020265

Lalli, C.M. & T.R. Parsons. 2002. *Biological oceanography: An introduction, 2nd Edition*. Butterworth-Heinemann, Oxford, 314 p.

Lauzier, L. & Trites, R. W. (1958). The deep waters in the Laurentian Channel. *Journal of the Fisheries Board of Canada, 15*(6), 1247-1257. https://doi.org/10.1139/f58-068

Lavoie, D., Lambert, N., Rousseau, S., Dumas, J., Chassé, J., Long, Z., Perrie, W., Starr, M., Brickman, D., & Azetsu-Scott, K. (2020). Projections of future physical and biogeochemical conditions in the Gulf of St. Lawrence, on the Scotian Shelf and in the Gulf of Maine using a regional climate model. *Canadian Technical Report of Hydrography and Ocean Sciences, 334,* 102 p.

Le Fouest, V., Zakardjian, B., Saucier, F. J., & Starr, M. (2005). Seasonal versus synoptic variability in planktonic production in a high-latitude marginal sea: The Gulf of St. Lawrence (Canada). *Journal of Geophysical Research*, *110*(C9), 1–21. https://doi.org/10.1029/2004JC002423

Le Quéré, C., Harrison, S. P., Colin Prentice, I., Buitenhuis, E. T., Aimont, O., Bopp, L., Claustre, H., Cotrim Da Cunha, L., Geider, R., Giraud, X., Klaas, C., Kohfeld, K. E., Legendre, L., Manizza, M., Platt, T., Rivkin, R. B., Sathyendranath, S., Uitz, J., Watson, A. J., & Wolf-Gladwor, D. (2005). Ecosystem dynamics based on plankton functional types for global ocean biogeochemistry models. *Global Change Biology*, *11*(11), 2016–2040. https://doi.org/10.1111/j.1365-2486.2005.01004.x

Levasseur, M., Fortier, L., Therriault, J.-C., & Harrison, P. J. (1992). Phytoplankton dynamics in a coastal jet frontal region. *Marine Ecology Progress Series*, *86*, 283–295.

Levasseur, M., Therriaultl, J.-C., & Legendre, L. (1984). Hierarchical control of phytoplankton succession by physical factors. *Marine Ecology Progress Series*, *19*, 211–222.

Li, Z., Li, L., Song, K., & Cassar, N. (2013). Estimation of phytoplankton size fractions based on spectral features of remote sensing ocean color data. *Journal of Geophysical Research: Oceans*, *118*(3), 1445–1458. https://doi.org/10.1002/jgrc.20137

Losa, S. N., Soppa, M. A., Dinter, T., Wolanin, A., Brewin, R. J. W., Bricaud, A., Oelker, J., Peeken, I., Gentili, B., Rozanov, V., & Bracher, A. (2017). Synergistic exploitation of hyper- and multi-spectral precursor sentinel measurements to determine phytoplankton functional types (SynSenPFT). *Frontiers in Marine Science*, *4*. https://doi.org/10.3389/fmars.2017.00203

Mackey, M. D., Mackey, D. J., Higgins, H. W., & Wright, S. W. (1996). CHEMTAX-a program for estimating class abundances from chemical markers: application to HPLC measurements of phytoplankton. *Marine Ecology Progress Series, 144*, 265–283. doi:10.3354/meps144265

Marañón, E. (2015). Cell Size as a key determinant of phytoplankton metabolism and community structure. *Annual Review of Marine Science*, *7*, 241–264. https://doi.org/10.1146/annurev-marine-010814-015955

McClain, C. R. (2009). A decade of satellite ocean color observations. *Annuel review of marine science, 1 (1),* 19-42. https://doi.org/10.1146/annurev.marine.010908.163650

Mei, Z. P., Lavoie, D., Lambert, N., Starr, M., Chassé, J., Perrie, W., & Long, Z. (2024). Modelling the bottom-up effects of climate change on primary production in the Gulf of St. Lawrence and eastern Scotian Shelf. *Frontiers in Marine Science*, *11*. https://doi.org/10.3389/fmars.2024.1416744

Mei, Z. P., Saucier, F. J., Le Fouest, V., Zakardjian, B., Sennville, S., Xie, H., & Starr, M. (2010). Modeling the timing of spring phytoplankton bloom and biological production of the Gulf of St. Lawrence (Canada): Effects of colored dissolved organic matter and temperature. *Continental Shelf Research*, *30*(19), 2027–2042. https://doi.org/10.1016/j.csr.2010.10.003

Mobley, C. D. (1999). Estimation of the remote-sensing reflectance from above-surface measurements. *Applied Optics*, *38*(36), 7442–7455. https://doi.org/10.1364/AO.38.007442

Morel, A., & Bricaud, A. (1981). Theoretical results concerning light absorption in a discrete medium, and application to specific absorption of phytoplankton. *Deep-Sea Research*, *28*(11), 1375–1393.

Morel, A., & Prieur, L. (1977). Analysis of variations in ocean color. *Limnology and Oceanography*, *22*(4), 709–722. https://doi.org/10.4319/lo.1977.22.4.0709

Mouw, C. B., Hardman-Mountford, N. J., Alvain, S., Bracher, A., Brewin, R. J. W., Bricaud, A., Ciotti, A. M., Devred, E., Fujiwara, A., Hirata, T., Hirawake, T., Kostadinov, T. S., Roy, S., & Uitz, J. (2017). A consumer's guide to satellite remote sensing of multiple phytoplankton groups in the global ocean. *Frontiers in Marine Science*, *4*, 41. https://doi.org/10.3389/fmars.2017.00041

Mouw, C. B., & Yoder, J. A. (2010). Optical determination of phytoplankton size composition from global SeaWiFS imagery. *Journal of Geophysical Research: Oceans*, *115*(C12). https://doi.org/10.1029/2010JC006337

Nair, A., Sathyendranath, S., Platt, T., Morales, J., Stuart, V., Forget, M. H., Devred, E., & Bouman, H. (2008). Remote sensing of phytoplankton functional types. *Remote Sensing of Environment*, *112*(8), 3366–3375. https://doi.org/10.1016/j.rse.2008.01.021

Nieke, B., Reuter, R., Heuermann, R., Wang, H., Babin, M., & Therriault, J. C. (1997). Light absorption and fluorescence properties of chromophoric dissolved organic matter (CDOM), in the St. Lawrence Estuary (Case 2 waters). *Continental Shelf Research*, *17*(3), 235–252. https://doi.org/10.1016/S0278-4343(96)00034-9

Not, F., Siano, R., Kooistra, W. H. C. F., Simon, N., Vaulot, D., & Probert, I. (2012). Diversity and ecology of eukaryotic marine phytoplankton. *Advances in Botanical Research, 64*, 1–53. https://doi.org/10.1016/B978-0-12-391499-6.00001-3

Paradis-Hautcoeur, J., Gosselin, M., Villeneuve, V., Tremblay, J. É., Lévesque, D., Scarratt, M., & Starr, M. (2023). Effects of riverine nutrient inputs on the sinking fluxes of microbial particles in the St. Lawrence Estuary. *Estuarine, Coastal and Shelf Science*, *284*. https://doi.org/10.1016/j.ecss.2023.108270

Parsons, T. R., Maita, Y., & Lalli, C. M. (1984). *A manual of chemical and biological methods for seawater analysis*. Pergamon Press.

Raitsos, D. E., Lavender, S. J., Maravelias, C. D., Haralabous, J., Richardson, A. J., & Reid, P. C. (2008). Identifying four phytoplankton functional types from space: An ecological approach. *Limnology and Oceanography*, *53*(2), 605–613. https://doi.org/10.4319/lo.2008.53.2.0605

Reynolds, C. S., Huszar, V., Kruk, C., Naselli-Flores, L., & Melo, S. (2002). Towards a functional classification of the freshwater phytoplankton. *Journal of Plankton Research*, *24*(5), 417–428. https://doi.org/10.1093/plankt/24.5.417

Röttgers, R., & Gehnke, S. (2012). Measurement of light absorption by aquatic particles: improvement of the quantitative filter technique by use of an integrating sphere approach. *Applied Optics*, *51*(9), 1336–1351. https://doi.org/10.1364/AO.51.001336

Roy, S., Blouin, F., Jacques, A., & Therriault, J. C. (2008). Absorption properties of phytoplankton in the Lower Estuary and Gulf of St. Lawrence (Canada). *Canadian Journal of Fisheries and Aquatic Sciences*, *65*(8), 1721–1737. https://doi.org/10.1139/F08-089

Roy, S., Chanut, J.-P., Gosselin, M., & Sime-Ngando, T. (1996). Characterization of phytoplankton communities in the lower St. Lawrence Estuary using HPLC-detected pigments and cell microscopy. *Marine Ecology Progress Series*, *142*, 55–73. doi:10.3354/meps142055

Roy, S., Llewellyn, C. A., Egeland, E. S., & Johnsen, G. (2011). *Phytoplankton pigments: characterization, chemotaxonomy and applications in Oceanography*. Cambridge University Press, 845p.

Roy, S., Sathyendranath, S., Bouman, H., & Platt, T. (2013). The global distribution of phytoplankton size spectrum and size classes from their light-absorption spectra derived from satellite data. *Remote Sensing of Environment*, *139*, 185–197. https://doi.org/10.1016/j.rse.2013.08.004

Ruddick, K. G., De Cauwer, V., Park, Y. J., & Moore, G. (2006). Seaborne measurements of near infrared water-leaving reflectance: The similarity spectrum for turbid waters. *Limnology and Oceanography*, *51*(2), 1167–1179. https://doi.org/10.4319/lo.2006.51.2.1167

Sadeghi, A., Dinter, T., Vountas, M., Taylor, B. B., Altenburg-Soppa, M., Peeken, I., & Bracher, A. (2012). Improvement to the PhytoDOAS method for identification of coccolithophores using hyper-spectral satellite data. *Ocean Science*, *8*(6), 1055-1070. https://doi.org/10.5194/os-8-1055-2012

Sathyendranath, S., Cota, G., Stuart, V., Maass, H., & Platt, T. (2001). Remote sensing of phytoplankton pigments: A comparison of empirical and theoretical approaches. *International Journal of Remote Sensing*, *22*(2–3), 249–273. https://doi.org/10.1080/014311601449925

Sathyendranath, S., Watts, L., Devred, E., Platt, T., Caverhill, C., & Maass, H. (2004). Discrimination of diatoms from other phytoplankton using ocean-colour data. *Marine ecology progress series*, 272, 59-68. https://doi.org/10.3354/meps272059

Schlüter, L., Mohlenberg, F., Havskum, H., & Larsen, S. (2000). The use of phytoplankton pigments for identifying and quantifying phytoplankton groups in coastal areas: testing the influence of light and nutrients on pigment/chlorophyll a ratios. *Marine Ecology Progress Series*, *192*, 49–63. doi:10.3354/meps192049

Schoemann, V., Becquevort, S., Stefels, J., Rousseau, V., & Lancelot, C. (2005). Phaeocystis blooms in the global ocean and their controlling mechanisms: a review. *Journal of Sea Research*, *53*(1-2), 43-66. https://doi.org/10.1016/j.seares.2004.01.008

Sharpe, H., Gosselin, M., Lalande, C., Normandeau, A., Montero-Serrasno, J. C., Baccara, K., Bourgault, D., Sherwood, O. & Limoges, A. (2023). Influence of a small submarine canyon on biogenic matter export flux in the lower St. Lawrence Estuary, eastern Canada. *Biogeosciences, 20*(24), 4981-5001. https://doi.org/10.5194/bg-20-4981-2023

Simard, Y., Lepage, R. & Gervaise, C. (2010). Anthropogenic sound exposure of marine mammals from seaways: Estimates for the Lower St. Lawrence Seaway, eastern Canada. *Applied Acoustics, 71*(11), 1093-1098. https://doi.org/10.1016/j.apacoust.2010.05.012

Sinclair, M. (1978). Summer phytoplankton variability in the lower St. Lawrence Estuary. *Journal of the Fisheries Research Board of Canada*, *35*, 1171–1185. https://doi.org/10.1139/f78-188

Soppa, M. A., Hirata, T., Silva, B., Dinter, T., Peeken, I., Wiegmann, S., & Bracher, A. (2014). Global retrieval of diatom abundance based on phytoplankton pigments and satellite data. *Remote Sensing*, *6*(10), 10089–10106. https://doi.org/10.3390/rs61010089

Spyrakos, E., O'Donnell, R., Hunter, P. D., Miller, C., Scott, M., Simis, S. G. H., Neil, C., Barbosa, C. C. F., Binding, C. E., Bradt, S., Bresciani, M., Dall'Olmo, G., Giardino, C., Gitelson, A. A., Kutser, T., Li, L., Matsushita, B., Martinez-Vicente, V., Matthews, M. W., Ogashawara, I., Ruiz-Verdu, A., Schalles, J. F., Tebbs, E., Zhang, Y., & Tyler, A. N. (2018). Optical types of inland and coastal waters. *Limnology and Oceanography*, *63*(2), 846–870. https://doi.org/10.1002/lno.10674

Stramski, D., Reynolds, R. A., Kaczmarek, S., Uitz, J., & Zheng, G. (2015). Correction of pathlength amplification in the filter-pad technique for measurements of particulate absorption coefficient in the visible spectral region. *Applied Optics*, *54*(22), 6763. https://doi.org/10.1364/ao.54.006763

Sun, X., Shen, F., Brewin, R. J. W., Li, M., & Zhu, Q. (2022). Light absorption spectra of naturally mixed phytoplankton assemblages for retrieval of phytoplankton group composition in coastal oceans. *Limnology and Oceanography*, *67*(4), 946–961. https://doi.org/10.1002/lno.12047

Sunda, W., Kieber, D. J., Kiene, R. P., & Huntsman, S. (2002). An antioxidant function for DMSP and DMS in marine algae. *Nature*, *418*(6895), 317–320. https://doi.org/10.1038/nature00851

Therriault, J. C., & Levasseur, M. (1986). Freshwater runoff control of the spatio-temporal distribution of phytoplankton in the lower St. Lawrence Estuary (Canada). In S. Skreslet (Ed.), *The role of freshwater Outflow in coastal marine ecosystems* (p. 251–260). Springer Berlin Heidelberg.

Uitz, J., Claustre, H., Morel, A., & Hooker, S. B. (2006). Vertical distribution of phytoplankton communities in open ocean: An assessment based on surface chlorophyll. *Journal of Geophysical Research: Oceans*, *111*(8). https://doi.org/10.1029/2005JC003207

Vidussi, F., Claustre, H., Bustillos-Guzman, J., Cailliau, C., & Marty, J.-C. (1996). Determination of chlorophylls and carotenoids of marine phytoplankton: separation of chlorophyll a from divinyl-chlorophyll a and zeaxanthin from lutein. *Journal of Plankton Research*, *18*(12), 2377–2382. https://academic.oup.com/plankt/article/18/12/2377/1483496

Vidussi, F., Claustre, H., Manca, B. B., Luchetta, A., & Marty, J. C. (2001). Phytoplankton pigment distribution in relation to upper thermocline circulation in the eastern Mediterranean Sea during winter. *Journal of Geophysical Research: Oceans*, *106*(C9), 19939–19956. https://doi.org/10.1029/1999jc000308

Vishnu, P. S., Xi, H., Belluz, J. D. B., Hussain, M. S., Bracher, A., & Costa, M. (2022). Seasonal dynamics of major phytoplankton functional types in the coastal waters of the west coast of Canada derived from OLCI Sentinel 3A. *Frontiers in Marine Science*, *9.* https://doi.org/10.3389/fmars.2022.1018510

Volk, T., & Hoffert, M. I. (1985). Ocean carbon pumps: analysis of relative strengths and efficiencies in ocean-driven atmospheric CO_2 changes. *The Carbon Cycle and Atmospheric CO_2: Natural Variations Archean to Present*, *32,* 99–110. https://doi.org/10.1029/gm032p0099

Werdell, P. J., Behrenfeld, M. J., Bontempi, P. S., Boss, E., Cairns, B., Davis, G. T., Franz, B. A., Gliese, U. B., Gorman, E. T., Hasekamp, O., Knobelspiesse, K. D., Mannino, A., Martins, J. V., McClain, C., Meister, G., & Remer, L. A. (2019). The plankton, aerosol, cloud, ocean ecosystem mission: Status, science, advances. *Bulletin of the American Meteorological Society*, *100*(9), 1775–1794. https://doi.org/10.1175/BAMS-D-18-0056.1

Winder, M., & Sommer, U. (2012). Phytoplankton response to a changing climate. *Hydrobiologia*, *698*, 5–16. https://doi.org/10.1007/s10750-012-1149-2

Wright, S. W., Jeffrey, S. W., Mantoura, R. F. C., Llewellyn, C. A., Bjørnland, T., Repeta, D., & Welschmeyer, N. (1991). Improved HPLC method for the analysis of chlorophylls and carotenoids from marine phytoplankton. *Marine Ecology Progress Series*, *77*(2), 183–196. https://www.jstor.org/stable/24826571

Xi, H., Bratagnon, M., Losa, S. N., Brotas, V., Gomes, M., Peeken, I., Alvarado, L. M. A., Mangin, A., & Bracher, A. (2023). Satellite monitoring of surface phytoplankton functional types in the Atlantic Ocean over 20 years (2002–2021). *State of the Planet*, *1*, 1–13. https://doi.org/10.5194/sp-1-osr7-5-2023

Xi, H., Losa, S. N., Mangin, A., Garnesson, P., Bretagnon, M., Demaria, J., Soppa, M. A., Hembise Fanton d'Andon, O., & Bracher, A. (2021). Global chlorophyll *a* concentrations of phytoplankton functional types with detailed uncertainty assessment using multisensor ocean color and sea surface temperature satellite products. *Journal of Geophysical Research: Oceans*, *126*(5). https://doi.org/10.1029/2020JC017127

Xi, H., Losa, S. N., Mangin, A., Soppa, M. A., Garnesson, P., Demaria, J., Liu, Y., d'Andon, O. H. F., & Bracher, A. (2020). Global retrieval of phytoplankton functional types based on empirical orthogonal functions using CMEMS GlobColour merged products and further extension to OLCI data. *Remote Sensing of Environment*, *240*. https://doi.org/10.1016/j.rse.2020.111704

Xie, H., Aubry, C., Bélanger, S., & Song, G. (2012). The dynamics of absorption coefficients of CDOM and particles in the St. Lawrence estuarine system: Biogeochemical and physical implications. *Marine Chemistry*, *128*, 44–56. https://doi.org/10.1016/j.marchem.2011.10.001

Zakardjian, B., Gratton, Y., & Vézina, A. F. (2000). Late spring phytoplankton bloom in the Lower St. Lawrence Estuary: the flushing hypothesis revisited. *Marine Ecology Progress Series*, *192*, 31–48. doi:10.3354/meps192031

Zapata, M., Rodriguez, F., & Garrido, J. L. (2000). Separation of chlorophylls and carotenoids from marine phytoplankton: a new HPLC method using a reversed phase C8 column and pyridine-containing mobile phases. *Marine Ecology Progress Series, 195*, 29–45. https://doi.org/doi:10.3354/meps195029

Zhang, Y., Shen, F., Li, R., Li, M., Li, Z., Chen, S., & Sun, X. (2024). AIGD-PFT: the first AI-driven global daily gap-free 4 km phytoplankton functional type data product from 1998 to 2023. *Earth System Science Data*, *16*(10), 4793–4816. https://doi.org/10.5194/essd-16-4793-2024